Effect of LC3 homologues on cytoplasmic TDP-43, stress granules and contents of small extracellular vesicles

Angelica Tristani

Thesis submitted to the University of Ottawa in partial fulfillment of the requirements for the Master's of Science degree in Cellular and Molecular Medicine

Department of Cellular and Molecular Medicine

Faculty of Medicine

University of Ottawa, Ontario, Canada

Abstract

Autophagy is a crucial process to maintain protein quality control and degrade cargo in the cell. Aberrant autophagy plays a crucial role in the pathogenesis of various neurodegenerative diseases, including Amyotrophic Lateral Sclerosis (ALS). ALS is the most common motor neuron disease, with 90% of cases occurring sporadically and 10% being familial. So far, there is no known cure for ALS; most therapeutics alleviate symptoms or delay their onset. ALS is primarily characterized by RNA binding proteins (RBPs) such as TDP-43, which is associated with 97% of cases.[1] In fact, aberrant dynamics of RBPs have been shown to lead to their aggregation and interaction with stress granules in ALS.[2] More specifically, stress granules unable to disassemble may persist in the cell, then requiring elimination by autophagy.[2,3] However, in ALS, we often find impaired autophagy and insufficient degradation of RBPs, leading to aggregate accumulation in the cytoplasm.[3] For this reason, fostering the autophagy pathway as a therapeutic method in ALS can potentially induce turnover and elimination of these pathogenic proteins, preventing their accumulation and ultimately cell death. Specifically, LC3 homologues offer a unique interest due to their direct involvement with later stages of autophagy, their selectivity, and their possible roles beyond autophagy. For the latter, LC3 has been implicated in secretory autophagy pathways, such as loading cargo for elimination into extracellular vesicles (EVs) to compensate for states of lysosomal inhibition. [4,5] Our goal was to analyze the effects of LC3 homologues in degradation of TDP-43 and stress granules and explore the involvement of LC3 stress granule protein loading into small EVs. Using high-throughput imaging microscopy, we compared the effects between different LC3 knockdowns on stress granule levels and cytoplasmic TDP-43. This allowed us to identify which LC3 homologues significantly impact clearance of these ALS-related substrates. The effect of LC3 knockdown on

cytoplasmic TDP-43 degradation is unclear; however, GABARAPL1 offers a promising role in the degradation of stress granules. Further investigation into the role of GABARAPL1 in stress granule clearance may offer therapeutic potential in ALS models to prevent the accumulation of stress granules. Lastly, knockdown of all LC3 homologues showed increased loading of stress granule proteins into EVs. In previous studies, LC3 appeared to be involved in packing RBPs and stress granule proteins into EVs; however, we saw opposing results in our mass spectrometry data. Analysing EV content in cells knocked down for LC3/GABARAP knockdown allowed us to depict the influence that LC3s have in EV cargo loading, specifically concerning stress granule proteins.

Statement of Contributions

I wrote this thesis and edited it, while Dr. Derrick Gibbings provided further edits before submission to examiners. Derrick Gibbings set the initial project idea and guidance throughout my project for experimental objectives. I did the actual experiments and data analysis.

Dr. Stephen Baird acquired images in the high-throughput screening lab at the Children's Hospital of Eastern Ontario (CHEO).

Charlotte Manser provided the initial image analysis pipeline for stress granule and TDP-43 quantification. I made minor adjustments/parameter changes as needed and performed the image analysis for my experiments.

U2OS-eGFP-G3BP2 cells were made and gifted from Dr. Laura Trinkle-Mulcahy's lab.

Ryan Reshke performed nanoparticle tracking analysis of small extracellular vesicle samples that I collected and provided guidance for EV isolation and mass spectrometry preparation.

Dr. Zhibin Ning, at the proteomics core facility at uOttawa, performed Mass Spectrometry for me after I had prepared my samples.

Acknowledgments

I would like to thank everyone who supported me throughout my Master's and provided me guidance these last two years, both in and outside of the lab.

Thank you to my supervisor Dr. Derrick Gibbings, I appreciate your guidance these last two years and the help you gave me in becoming the young scientist I am today. You helped me navigate my way through this project and transition into research, which I am very grateful for. I will forever appreciate the opportunities presented, which wouldn't have been possible without your support and guidance.

Thank you to all the members of the Gibbings Lab for your guidance and help throughout my time at the lab. Specifically, Ryan Reshke and Kallol Dutta, who both helped me immensely in transitioning into research for the first time. Thank you for answering all of my questions, and always being willing to provide guidance. Thank you Charlie for teaching me the ropes of high-throughput imaging, and Stephen Baird for imaging my numerous plates. To Charlie and Nick, thank you for putting up with my endless UK accents, lab zoomies, and brightening my days.

Thank you to my TAC members, Dr. Ryan Russell and Dr. Max Rousseaux, for all your helpful feedback and guidance - I greatly appreciate it. Thank you to the uOttawa Eric Poulin Centre for Neuromuscular Disease for helping fund my research.

To my Aunty Kenny and Aunty Lee, thank you for all your love and support. You both have helped me grow into the woman I am today and supported my dreams since I was little. You are both incredibly strong women that I will always look up to.

To my best friend Olivia (maguy), I will forever be grateful for our beautiful friendship. Thank you for supporting me, cheering me on and reminding me to be kind, proud, and patient with myself when navigating my ups and downs. You never fail to bring a smile to my face.

To Thomas, thank you for everything. You've supported me in so many ways these last two years; from learning to make lentivirus at the lab together, being an awesome lab manager to becoming my forever friend, you've been there for me through up and down. Thank you for always supporting me, believing in me, and reminding me that I am more than capable of accomplishing my dreams and goals. I love you so much and am sincerely grateful for all the love and warmth you bring into my life.

To my Mama and Papa, words can't capture how lucky I am to have such loving and supportive parents. You have both been incredible role models. You've been my number one cheerleaders since day one and support me through all my ups and downs. I wouldn't have been able to do this without your unconditional love and support. You've always believed in me no matter what and helped me face new beginnings, chapters, changes, and challenges with strength and love. Thank you for supporting me through university these last six years and reminding me I can accomplish whatever I put my mind to. I love you both so much!

Table of Contents

List of Figures

List of Tables

List of Abbreviations

AB: Amyloid beta

AD: Alzheimer's disease

ALS: Amyotrophic Lateral Sclerosis

AMPK: AMP-activated protein kinase

ATAXN1L: Ataxin 1-Like

ATG: Autophagy-related

ATTECs: Autophagosome-tethering compounds

AUTACs: Autophagy targeting chimeras

C9orf72: Chromosome 9 open reading frame 72

CLEAR: Coordinated lysosomal expression and regulation

CMA: Chaperone mediated autophagy

DIA: Data-independent acquisition

ESCRT: Endosomal sorting complex required for transport

EV: Extracellular vesicle

FIP200: FAK family kinase-interacting protein of 200 kDa

FTD: Frontotemporal Dementia

FUS: Fused in sarcoma

FYCO1: FYVE and coiled-coil domain-containing protein 1

G3BP1/G3BP2: Ras GTPase-activating binding protein (1/2)

GABARAP: Gamma-aminobutyric acid receptor protein

GO: Gene Ontology

HD: Huntington's disease

HOPS: Homotypic fusion and protein sorting

HSPA8: Heat shock 70 kDa protein 8

HTT: Huntington

ILV: Intra-luminal vesicles

LDELS: LC3-dependent extracellular vesicle loading and secretion

LIR: LC3-interacting region

LLPS: Liquid-liquid-phase separation

MAP1LC3: Microtubule-associated proteins 1A/1B light chain 3

MTX1: Metaxin-1

MVB: multi-vesicular body

NES: Nuclear export signal

NLS: Nuclear localization signal

OPTN: Optineurin

PAS: Phagophore assembly site

PE: Phosphatidylethanolamine

PI3P: Phosphatidylinositol 3-phosphate

PKA: Phosphorylation from protein kinase A

PLEKHM1: Pleckstrin homology domain-containing family M member 1

PP2A: Protein phosphatase 2A

PROTAC: Proteolysis-targeting chimeras

PTM: Post-translational modification

PTM: Post-translational modifications (PTM)

RB1CC1: RB1-inducible coiled-coil protein

RBP: RNA binding protein

RNA: Ribonucleic acid

SALI: Secretory autophagy during lysosome inhibition

SNAP29: Synaptosomal-associated protein 29

SNARE: Soluble N-ethylmaleimide-sensitive factor attachment protein receptor

SQSTM1: Sequestosome1

STX17: Syntaxin17

TDP-43: TARDBP

TFEB: Transcription Factor EB

TIAR: TIA1-related protein

TOLLIP: Toll-interacting protein

Ub: Ubiquitin

UBD: Ubiquitin-binding domain

UBQLN2: Ubiquilin2

ULK1/2: Unc-51-like kinase 1/2

UPS: Ubiquitin proteasome system

VAMP7/8: Vesicle-associated membrane protein 8 or 7

VCP: Valosin-containing protein

VPS34: Vacuolar protein sorting 34

WIPI: WD repeat domain phosphoinositide-interacting protein

Chapter 1: Introduction & Background

1.0 Autophagy

Autophagy is the process in which contents of the cell can be degraded by the lysosome via an autophagosome, a double membrane organelle[6]. Cargo can include and is not limited to damaged/misfolded proteins, bacteria, pathogens, viruses and organelles[6]. Autophagy allows for maintaining proteostasis and turnover of damaged/aggregated proteins in the cell to prevent accumulation, which leads to cell stress and damage[6].

Protein homeostasis is controlled by the ubiquitin proteasome system (UPS) and the autophagy system[7]. The UPS degrades targets through the ubiquitination of targeted substrates. The UPS system depends on the 26S proteasome and small ubiquitin molecules, which tag substrates for degradation by the protease complex.[8] It is generally thought that the UPS targets are soluble proteins, whereas autophagy can target insoluble proteins. The UPS system can degrade smaller misfolded proteins, whereas the autophagy system can degrade insoluble proteins or entire organelles.[7,8] The UPS system and autophagy are similar but have different mechanisms and specificity. Autophagy can degrade larger cellular cargo under stressful conditions, where the UPS system is more specific to maintaining protein quality and essential regulatory proteins. Both are essential for health and maintaining protein homeostasis in the cell.

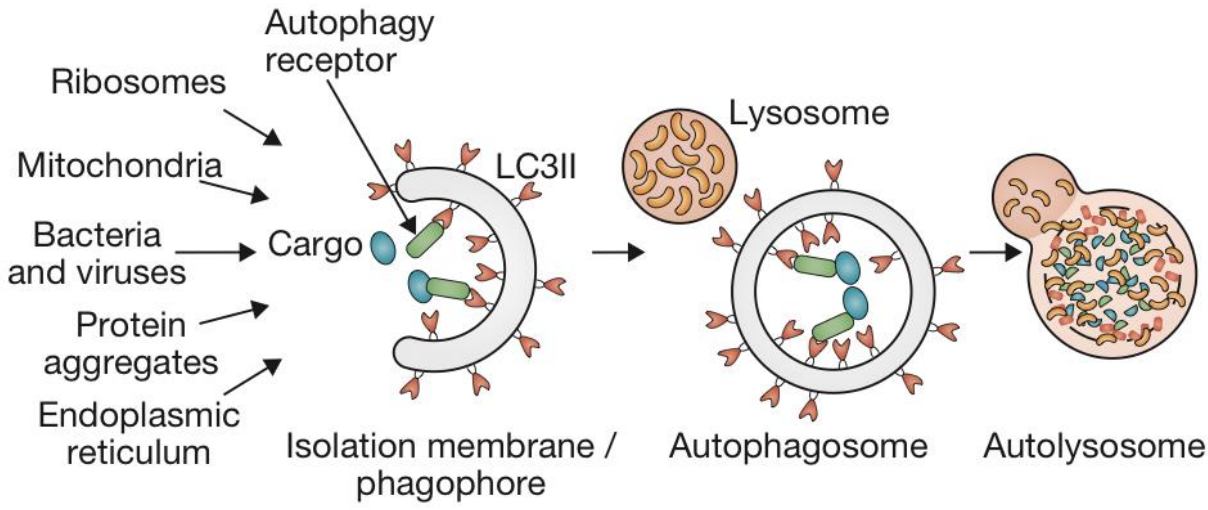

Figure 1. Graphic representation of macroautophagy. Image retrieved from Stolz A, Ernst A, Dikic I. Cargo recognition and trafficking in selective autophagy. *Nat Cell Biol*. 2014;16(6):495-501. doi:10.1038/ncb2979 Licence #: 5876671052259 Date: Sept, 26, 2024 License Content Publisher: Springer Nature Journal: Nature Cell Biology.

1.0.1 Forms of Autophagy:

There are forms of both selective and non-selective autophagy. Non-selective autophagy performs general bulk degradation during stress or nutrient deprived conditions to generate energy.[9] The engulfment of cargo during bulk degradation is not specific and is done to meet the cell's metabolic needs.[9] Selective autophagy is a more targeted degradation approach in which specific cargo, such as damaged organelles, aggregated proteins, etc., are engulfed. Autophagy contains three major types: macroautophagy, microautophagy and chaperone mediated autophagy (CMA).[10] All three complement one another by fusing with the lysosome for cargo degradation.[10] Microautophagy utilizes small invaginations of the lysosome to uptake cargo for degradation, whereas CMA uses a chaperone to individually transfer proteins into the lysosome directly.[6,10] The uptake of microautophagic cargo occurs directly at the lysosome as well. However, CMA utilizes chaperones to identify specific substrates, making it a precise process relative to macro and microautophagy. All CMA substrates have a specific pentapeptide motif known as the KFERQ motif.[6] These substrates are recognized by chaperones in the cytoplasm, such as heat shock 70 kDa protein 8 (HSPA8) and other co-chaperones.[6] Once the KFERQ motif containing protein is recognized and bound by a co-chaperone, it is translocated into the lysosome, in a process requiring Lamp2b.[6] Lamp2b facilitates the translocation of the CMA target/substrate across the membrane.[6]

1.1 Macroautophagy:

Macroautophagy (hereafter referred to as autophagy) targets cargo from the cytoplasm and sequesters it to the lysosome for degradation using a double lipid layered membrane to engulf/carry the cargo.[9] These double-membrane organelles are called autophagosomes. Their formation starts with an isolated double membrane called a phagophore, which is nucleated at a phagophore assembly site (PAS).[9] The phagophore is elongated and sealed around selected substrates, now termed autophagosomes. The autophagosome then fuses with the lysosome to form an autolysosome, where the autophagic substrates are degraded (Figure 1).[9] The phagophore nucleation is elicited in response to stimuli and signals such as oxidative stress, endoplasmic reticulum (ER) stress, protein aggregation or starvation. [9] The PAS can be at the ER, mitochondria-ER contact sites, recycling endosomes, Golgi, and plasma membrane, which are all suggested membrane sources for phagophores.[9]

1.1.1 Signal/regulation that triggers autophagy:

During stress or nutrient deprivation, mTOR is inhibited and autophagy is induced.[11] Stress stimuli can include ER stress, oxidative stress, hypoxia, or accumulation of misfolded proteins.[11] Basal-level autophagy is relatively low in normal conditions. [11,4] However, it is significantly induced by stress and cellular cues.[10] While autophagy can be activated by a variety of signals, it is inhibited by mTORC1, a negative regulator of unc-51-like kinase 1/2 (ULK1/2). [11,10] In nutrient-rich conditions, mTORC1 promotes anabolic processes such as cell growth and inhibits catabolic processes such as autophagy.[12,13] When ULK1 is phosphorylated by mTORC1, autophagy is repressed. [12,13] Autophagy is induced when ULK1 is dephosphorylated by component protein phosphatase 2A (PP2A) and dissociated from mTORC1. [12,13] ULK1 is also

activated by AMP-activated protein kinase (AMPK) via direct phosphorylation, which, in turn, induces autophagy. [12,13] Conversely, AMPK, which responds to energy stress, can negatively regulate mTORC1.[13] For example, when ATP levels are depleted during oxidative stress, AMPK is activated, suppressing mTORC1 and phosphorylating ULK1, thereby inducing autophagy.[14]

Another important regulator of the autophagy pathway is Transcription Factor EB (TFEB), which is responsible for the transcription of genes whose promoter contains a Coordinated Lysosomal Expression and Regulation (CLEAR) motif.[15] This helps induce the formation of phagophores, fusion to the lysosome, and lysosomal degradation.[16] Overexpression of TFEB increases lysosomal biogenesis and therefore degradation of autophagy substrates.[16] Furthermore, it has been shown that TFEB and mTORC1 co-localize and inhibition of mTORC1 activates TFEB and nuclear translocation of TFEB.[17] mTORC1 phosphorylates TFEB, which forces it to remain inactive and prevents its translocation into the nucleus.[17] During stress, mTORC1 is inactive and unphosphorylated TFEB accumulates in the nucleus.[17] In turn, mTORC1 can prevent the nuclear translocation of TFEB, suppressing the transcription of autophagic and lysosomal genes.[14]

1.1.2 Initiation

Autophagy is initiated by the ULK complex, which consists of ULK1/2, RB1-inducible coiled-coil protein (RB1CC1), also known as FAK family kinase-interacting protein of 200 kDa (FIP200), as well as ATG13 and ATG101.[6,11,14] As mentioned, when ULK1 is activated by AMPK or following the inactivation of mTORC1, it phosphorylates its substrates ATG13, ATG101 and FIP200.[18] The ULK1 complex is one of the earliest factors involved in phagophore formation for membrane recruitment. [19]Another crucial complex for autophagosome

initiation/formation is the PI3KC3 complex otherwise known as the Beclin1 complex, which consists of Beclin1, vacuolar protein sorting 34 (VPS34) and ATG14. The Beclin1 complex produces phosphatidylinositol 3-phosphate (PIP), by converting PI to PI-3-phosphate (PI3P).[19] PI3P is responsible for recruiting downstream autophagy proteins to the forming phagophore.[19] WD repeat domain phosphoinositide-interacting proteins (WIPI) sense PI3P during phagophore nucleation and interact directly with the forming membrane, which is important for recruiting downstream ATG proteins.[19] Downstream is the ATG12 complex, which consists of the ATG5-ATG12 conjugate and ATG16L1. ATG5-ATG12 facilitates the transfer of the LC3/ATG8 homologue to the lipid phosphatidylethanolamine (PE). While Atg16L1 determines the site of this conjugation by targeting the ATG5-ATG12 conjugate.[19,20] The ATG12-ATG5-ATG16L1 complex acts as a scaffold on the phagophore at the PAS.

1.1.3 Expansion and Elongation

Once the ATG16L1 complex is recruited to the PAS, it mediates the lipidation of ATG8, otherwise known as LC3. There are two forms of LC3, LC3-I and LC3-II. LC3-I is the unconjugated version, and LC3-II is the lipid-conjugated version. Before LC3 can be conjugated to lipid, its C-terminal must be cleaved by ATG4 to expose a glycine residue. From this point, ATG7 acts as an E1 enzyme, activating LC3, and ATG3 acts as an E2 enzyme that helps the lipidation process of LC3. The ATG16L1 complex transfers LC3-I from ATG3 to the lipid PE on the phagophore membrane.[21] After the lipidation of the LC3 protein to the autophagosomal membrane, other ATG proteins detach from the membrane; however, the LC3-II proteins remain attached/conjugated. Lipidated LC3 remains on the inside of the autophagosome, aiding in elongation and formation of the autophagosome. [21] ATG9 aids in expanding phagophores and

delivering phospholipids to the growing membrane.[22] In addition, LC3 homologues act as the cargo docking site for autophagic substrates during selective autophagy. [21] Autophagy receptors recruiting cargo will bind LC3-II via its LC3-interacting region (LIR) motif, anchoring cargoes to the forming autophagosome. [21] The autophagy receptors recognize cargo that needs to be delivered to an autophagosome. If phagophore expansion needs to be limited, ATG4 can deconjugate LC3s from the lipid PE outside of the autophagosome. [21] In addition, targeting LC3 homologues to an autophagic membrane can be regulated by post-translational modifications (PTM). Some examples include negative regulation by phosphorylation from protein kinase A (PKA). [23] LC3s are also thought to be implicated in the sealing of the phagophore.

1.1.4 Maturation and Fusion to Lysosome

After phagophore expansion, the phagophore is sealed to form an autophagosome. Endosomal sorting complex required for transport (ESCRT), ATG proteins, and SNAREs mediate the closer and fusion of the autophagosome to the lysosome.[24,25] As the autophagosome matures, ATG proteins, including LC3 proteins, begin to clear from the outer, cytosol-facing membrane and proteins involved in lysosomal delivery/fusion come into action. These include soluble N-ethylmaleimide-sensitive factor attachment protein receptor (SNARE) proteins such as syntaxin17 (STX17) and synaptosomal-associated protein 29 (SNAP29) which are on the autophagosome.[9] STX17 is located on the autophagosome membrane. Vesicle-associated membrane protein 8 or 7 (VAMP8 or VAMP7) and homotypic fusion and protein sorting (HOPS) complex are located on the lysosome, helping to tether the lysosome to the autophagosome membrane.[9] SNAP29 is a bride between STX17 and VAMP8, allowing the autophagosome to fuse with the lysosome.[9] In addition to this, LC3 themselves can drive the

maturation of the autophagosome by linking the autophagosome to kinesins and motor proteins using adaptors such as FYVE and coiled-coil domain-containing protein 1(FYCO1). [9] The LC3 homologues also recruit the HOPS complex through pleckstrin homology domain-containing family M member 1 (PLEKHM1). Genetic deletion of PLEKHM1 inhibits autophagosome-lysosome fusion. [26] PLEKHM1 bridges the autophagosome and lysosome by binding RAB7 and HOPS/SNARE complexes on the lysosome and autophagosomal surface protein LC3.[26] Lysosomal hydrolases are responsible for digesting and degrading the autophagic material.[27] These enzymes are relatively inactive at the pH of the cytosol but are activated by the acidic pH in the lysosome.[27] The V_1V_0-ATPAase acidifies the lysosome by pumping protons into the lysosome.[27] The lysosome can also be chemically inhibited with the treatment of BafilomycinA1, which inhibits V-ATPase.[27]

1.2 LC3 homologues

The mammalian ATG8 homologues are essential in all parts of autophagosome biogenesis, as well as mediating the selectivity of autophagy.[28,29] In mammalian cells, there are six ATG8 homologues total and two subfamilies: Microtubule-associated proteins 1A/1B light chain 3 (MAP1LC3/LC3) and Gamma-aminobutyric acid receptor protein (GABARAP). There are 3 LC3s total: *MAP1LC3A*/LC3A, *MAP1LC3B*/LC3B, *MAP1LC3C*/LC3C and 3 GABARAPS: *GABARAP*, *GABARAPL1*, *GABARAPL2*. The 6 LC3 homologues share a similar molecular weight between 16-18 kDa.[30,31] Overall, the six homologues have high structure similarity, although substantial sequence differences exist amongst the subfamilies and individual homologues.[32] They each have different expression activity and levels, for example, LC3C is primarily expressed in the lung, while GABARAPs are expressed in the central nervous

system.[33] All of the six homologues conjugate to the lipid PE via the C-terminus, and each of them has a conserved ubiquitin fold with slightly varying N-terminal helices.[34,35] The varying N helices support the notion that the individual LC3 proteins have different selective interactions based on their N-terminus.[34,36] Mutations in LC3 homologues, specifically on the C-terminus, are associated with the accumulation of that homologue in the cell and possibly inhibited proteolytic cleavage.[37,38]

However, PTMs of LC3 homologues can also influence their affinity for selective interactions. Particularly, phosphorylation of LC3/GABARAPs influences selective autophagy. For example, phosphorylation of LC3C and GABARAPL2 by TBK1 prevents binding to ATG4, possibly a mechanism to prevent pre-mature de-lipidation from the membrane.[39] Another proposed PTM is the acetylation of nuclear LC3 by SIRT1, which then promotes translocation to the cytoplasm where LC3 interacts with autophagic machinery, promoting ATG7-LC3 binding.[40] Conversely, ubiquitination of LC3B by UBA6 and BIRC6, promotes proteasomal degradation of LC3B, negatively regulating autophagy. [41] All binding partners of LC3 have an LIR motif and are involved in many processes, such as autophagosome initiation, elongation, vesicle trafficking, lysosomal fusion and selective autophagy, amongst other functions.[34] The exact molecular details and factors for how these homologues differ from one another are still unclear and is an ongoing area of research.[34] Majority of LC3 research and understanding stems from the LC3B homologue, which may not encompass the behaviour of all 6. Both subfamilies are involved in autophagosome biogenesis, although some research has shown that the GABARAP subfamily is involved in the later stage of autophagosome sealing.[34] The LC3 subfamily acts more upstream for phagophore elongation.[29] However, both promote membrane fusion processes through their N-terminus. [42] Lipidation of LC3 homologues to lipid PE, on their C-terminal, is

important for phagophore elongation and autophagosome-lysosome fusion and is reliant on cleavage from ATG4.[43,44] Cells that are deficient for LC3 show poor autophagosome formation but are unable to fuse to the lysosome successfully.[43]

Specifically, in selective autophagy, LC3 homologues mediate the engulfment of cargo into the autophagosome by binding to autophagy receptors via the LIR motif. The binding of Sequestosome1, otherwise known as p62, directly to LC3A and B, as well as the GABARAP subfamily, facilitates the degradation of p62 positive cytoplasmic aggregates.[45] Autophagy receptor NBR1 has been shown to bind to LC3B, GABARAP and GABARAPL2 for degrading p62 positive bodies in the cytoplasm.[46] Similarly, specific binding of NDP52 to LC3C is required for autophagic degradation of bacteria such as *Salmonella*.[47] Although there are a lot of similarities and overlapping functions between the LC3 homologues, ongoing research demonstrates functional differences between the two subfamilies and individual homologues.[42–44,47] Different LIR containing proteins show some selectivity for specific LC3 homologues, and the various homologues display overlapping but unique interactomes.[48–50] Proteomic data of the various LC3 homologues has demonstrated that not all identified autophagy receptors interact with each LC3 homologue, suggesting that LC3s may also have some specificity in the type of autophagy they are selective for. [49,51,52] However, LC3 interactomes go beyond autophagy related functions and are linked to other functions, such as vesicle trafficking.[53]

1.3 Role of Autophagy Receptors in Selective Autophagy:

Autophagy receptors bind cargo for autophagic degradation and bring them to LC3-II, located on the forming autophagosome. Autophagy receptors contain a ubiquitin-binding domain (UBD) and an LIR motif, which allows for docking to LC3-II.[45] Autophagy receptors are also

degraded in the lysosome as they dock on the inner membrane of the growing autophagophore on LC3-II. Supposedly, p62, OPTN, and NDP52 interact with the ATG12-ATG5-ATG16L1 complex to help mediate binding to the LIR sites. [54] Some types of selective autophagy include reticulophagy, which is the degradation of portions of the ER, and ribophagy, which is the targeted degradation of ribosomes.[32,55] Aggrephagy, which includes the targeted degradation of protein aggregates.[32,55] Lysophagy is the selective degradation of the lysosome, and granulophagy is the targeted degradation of granules in the cytoplasm. [32,55] Some autophagy receptors for aggrephagy include sequestosome1/p62, NBR1, OPTN, toll-interacting protein (TOLLIP) and others.[32,56] Other examples include Lipophagy, the degradation of lipids, or xenopohagy, which includes the removal of bacteria or virions in the cytoplasm. Many other forms of selective autophagy exist, based on the cargo targeted for autophagic degradation.[32] However, some studies have displayed that specific LC3s are involved in certain types of selective autophagy and not others, such as selective degradation of mitochondrial protein metaxin-1 (MTX1) dependent on LC3C.[51] Only knockdown of LC3C led to accumulated MTX1 in the cell.[51] This selectivity is influenced by the autophagy receptors the LC3 homologue preferentially interacts with via the LIR motif.[57] The LIR motif on autophagy receptors ensures binding ability to an LC3/GABARAP homologue on a hydrophobic pocket. However, differences in structure and charge of these hydrophobic pockets influence the binding affinity to certain LIR motifs, thereby influencing the affinity for certain receptors and cargo. [57]

1.3.1 Cargo Recognition and Binding

Ubiquitin, which has a vital role in the UPS system for marking proteins for degradation, is also crucial in autophagy.[58] Autophagy receptors bind through their UBD to ubiquitin chains on intracellular cargo. For example, NBR1 can recognize cargo ubiquitin-dependently, binding

to ubiquitinated protein aggregates through a UBD domain on its C-terminus. [59] Similarly, p62 binds to ubiquitinated cargo to facilitate the degradation of protein aggregates and links them to autophagy by binding to LC3 through its LIR motif. Mutations in the UBD domain of p62 have been linked to Paget's disease and associated with increased inclusion bodies. [60] Furthermore, TDP-43 aggregates have displayed ubiquitin chains, markers for ubiquitin-dependent degradation systems.[61,62] Soluble TDP-43 is degraded by the UPS system, and insoluble/aggregated forms are directed to the autophagy system, suggesting a Ub-dependent autophagy mechanism for its clearance.[61,62] Another receptor, optineurin (OPTN), is shown to bind ubiquitinated mitochondrial membranes through its UBD and facilitate mitophagy by interacting with LC3 through its LIR domain.[63] However, some autophagic cargo are also selectively degraded through ubiquitin-independent mechanisms by binding Ub-like tagged cargos, as reviewed by Khaminets et al., 2016.[58] Such as Ub-independent mitophagy through autophagy receptor NIX. NIX, which is shown to interact with GABARAPL1 through its LIR motif and binds to mitochondria through a second LIR motif.[64] Although p62 is associated with Ub-dependent autophagy, it can also contribute to Ub-independent degradation of stress granules. P62 and C9ORF72 can recognize arginine-methylated Fused in sarcoma (FUS) via association with SMN to facilitate autophagic degradation of stress granules.[65] Overall, the mechanisms that mediate selective autophagy are diverse and complex.

1.4 Autophagy in Disease:

Many defects in autophagy are linked to many neurodegenerative diseases, and disruption to proteostasis is a pathological driver in many diseases. Particularly, many neurodegenerative diseases, such as Alzheimer's disease (AD), Huntington's disease (HD) and Amyotrophic Lateral

Sclerosis (ALS), are driven by proteinopathies and neuronal toxicity, as reviewed in Rubinzstein et al.,.[66] The pathogenic correlation of aggregates is debatable; however, we often see improvement in symptoms when reducing aggregates and worsening when they accumulate. Therefore, autophagic dysregulation and machinery deficits further worsen proteostasis and cellular health.[66] Increasing or promoting autophagy has been shown to improve health and suppress protein aggregation or accumulation of misfolded and pathological proteins. Impairment of autophagy has been associated with diseases and accelerating neurodegenerative diseases. Impairment of autophagy leads to an increase in cytosolic aggregated insoluble proteins. For example, a study using mice with an ATG16L1 deletion, which is necessary for PE conjugation in autophagy, led to impaired LC3-II, demonstrated increased neuroinflammation and amyloid beta (AB) aggregates[67] Furthermore, a linker compound that bound mutant Huntingtin and LC3 together, resulted in lower levels of polyQ HTT and ATAXIN3 in HEK cells and also rescued HTT toxicity in neuronal cells from Huntington disease (HD) patients.[68] In addition, using a chemical compound that stimulates autophagy decreased TDP-43 inclusions and reduced cytoplasmic mislocalization.[69] Autophagy induction was verified by enhanced LC3-II/LC3-I ratios, in primary rodent cortical neurons.[69] Reduced TDP-43 levels were correlated to autophagy induction. Autophagy receptors bind to aggregated proteins for autophagic degradation, which is important in neurodegenerative diseases.[45,59,66] Autophagy receptors such as p62 and OPTN have been spotted in protein aggregates of numerous neurodegenerative diseases, as reviewed in Rubinzstein et al., 2015. Both p62 and LC3 were co-localized around mutant huntingtin in HeLa cells, while mutant p62 increased cell death.[70] Overall, the paper suggested that p62 may work to eliminate mutant huntingtin by promoting autophagy through

recruitment of LC3, and lack of p62 in the presence of protein aggregates promoted further pathogenesis.[70]

In ALS and Frontotemporal Dementia (FTD), defects in autophagy receptors are linked to the disease. Mutations in genes encoding *OPTN* and *SQSTM1/p62* are tightly associated with ALS. Mutations in the UBD and LIR domains of *OPTN* cause disrupted autophagosome recruitment to damaged mitochondria, interrupting mitophagy.[71] This highlights a possible mechanism in ALS, which leads to the accumulation of damaged mitochondria and cell death.[71] Similarly, patients with p62 mutations displayed an accumulation of p62 positive inclusions and increased TDP-43 levels in the spinal cord, suggesting p62 mutations participated in TDP-43 proteinopathies.[72] TDP-43 pathologies are present in roughly 97% of ALS cases, however, not all TDP-43 dysfunction is associated with autophagy receptor mutations.[1] Only 2-5% of ALS patients carry *p62* mutations, and even fewer carry *OPTN* mutations.[73] In the case of ALS, there are many strong links between autophagic dysfunction and the pathogenesis of the disease. A study using $SOD1^{G93A1}$ mice demonstrated autophagosomal uptake in the axon; however, autophagic flux did not increase, showing that SOD1 mutations may limit autophagic degradation in response to stress.[74]

1.5 ALS

Amyotrophic Lateral Sclerosis (ALS) is the third most common neurodegenerative disease, characterized by death of upper and lower motor neurons.[75] Disease onset varies, as does preferential degeneration of either upper or lower motor neuron.[75] Phenotypically, motor dysfunction manifests in loss of mobility and coordination. At onset, muscle weakness is usually first seen in either limb or bulbar muscles.[76] Typically, upper motor neurons in the primary

cortex and brainstem are some of the first to begin degenerating in bulbar-onset ALS.[76] Impaired eye movement, facial movement, or swallowing are often observed.[76] Bulbar onset consists of muscle weakness related to breathing and swallowing, and limb onset appears in either the upper or lower limb.[76] Additionally, cognitive and behavioural impairment is a common phenotype.[75] Typically, prognosis after diagnosis ranges from three to five years, with an eight-year survival rate as low as 10%. Most ALS cases are sporadic, whereas very few are familial.[75] Few treatments are available for ALS, and even then, they mainly target symptom management.[75] For example, edavarone and riluzole can slow early disease progression. ALS is characterized by RNA binding proteins (RBPs), including but not limited to TDP-43.

1.5.1 Mutations in ALS

Most disease related mutations in ALS form aggregates when protein quality systems such as autophagy are impaired. The disease is also primarily characterized by mutations in RNA binding proteins such as TDP-43, FUS, C9ORF72, hnRNAPA2BP1and ATAXIN-2.[3] Mutations in TARDBP lead to increased baseline cytoplasmic levels of TDP-43.[1] Over 50 mutations of TDP-43 have been linked to ALS, as reviewed in Suk et al., 2020. Almost all TDP-43 mutations are in its C-terminal domain, which is aggregation prone due to its unstructured nature and low complexity.[1] In many ALS causing mutations of TDP-43, the protein displays altered nucleocytoplasmic distribution, with increased cytoplasmic levels and decreased nuclear levels.[1] TDP-43 mis-localization displays gain and loss of function effects and may be a key mechanism of ALS pathogenesis. Mutations in *FUS* are associated with early-onset ALS and are responsible for approximately 4% of familial ALS and less than 1% of sporadic ALS. FUS is an RNA-binding protein (RBP) primarily localized in the nucleus.[77] Its exact cellular function is unknown

but involves processes such as DNA repair, transcription, mRNA transport and splicing. Abnormal aggregation of FUS is linked to ALS, as well as variants of *FUS*.[77] Multiple mutations in FUS have been associated with increased neuronal and glial cytoplasmic inclusions in ALS patients.[77] Furthermore, FUS mutations display altered RNA and protein homeostasis, increased aggregation and altered subcellular localization.[77] The ribonucleoprotein hnRNPA1 and hnRNPA2B1 regulate alternative splicing and transport of pre-mRNA transcripts. Mutations in *hnRNPA1* and *hnRNPA2B1* also lead to stress granule formation.[3] A prevalent mutation in ALS is a repeat expansion in *C9orf72*, associated with abnormal TDP-43 aggregation and is thought to act upstream in TDP-43 proteinopathy. The precise function of C9ORF72 is unknown, however, it is believed to activate a Rab guanosine triphosphatases (Rab GTPase), and accumulating research has demonstrated links to autophagy and stress granule formation.[65] Our lab demonstrated a role in which p62 and C9ORF72, alongside SMN, are involved in the autophagic degradation of stress granules. Cells with C9ORF72 expansion demonstrate a lack of p62 dependent stress granule degradation.[65] The recent work regarding C9ORF72 suggests a possible ALS mechanism in which C9ORF72 prevents autophagic elimination of stress granule components and promotes stress granule formation. Polyglutamine (polyQ) expansion in the cytoplasmic RNA binding protein ATAXIN2 has also been linked to ALS and is a component of stress granules. [78] As reviewed by Daisuke et al., 2017, polyQ ATAXIN2 can modify the subcellular distribution of TDP-43. [78] Mutations in many ALS linked RNA binding proteins promote stress granule formation, which can cause dysfunctional RNA quality control. [78] Another similar pathological theme in ALS is the mislocalization of RNA binding proteins in the cytoplasm and the formation of cytoplasmic aggregates.[78] Furthermore, mutations in several autophagy related genes such as *SQTSM1/p62*, *Ubiquilin2* (UBQLN2), *Valosin containing*

protein (VCP), and *OPTN* are associated with ALS. [78-80] Mutations in these genes often lead to impaired autophagy and the accumulation of damaged organelles and proteins.[79–82] Many of them have been spotted in pathological inclusion bodies present in CNS tissue from ALS patients. [78] Both p62 and OPTN are known autophagy receptors that interact with LC3 to promote the degradation of cytoplasmic cargo. TBK1 enhances binding affinity of p62 and OPTN to LC3 through phosphorylation.[78] Defects of TBK1 lead to decreased clearance of aggregated proteins.[78] Similarly, mutations in UBQLN2 have been associated with interrupted protein degradation. Likewise, mutations in VCP, which is involved in RNA and ubiquitin dependent autophagy, are linked to persistency/altered dynamics of stress granules. [78]Altogether, these mutations highlight a mechanism for the pathogenesis of ALS, in which RNA and protein quality control are dysregulated.

1.5.2 sALS

The majority of ALS cases occur sporadically. A prominent feature of some sporadic ALS cases is the presence of RNA binding protein abnormalities such as TDP-43, FUS, HNRNPA1/HNRNPA2B1 and other proteins. The abnormal cytoplasmic accumulation of RBPs is also present in sALS. [78] During normal stress response, some of these RBPs, such as FUS and TDP-43, are recruited to stress granules, however, during chronic stress, their deposition can be prolonged, leading to persistent inclusions.[83] Similar to fALS, disrupted autophagy and protein quality control are common themes in sALS. Pathological inclusions in motor neurons from sALS patients have demonstrated LC3 and P62, which suggested interrupted autophagy in sALS.[84] The common connection between RBPs and autophagy is their tendency to aggregate and burden the autophagic system. The sequestration of autophagy receptor p62 into TDP-43

aggregates, disrupts autophagy and promotes the accumulation of toxic proteins in the cytoplasm.[1] Conversely, decreased autophagic function is associated with TDP-43 mislocalization and aggregation, as reviewed by Suk et al., 2020.

1.5.3 TDP-43

TDP-43 is a major player and influence in the pathogenesis of ALS, present in both sALS and fALS, observed in 97% of ALS patients. [85] TAR-DNA binding protein 43 (TDP-43) is predominantly localized to the nucleus, but in ALS, it is commonly found in cytoplasmic inclusion bodies (Figure 2.).[85] TDP-43 is an RNA binding protein that is involved in tasks such as pre-mRNA splicing mRNA transport and is involved in genes that regulate neuronal development. Genetic deletion of *TDP-43* is embryonic lethal, and overexpression can cause cell death in animal/cell models .[86,87] Typically when the nuclear localization signal is not properly functioning, TDP-43 protein mislocalizes to the cytoplasm, displaying a loss of nuclear function, and ends up accumulating in the cytoplasm where it can begin to aggregate, and may exert gain of toxic function.[85] Mislocalization of TDP- 43 is thought to induce toxicity through both gain and loss of function mechanisms. When nuclear levels of TDP-43 decrease, this leads to a loss of function in TDP-43 splicing activity.[85] Mis-localization of TDP-43 from the nucleus to the cytoplasm is found in both sporadic and familial types of ALS.[85]The N-terminal of TDP-43 contains a nuclear export signal (NES) and a nuclear localization signal (NLS) sequence. These domains are essential for successful shuttling between the nucleus and cytoplasm. The C-terminal domain, often referred to as the low-complexity domain, is a glycine-rich region with an unstructured nature, which is considered important for TDP-43 toxicity in disease. Motor neurons exhibit TDP-43 inclusions, along with neurons in the brain stem, spinal cord, glial, and

cortex.[85] It is still unclear what causes cytoplasmic TDP-43 to adopt insoluble forms.[85] The neuronal dysfunction seen in ALS is brought on by the accumulation of cytoplasmic TDP-43 and by depletion in the nucleus.[85] Although mutations of TDP-43 can cause ALS, abnormal levels or localization of wild-type TDP-43 can cause ALS-like symptoms in mice as well. It is not clear how mislocalization and aggregation of TDP-43 are linked, however, some hypothesize that mislocalization acts upstream, promoting the aggregation and misfolding of TDP-43 in the cytoplasm.[1] PTMs of TDP-43 also play a role in its subcellular localization and functionality. Some examples of TDP-43 PTMs are phosphorylation, ubiquitination, and poly-ubiquitination.[88] Accumulation of these PTMs is an indicator of aggregated TDP-43, specifically phosphorylation of TDP-43.[1,88]

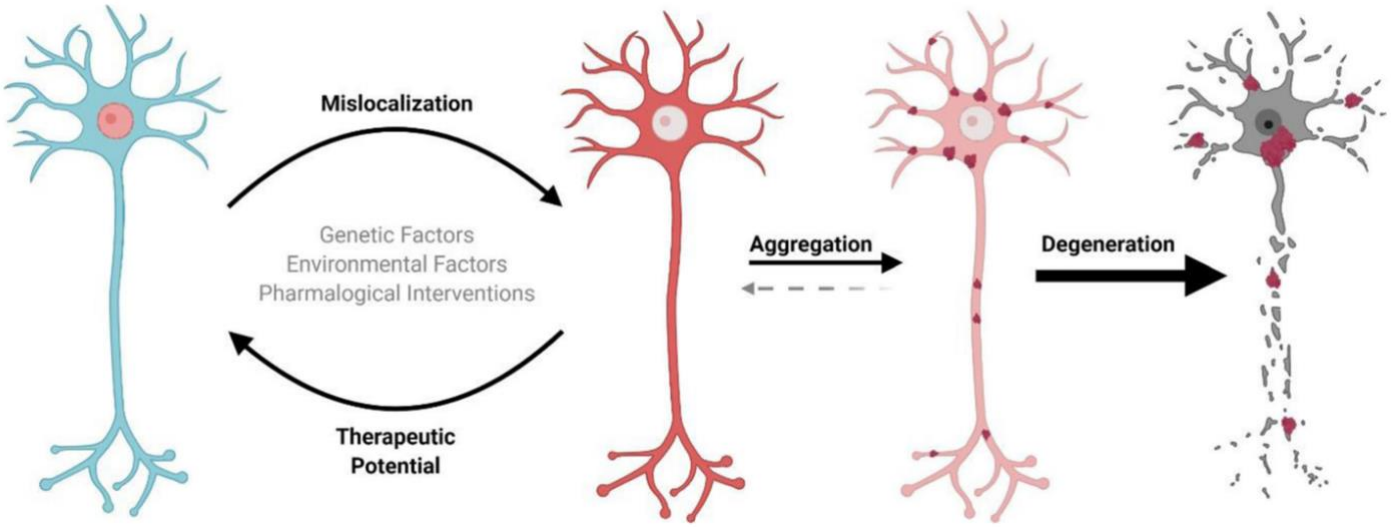

Figure 2. Schematic representation of aggregation and degeneration process in neurons from ALS. Red dots symbolize TDP-43 mislocalizing from the nucleus and aggregating. Retrieved from Suk TR, Rousseaux MWC. The role of TDP-43 mislocalization in amyotrophic lateral sclerosis. *Mol Neurodegener*. 2020;15(1). doi:10.1186/s13024-020-00397-1 https://creativecommons.org/licenses/by/4.0/ No changes were made to the graphic.

1.5.4 Autophagy and TDP-43

Typically, the autophagy system would target TDP-43 inclusions for degradation. In ALS, the machinery is not functioning well or efficiently[89]. This causes an accumulation of the

inclusion bodies and aggregates.[69,90] The number of inclusion bodies correlates with neuronal loss, therefore, impaired clearance of aggregated TDP-43 is proposed to increase neuronal death. TDP-43 positive inclusions are seen in ALS, and aggregated TDP-43 is supposedly degraded by autophagy. Autophagy induction improves TDP-43 turnover and also prevents cell death from aggregated TDP-43. This has been demonstrated in both cell and mouse models in a study using TDP-43^{A315T} mice, inducing autophagy reduced cytoplasmic TDP-43 related proteinopathy in the spinal cord and brain of mice expressing mutant human TDP-43.[91] The co-localization of TDP-43 and p62, which binds ubiquitinated cargo, further supports the selective autophagic degradation of aggregated TDP-43. [92]

1.5.5 Stress Granules

Many ALS related proteins, including TDP-43, interact with cytoplasmic stress granules and have been found to co-localize with stress granules.[2,93] Stress granules are non-membrane-bound cytoplasmic condensates that contain RNA binding proteins (RBPs), mRNAs, and ribosomal subunits. Common stress granule proteins include TIA1-related protein (TIAR) and Ras GTPase-activating binding protein (G3BP1/G3BP2).[93] Stress granules play an important role in the cellular response to stress. In response to cellular stress, including environmental or chemical triggers such as sodium arsenite[94], stress granules form to pause translation initiation. Not only does this protect mRNA from the stressor, but it helps prioritize ATP consumption during stress. Stress granule dynamics is a complex process that varies according to the exact stressor. Generally, upon exposure to stress, translation halts. Core stress granule proteins, such as GTPase-activating binding protein (G3BP), initiate formation of the stress granule shell. Other RBPs, such as TDP-43, are then recruited to the shell of the granule.[94] TDP-43 assists in liquid-

liquid-phase separation (LLPS), which allows granule components to transition from a bulk soluble state to concentrated droplets, and thus plays a part in both assembly and disassembly. [95] When the stressful stimulus is removed, stress granule disassembly allows resumption of translation, though disassembly time does vary depending on the nature of the stressor.[95] Stress granules can persist in the cytoplasm under chronic stress, amongst other things. When this occurs, autophagy offers a method of stress granule clearance. In fact, evidence has demonstrated that a significant portion of stress granules relies on autophagy for degradation.[96,97] Inhibition of valosin-containing protein (VCP), an AAA-ATPase that promotes autophay, stalls stress granule disassembly. Pathogenic mutations in VCP have also displayed reduced stress granule clearance, which is linked to ALS, a disease often characterized by accumulated stress granules and aggregates. [96,97] Furthermore, our lab has demonstrated autophagic elimination of stress granules by p62, suggesting an implication of mutant p62 in ALS. Overall, accumulating evidence has demonstrated that inhibited autophagy supports ALS pathology. When stress granules do not disassemble and are persistent, this can lead to aggregation, further accelerating cellular stress and toxicity to the cell.

1.5.6 ALS and stress granules

There are altered stress granule dynamics in ALS, leading to persistent granules and aggregation. TDP-43 is recruited to stress granules for stalled translation, although under prolonged stress, this can lead to persistent aggregation.[98,99] Localization of TDP-43 to stress granules is mediated by its C-terminal, also known as the low complexity domain, which is aggregate-prone.[86]Cells treated with siRNA targeting TDP-43 displayed interrupted SG formation and reduced assembly.[100] However, neuronal models displayed accelerated SG disassembly when TDP-43 levels were depleted.[100] Conversely, mutant forms of TDP-43 have

been associated with stress granule persistency and failed disassembly. When important RBPs, such as TDP-43, are sequestered into granules, these proteins' functions are interrupted, leading to downstream consequences on mRNA metabolism and transcriptional regulation.[3,101] When disassembly is impaired stress granules persist and can transition from a liquid to a solid state. [101] This dynamic promotes inclusions and possibly promotes TDP-43 cytoplasmic inclusions. Therapeutically targeting autophagy may be able to rebalance proteostasis in these pathological dynamics.

1.6 Need of Therapeutics Harnessing Autophagy in ALS

Impaired autophagy and interrupted protein quality control are hallmarks of many neurodegenerative diseases and highly correlate with ALS pathogenesis. This makes autophagy an attractive therapeutic target. Since ALS is currently an incurable disease, with few medications being available, that mainly target the delay of symptom onset, there is a dire need for a therapeutic to target TDP-43 pathology and repair autophagy machinery. So far, many autophagy targeting strategies and modifiers have shown great promise concerning ALS. Rapamycin delivery to an ALS mice model shows decreased motor impairments, reducing TDP-43 positive inclusions.[102] Similarly, using a mutant FUS neuronal model under oxidative stress, treatment with the mTOR chemical inhibitor rapamycin reduced cell death and decreased stress granules.[103]

1.6.1 New Avenues for Autophagy based Therapeutics

Many new therapeutics are targeting the protein degradation pathways using smaller pharmacological agents.[104] One example is proteolysis-targeting chimeras (PROTACs);

however, one limitation of this system is its compatibility with certain neurodegenerative diseases as it relies on the UPS system. This requires smaller proteins that can fit through the small pores of the proteasome rather than the larger aggregated proteins we see in diseases like ALS.[105] This makes targeting chimeras that rely on the autophagy-lysosome system much more attractive for neurodegenerative diseases. Another system is autophagy targeting chimeras (AUTACs,) which utilize the selective autophagy pathway.[106] AUTAC uses a degradation tag, ligand and the linker compound to accelerate ubiquitination and enhance selective autophagy.[106] Similarly, this system can target larger damaged proteins and organelles. Lastly, another early therapeutic mechanism is autophagosome-tethering compounds (ATTECs). In investigating Huntington's disease, ATTEC was a linker compound used to tether mutant Huntingtin to LC3 to facilitate the recruitment of mutant HTT into autophagosomes. Without targeting wild type Huntington. The linker compound showed depleted expanded polyQ proteins and did not influence overall autophagy function. [107]

1.7 Other applications of autophagic machinery and LC3 Homologues

LC3 homologues are essential players in the autophagy pathway, although some papers have shown that some autophagic machinery may be involved in extracellular vesicle secretion and loading.[53] A paper identified some components of the LC3 conjugation system to be involved in specifying the secretion of RBPs into extracellular vesicles (EVs), which they called LC3-dependent extracellular vesicle loading and secretion (LDELS). This proposed pathway would involve the components of the LC3 lipidation/conjugation machinery but not all of the ATG proteins.[4] Proteomic studies revealed some overlap between the LC3 secretome and

proteins detected in EVs, including LC3-II. The study also detected many RNA and stress granule related proteins as LDELS targets. The proposed mechanism is a pool of LC3s at the multi-vesicular body (MVB) to capture and package RBPs into intra-luminal vesicles (ILVs), which are then released as small EVs.[4] Autophagy is responsible for the clearance of stress granules, however, this proposed mechanism provides more insight into how autophagy machinery might interact with these granules.[97]

However, one caveat to this study is the use of ATG7 and ATG14 knockout HEK293T models, still leaving room to question whether LC3 is genuinely involved. A similar proposed pathway involving autophagic machinery with EVs includes the secretion of autophagy cargo receptors outside the cell when autophagosome maturation or lysosomal function is impaired.[108] This proposed process is termed secretory autophagy during lysosome inhibition (SALI) (Figure.3). They also propose that machinery similar to the LDELS pathway, such as ATG7, ATG12, ATG2, ATG14, and FIP200, are necessary for SALI.[5] They suggest that the co-localization of LC3B and p62 is crucial for this process in cells experiencing lysosomal inhibition and using RAB27A for extracellular release. [5]

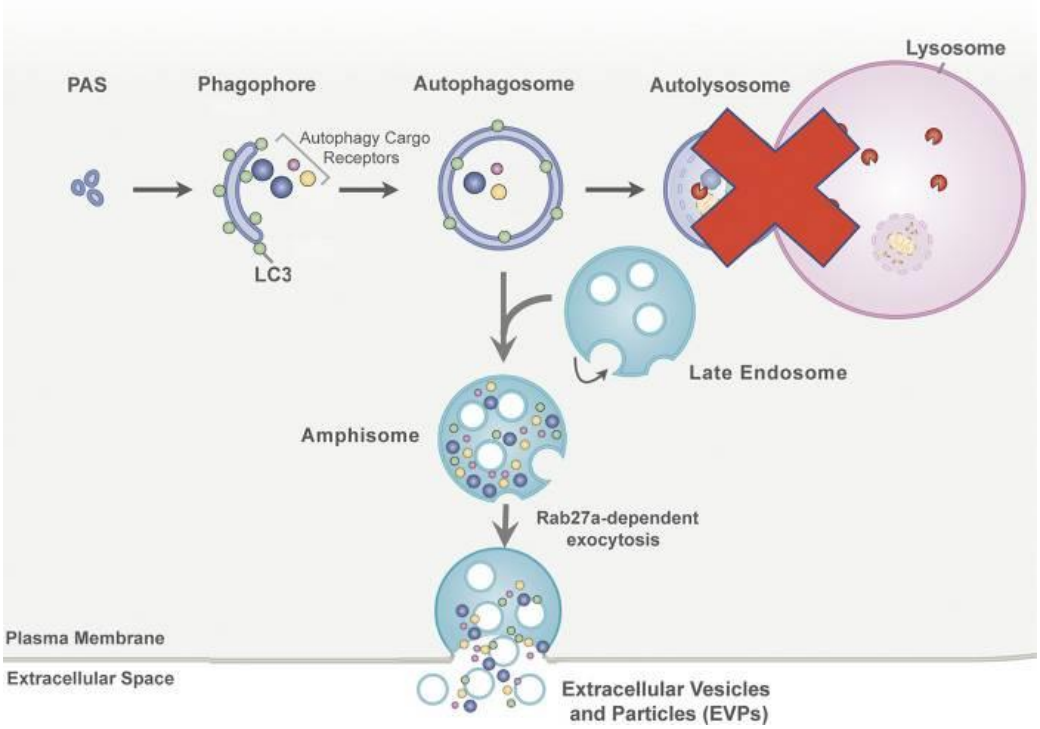

Figure 3. Schematic representation of SALI pathway. Retrieved from
Solvik TA, Nguyen TA, Lin YHT, et al. Secretory autophagy maintains proteostasis upon lysosome inhibition. *Journal of Cell Biology*. 2022;221(6). doi:10.1083/jcb.202110151
https://creativecommons.org/licenses/by/4.0/ no changes were made

1.7. 1 Extracellular Vesicles

Extracellular vesicles (EVs) are small lipid-bound vesicles secreted in cells that are released into extracellular space. [109] Cargo in EVs can consist of nucleic acids, proteins and lipids. EVs are responsible for cell communication, the release of unwanted material, and cell maintenance.[109] Furthermore, they can be used as biomarkers for diseases, as they often carry proteins associated with a disease if present, such as detecting biomarkers related to ALS from the cerebral spinal fluid of patients. [110]

1.8 Rationale:

The impaired autophagy machinery and decreased RNA/protein quality control linked to ALS and neurodegenerative diseases highlight the need to target these proteinopathies to a proper degradation system. The ability of autophagy to aid in the clearance of aggregated ALS proteins such as wild-type and mutant TDP-43, along with the elimination of persistent stress granules, highlights the importance of harnessing autophagy as a therapeutic. Although there are many crucial proteins and players in the autophagy pathway, the role of LC3 homologues suggests a promising avenue. Their selectivity and importance in autophagosome biogenesis, cargo docking, and auto-lysosome fusion highlight their essential role in the pathway. Although some distinct roles have been uncovered, the role of specific LC3 homologues in the degradation

of ALS substrates TDP-43 and stress granules remains unclear. Their speculated involvement in vesicle trafficking pathways such as LDELS/SALI also offers a mechanism in which these crucial proteins may be involved in counteracting ALS substrates and how they might be implicated in other pathways.

Hypothesis:

Silencing of specific LC3 Homologues via siRNA transfection will impair autophagy, leading to increased cytoplasmic TDP-43 and stress granules and altered packaging of stress granule proteins into EVs.

Chapter2: Methods & Materials

2.0 Cell Lines

1. U2OS (ATCC)
2. U2OS-eGFP-G3BP2 cells – were generated with U2OS cells from ATCC from Dr. Trinkle-Mulcahy's lab, Methods used to generate the cells are described in: Trinkle-Mulcahy et al. 2007 (Visualization of intracellular PP1 targeting through transiently and stably expressed fluorescent protein fusions**)** PMID: 17200560

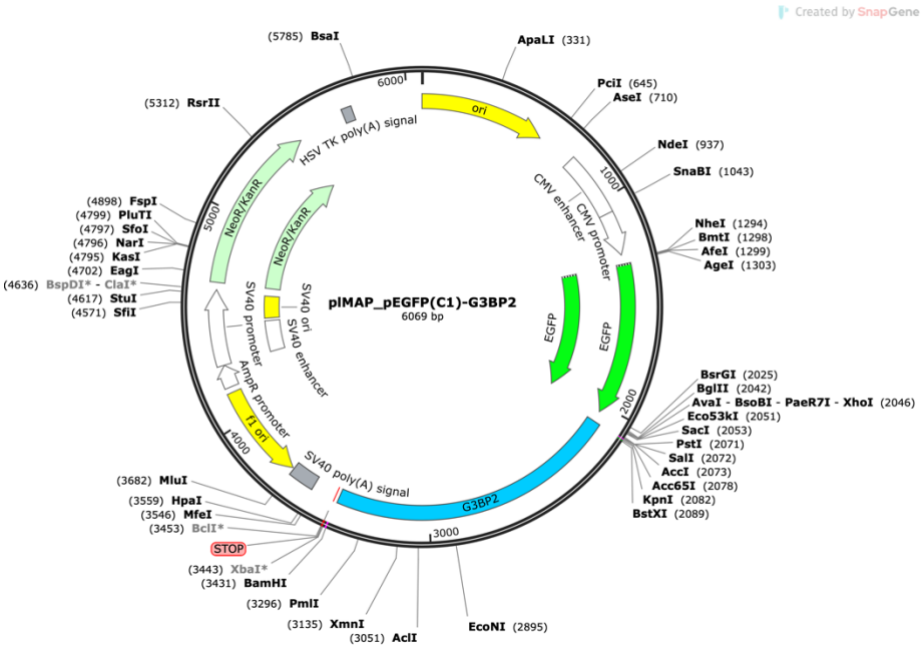

Figure 4. Plasmid map for pEGFP(C1)-G3BP2. Plasmid used to generate the stable expressing U2OS-eGFP-G3BP2 cell lines, exported from snap gene. Gifted from the Trinkle-Mulcahy lab.

2.1 Cell Culture

U2OS and U2OS-eGFP-G3BP2 cells were cultured in 10% fetal bovine serum (FBS) (ThermoFisher,12484028) and 1% Penicillin-Streptomycin (Wisent,450-201 EL). Cells were cultured at 37 °C, 5% CO_2. Cells were rinsed with PBS (319-015-CL, Wisent) before being trypsinized and passaged using Trypsin/EDTA (Wisent, 325-045 EL) when confluent. If cells

were seeded, they were done so using a hemacytometer to determine concentration and seed desired amount.

2.2 High-Throughput Microscopy:

2.2.1 siRNA transfection

Reverse transfection of siRNA was performed using 0.05 ul of 10uM siRNA (final concentration of 10nM), and 5ul of opti-mem (ThermoFisher, 31985070) was used per well and incubated at room temperature for 5 minutes. If a pooled siRNA knockdown was performed, consisting of multiple siRNAs transfected at the same time, they were transfected at a final concentration of 10nM collectively, as well. Then RNA iMAX (13778150, ThermoFisher) was diluted 1/50 using 5ul per well and incubated with siRNA for 20 minutes prior to seeding cells. Cells were seeded so each well contained $0.12x10^4$ cells/mL in antibiotic free media on a 384 well imaging plate (ABD2-01201A, Aurora). 72 hours after knockdown, cells were treated with sodium arsenite (S7400-100G, Sigma-Aldrich) to induce oxidative stress. If cells were treated with arsenite and had a recovery period without sodium arsenite, wells were washed with PBS in between. All siRNAs used are listed in Table 1.

2.2.2 Immunofluorescent Staining:

Cells were washed once with PBS after arsenite treatments prior to fixing. Cells were fixed with 4% formaldehyde (F79-1, Fisher) for 10 minutes at room temperature. Following fixing, cells were washed with PBS two times and then permeabilized with Permeabilization buffer (0.1% Triton, 2mM ammonium chloride in PBS) for 10 minutes at room temperature. Cells were washed again prior to blocking in 10% GSA (S36-100ML, Sigma) for 1 hour at room

temperature. Then, using 10% GSA, the primary antibody was diluted and incubated for 1 hour at room temperature on cells. Afterwards, plates were washed with PBS, and the secondary antibody was diluted in 10% GSA, cells were incubated in the dark at room temperature for one hour. After secondary, cells were washed again with PBS before being incubated in 20% Hoechst (H3570, ThermoFisher) for 10-15 minutes before being washed and left in PBS. The plate was imaged at the High-Throughput screening lab at Children's Hospital of Eastern Ontario (CHEO) by Dr. Stephen Baird on the Opera-Phoenix by Perkin Elmer. All antibodies used are listed in Table 3. Workflow is depicted in Figure 5.

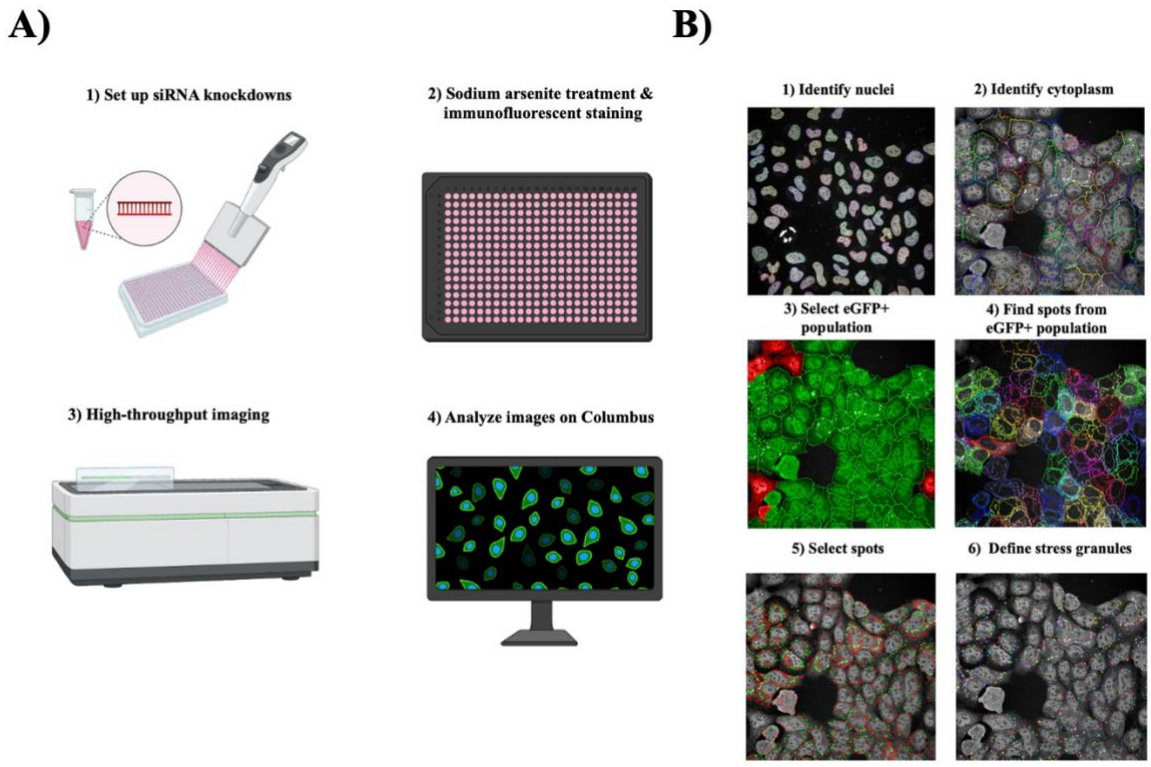

Figure 5. Graphic representation of workflow for high-throughput imaging of LC3 knockdown experiment. (A) siRNA was reversely transfected in a 384 well plate and then incubated for 72 hours. Afterwards, cells were treated with sodium arsenite at the desired concentration, then fixed and immunofluorescent staining. The plate was then sent for high throughput microscopy, where images were loaded and analyzed in Columbus. (B) Columbus image analysis pipeline for stress granule quantification.

2.2.3 Data Analysis on Columbus:

Data was analyzed on PerkinElmer's Columbus Image Analysis server. The image analysis pipeline was designed by Charlotte Manser, and the pipeline was adjusted as needed to best suit the images being analyzed. Between 3-5 technical replicates were used for each condition/knockdown, and approximately 20 fields of view per technical replicate/well. A pipeline was used to define regions and objects of interest, such as cell cytoplasm boundaries and nuclei. Such as defining the nuclei cytoplasm using TDP-43 staining to set cytoplasmic boundaries and cell ring region. Find nuclei module is with method B to detect nuclei from the input image. Find Cytoplasm using the corresponding channel (AF546 or AF568 for TDP-43), using method A. Afterwards, select cell region is used to detect the ring region from the cell. These modules help determine the population and boundaries and are available in Columbus software. After, Intensity properties are calculated for any channels used (for example, AF546/AF568 for TDP-43, eGFP for G3BP2, and Hoechst for nuclei). The intensity of eGFP in the cytoplasm was calculated, and the intensity of TDP-43 in both nuclei and cytoplasm was also calculated in the software for the image analysis. Cells that were not expressing eGFP were excluded from analysis and not included in the population for image analysis. In order to calculate stress granules/cells, the find spots module was used to detect the region of interest population using eGFP+ cells, only looking within the cytoplasmic boundaries. Parameters such as region intensity, corrected spot intensity, spot area, spot contrast, relative spot intensity and uncorrected spot peak intensity were used to filter the population out false positives or negatives and detect stress granules from ambiguous spots or debris in the images. These values were adjusted in every experiment using our negative control wells and positive controls to set thresholds appropriate to those image sets. Cytoplasmic TDP-43 and nuclear intensity were

measured as a ratio: cytoplasmic intensity/nuclear intensity within the eGFP+ population. eGFP+ intensity was also calculated to measure and calculate sieGFP knockdown using immunofluorescence intensity in order to ensure sufficient knockdown of sieGFP each round to gauge successful siRNA transfection. The image analysis pipeline was run on the Columbus image analysis server, where data was analyzed using Excel and Prism afterward.

2.2.4 Statistical Analysis:

Statistical analysis for image analysis and graphs was made on GraphPad Prism 10 software. One-way ANOVA tests were used to compare the mean of control to every other mean. Values were measured as mean and standard error. Statistical significance is as follows: * = $p<0.05$, **< p= 0.01, ***=$p<0.001$, ****=$P<0.0001$

2.3 Validation of siRNAs via qPCR:

2.3.1 siRNA transfection

Reverse transfection of siRNA was performed using a 2ul of 10mM siRNA (final concentration of 10nM), and 200ul of opti-mem was used per well and incubated at room temperature for 5 minutes. Then, 20ul RNA iMAX (13778150, ThermoFisher) was incubated with siRNA for 20 minutes prior to seeding cells. Cells were seeded at $12x10^4$ cells/mL in antibiotic free media.

2.3.2 RNA Isolation

After siRNA transfection, U2OS cells were seeded on a 6-well plate at $20x10^4$ cells/mL and harvested 72 hours after siRNA transfection. Using 500uL of TRIzol Reagent (Thermofisher

15596018), cells were collected into a 1.5 mL tube, and 100ul of chloroform was added to each sample. Samples were shaken for 15 seconds and then sat at room temperature for 2-3 minutes. Samples were then centrifuged at 15,000xg for 15 minutes at 4°C. The top aqueous layer was collected into a fresh 1.5mL tube, and 500ul of 100% Isopropanol was added (Fisher Scientific, BP26181) and 1ul GlycoBlue coprecipitate (Thermofisher, AM9516). Samples were stored overnight at -20 or at room temperature for 10 minutes. Samples were then centrifuged at 15,000xg for 10 minutes at 4°C. The supernatant was removed, and 75% ethanol (P016EAAN, uOttawa Biobar) was used to resuspend the pellet. Another centrifugation of 15,000xg for 15 minutes at 4°C was done before the supernatant was removed, not disturbing the pellet. Pellet was dried in fumehood for 10 minutes at room temperature, then resuspended in 20ul of nuclease free water (MC1191, Promega). Samples were incubated in a thermomixer at 55°C for 5 minutes. Sample concentrations were then measured using a nanodrop.

2.3.3 Rt- qPCR

Using between 500-1000ug of RNA, bringing to a total of 7ul with nuclease free water per sample, 1ul of dNTP (D-5-10, Froggabio) and 2ul of oligodT (idt) were added to each sample. Samples were incubated for 5 minutes at 65°C. Afterwards, 6.8ul of nuclease free water, 0.2ul of RiboLock (EO0382, ThermoFisher), 1ul of M-Mulv Reverse Transcriptase and 2ul of M-Mulv Buffer (New England Biolabs, (M0253S). No RT control was included of all the above reagents, except 3ul of M-Mulv buffer and no M-Mulv Reverse Transcriptase. The primers used are indicated in the table below. cDNA was diluted 1/5 with nuclease-free water before being added to the qPCR reaction. In total, 6ul of primer and goTAQ master mix (A6001, Promega) and 4ul of cDNA. Plates consisted of 2-3 technical replicates per primer on 384 well qPCR

plate (HSP3801, Bio-Rad). All primers used are listed in Table 2 and were ordered/manufactured from IDT.

2.3.4 qPCR Analysis

CT values were exported to analyze qPCR results. Each technical replicate was averaged and normalized to the GAPDH average CT value. Delta CT was solved by subtracting the average housekeeping CT value from each sample of interest. Delta Delta CT was solved by subtracting scramble control CT value from knockdown sample CT value, whereafter -log2 fold of each delta delta CT value was calculated and converted into a percentage of expression by multiplying by 100. Statistical analysis for results and graphs was performed on GraphPad Prism 10 software. Unpaired t-tests were used to compare the mean between knockdown and scramble control. Values were measured as mean and standard error. Statistical significance is as follows: * = $p<0.05$, **< p= 0.01, ***=$p<0.001$, ****=$P<0.0001$. siLC3ABC knockdown, displayed high error bars for MAP1LC3A gene expression for siLC3A. One of the three biological replicates was drastically higher than the other two, and therefore, an outlier test was conducted on Prism using the ROUT method (Q=1%).

2.4 Validation of siRNAs via Western Blot:

2.4.1 Protein Isolation and Assay

Using (1mL for 10cm plate) or (500ul – 6 well plate) of RIPA buffer (5M NaCl, 100ul NP40, 500ul 10% sodium deoxycholate, 500ul 20% SDS, 500ul of 1M TRIS in ddh20 with a protease inhibitor tablet) for protein harvest. Cells were scraped off and collected with RIPA buffer. Samples were sonicated for 30 seconds and then centrifuged at 13,000xg for 5 minutes at

4 degrees Celsius. The supernatant was collected into a new tube, and the pellet was discarded. A BCA assay was used to measure protein concentrations. 5ul of sample and/or standard were loaded into each well. Adding 25 ul of reagent SA (20ul of Reagent S (500-0115, bio-rad) per 1ml of Reagent A (500-113)) and 200ul of Reagent B (500-0114) to each well. After 15 minutes of incubation at room temperature, the read absorbency was at 750nm. Calculations were done in Excel to solve for the mass of each protein sample (c=m/v), and concentration was calculated based on the trendline of the absorbancy curve by solving for x in y=mx+b. To prep samples, they were mixed with 4X Laemmli buffer (100ul B-mercapethanol (1610710, biorad) and 900ul laemelli blue buffer (1610747, bio-rad) and PBS. Samples were incubated at 95 degrees Celsius for 10 minutes before being loaded into the gel.

2.4.2 Western Blot

Using 10% polyacrylamide gels (ddH2O, 40% Acrylamide, 1.5M Tris Ph 8.8, 10% SDS, 10% APS and TEMED for running gel and ddh2o, 40% Acrylamide, 0.5M Tris ph 6.8 and 10% SDS and 10% APS and TEMED for stacking gel). Samples were loaded, and 5ul of protein ladder (PM008-0500, FroggaBio). Using 1x Running Buffer, samples were run for 1 hour at 150V. Samples were then transferred for 1 hour at 100V in 1x transfer buffer onto a PVDF membrane. Afterwards, the membranes were blocked in 5% milk in 1% TBST (150mM NaCL, 10mM Tris-HCl Ph8, 0.05% Tween 20). They were then probed overnight at 4 degrees on a shaker in primary antibody in 1% TBST. The next day, they were washed 3 times for 5 minutes in 1% TBST then incubated for 1 hour at room temperature in secondary antibody. They were then washed again 3 times for 5 minutes at room temperature in 1% TBST. After they were

ready to be imaged, using HRP substrate (WBLUR0500, Fisher) on Li-COR. All antibodies used are listed in Table 3.

2.5 Extra Cellular Vesicle Isolation

2.5.1 Knockdown for EVs:

Knockdowns were set up using the protocol described above, although 5ul of siRNA, 500ul of opti-mem and 10ul of RNA iMax were used per sample. LC3 siRNAs were pooled at 10uM, creating a 60uM siRNA (60nM final concentration) and using a 60uM scramble control (60nM final concentration). Cells were reversely transfected using the same protocol and set aside for knockdown validation via western blot using the same protocol described previously. U2OS cells were seeded afterwards on a 10cm plate. Media was changed at 24 hours to exosome free media (DMEM F12 (319-075-CL, wisent), 1% penicillin-streptomycin and 10% exosome depleted FBS (A2720801, ThermoFisher). Media was collected at 48 hours and 72 hours. Cells were lysed using RIPA buffer and harvested for protein isolation. Exosome samples were spun at 300g for 10 minutes and 1000xg for another 10 minutes, then transferred to a new tube.

2.5.2 EV purification

Samples were spun at 10,000xg for 30 minutes and then prepped for ultracentrifugation. Samples were spun at 25,800rpm for 2 hours at 4 degrees Celsius. Media was remixed, and the pellet was resuspended in 1mL of PBS, then spun for 30 minutes at 49000 rpm at 4 degrees Celsius. The supernatant was discarded, and the pellet was resuspended in 20ul of PBS.

2.6 Mass Spectrometry:

2.6.1 Preparation of samples

After proteins were isolated from cell lysates, 1% triton and 1% SDS were added to exosome samples. Proteins were precipitated from lysates using 4 volumes of acetone (BDH1101-1LP, vwr) and vortexed. Samples were incubated in ice cold acetone for 1 hour at -20, then spun at 15,00xg for 10 minutes. Precipitate was resuspended in 6M urea and 100mM Tris ph8. Reuspension was diluted with 5 fold 100mM Tris ph8 without urea. Samples were then trypsinized. Add 50mM DTT to a final concentration of 10% and incubate for 5 minutes at 65 degrees. 100mM IAA to a final concentration of 10% in the sample was added. The following steps were done using tinfoil to cover from light. Samples were incubated at 30 degrees Celsius for 30 minutes. Then 70ul of 100ng/ul of proteomics grade trypsin was added to each sample and incubated at 37 degrees Celsius overnight. The following day, acetic acid was added to each sample to create a final concentration of 0.5%. Samples were desalted using Sep-Pak tc18 cartridges (WAT054960, Waters) (1cc, 50mg). The cartridges were washed and conditioned with 900ul of acetonitrile (ACN), followed by 300ul of 50% ACN and 0.5% acetic acid (HAcO), then 900ul of 0.1% HAcO. Samples were loaded into cartridges afterwards. Afterwards, they were washed and desalted with 900ul of 0.1% HAcO, then 90ul of 0.5% HAcO. Waste was discarded, and sample was eluted into a fresh tube with 500uk of 50% ACN and 0.5% HAcO. Samples were stored at -20 and then fractionated the following day on a Pierce SCX column. Columns were first washed with 25mM sodium acetate at ph4 and spun at 2,000xg for 5 minutes. Flow through was discarded, and sample was loaded into column and spun at 200g for 5 minutes. Columns were washed and spun once more with sodium acetate again and then eluted with 100ul of 25mM sodium acetate at pH 5.5 with 1M NaCl into a fresh tube to collect samples using another 2000xg spin for 5 minutes. Samples were desalted again using tc18 columns and then

dropped off at the Rodger Guindon proteomics facility. Mass spectrometry was performed by Dr. Zhibin Ning.

2.6.2 Nanoparticle Tracking Analysis

Nanoparticle Tracking Analysis (NTA) was performed on a ZetaView PMX-110 by Ryan Reshke. The ZetaView was calibrated upon each start-up using 102 nm polystyrene beads (Microtrac, 900383). Small EVs were diluted in 1X PBS to be in the instrument's range for accurate measurement. Video acquisition was performed with the following settings: Sensitivity 85, Shutter Speed 40, Frame Rate (fps) 30, Resolution Highest, Camera Gain 770, Positions Measured 11, Minimum Brightness 15, Minimum Size (pixels) 10, Maximum Size (pixels) 500.

2.6.3 Data Analysis and Processing

The Mass Spec data-independent acquisition (DIA) file was exported, and the intensities of each protein/gene were analyzed to determine expression levels. There were 3 biological replicates in total for each condition (scramble and siLC3 knockdown). Each biological replicate was used to calculate their averages in order to calculate a ratio or LOG2 fold change. A two-tailed T-test was used to calculate significance on Excel ($p<0.05$). Proteins detected in only one of three biological replicates were excluded from calculations as false positives. Results were graphed using Prism. Significant hits were compared to supplementary data from Leidal et al., 2020 and Debnath et al., 2021 as well as Anne-Claude Gingras et al., 2018 in Excel to spot overlap/common proteins. Further analysis using Gene Ontology (GO) enrichment analysis was performed on Panther of significant EV hits ($p\leq0.05$). Table was exported to graft -log10 False Discovery rate (FDR) across molecular function and cellular components identified by GO Analysis on Panther. Furthermore, protein functions were obtained from UniProt human protein database.

Table 1: siRNAs used

siRNA gene	Catalogue name	Company
MAP1LC3A	439240	ThermoFisher
MAP1LC3B	4329240	ThermoFisher
MAP1LC3C	4329240	ThermoFisher
MAP1LC3C	4329240	ThermoFisher
GABARAP	4329240	ThermoFisher
GABARAPL1	4329240	ThermoFisher
GABARAPL1	439240	ThermoFisher
GABARAPL2	439240	ThermoFisher
Negative control	4390847	ThermoFisher
eGFP	AM4626	ThermoFisher
ATG16L1	4392420	ThermoFisher
ATG7	4392420	ThermoFisher
P62	4392420	ThermoFisher

Table 2: Primers used for rt-qPCR

Gene	Forward primer sequence 5'-3'	Reverse primer sequence 5'-3'
MAP1LC3A	CAGCATGGTGAGTGTGT CCA	TCAGAAGCCGAAGGTTTCCT
MAP1LC3B	AGGCCTTCTTCCTGTTGGTG	GGCTCTGCAGTCTAGCAAGT
MAP1LC3C	GGCTCTGCAGTCTAGCAAGT	GGCTCTGCAGTCTAGCAAGT
GABARAP	AGAAGAGCATCCGTTCGAGA	CAGACCGTAGACACTTTCGTCA
GABARAPL1	CCCTCCCTTGGTTATCATCCA	ACTCCCACCCCACAAAATCC
GABARAPL2	AAATATCCCGACAGGGTTCC	CAGGAAGATCGCCTTTTCAG
BETA-ACTIN	GGGGTGTTGAAGGTCTCAAA	GGCATGGGTCAGAAGGATT
GAPDH	GCCTGCTTCACCACCTTCTTG	AGGTCATCCCTGAGCTGAACG
G3BP1	AGCCTGTTCAGAAAGTCCTTAGC	CGAAGGCGATTATCTCGTCGGT
G3BP1	GTCCAGAGTCTAAGCCTGAATC	ATGTCACCTTGCTCACCAG
G3BP2	CCTCGTGTGCGTGAACAAC	CATGTGGCAAGTTACCAACAAAA
G3BP2	TGTGGAACTTCGCATCAATACC	AAACGTACTTCCCCTCGAAACA

Table 3: Antibodies (IF: immunofluorescence, WB: western blot)

Antibody name/ target	Application	Catalogue number	Company	Species
AF546	IF	A-11010	ThermoFisher	rabbit
AF 568	IF	A-11011	ThermoFisher	rabbit
C-term TDP-43	IF	T1580-200UL	sigma	rabbit
Hoechst	IF	H3570	ThermoFisher	n/a
ATG7	WB	2631s	Cell Signalling	mouse
ATG16L1	WB	8089	Cell Signalling	rabbit
P62/P62	WB	P0067	Sigma	rabbit
GAPDH	WB	Sc-32233	Santa Cruz Biotechnology	Mouse
LC3B	WB	L7543	Sigma	Rabbit
Gabarap,L1,L2	WB	Ab109364	Abcam	Rabbit

Chapter 3: Results

3.1 siRNA Validation for High-Throughput Microscopy:

Knockdowns were validated via rt-qPCR of each LC3 homologue. A pooled knockdown of all siLC3/GABARAPs was included, which consisted of each siRNA pooled together in one transfection. For example, siLC3ABC pool consisted of siRNA for MAP1LC3A, MAP1LC3B, MAP1LC3C, combined at a final 10nM concentration collectively. SiGABARAP pool consisted of siRNA for: GABARAP, GABARAPL1, GABARAPL2 combined at a final concentration of 10nM collectively. All 6 siLC3 pool consisted of: siRNA for MAP1LC3A, MAP1LC3B, MAP1LC3C, GABARAP, GABARAPL1, and GABARAPL2 combined at a final concentration of 10nM collectively. Due to the lack of specificity among antibodies to detect the different LC3 homologues, knockdowns were validated via rt-qPCR instead of western blot. Expression levels were normalized to GAPDH levels. All knockdowns yielded over 70% knockdown, except for siLC3A (Figure 6A). In pooled knockdowns, the level of knockdown amongst the several genes varied. Specifically, in the LC3 pool, most genes displayed approximately over 70% knockdown. However, in the Gabarap pool, the knockdown percentage was above 50% but below 70% (Figure 6B). Lastly, in all 6 siLC3 pooled knockdown, there was a lot of variation amongst the various knockdowns, however all knockdowns except for siLC3A displayed minimum 70% knockdown (Figure 6B).

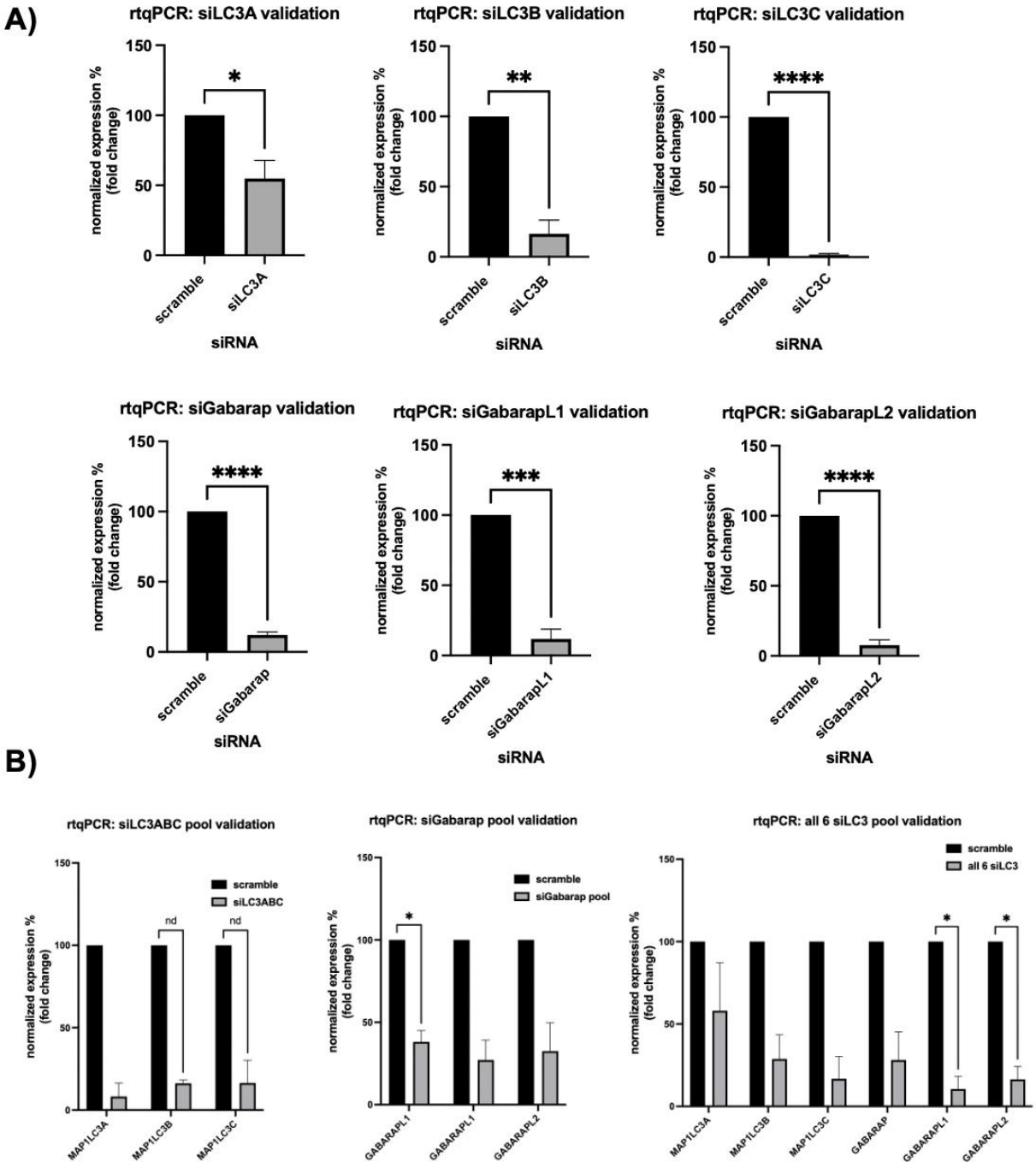

Fig 6. Validation of knockdowns via rt-qPCR. (A) rt-qPCR results of each LC3 homologue siRNA. Data consisted of 3 technical replicates/knockdown. Significance testing by unpaired t-test ($p<0.05$). Data represented as means and standard error. B) rt-qPCR results of pooled LC3 knockdowns by siRNA. Data consistent of 2-3 technical replicates. Significance testing by multiple unpaired t-tests ($p<0.05$).

3.1.2 Effects of siLC3 on stress granules and cytoplasmic TDP-43 at 500uM sodium arsenite:

U2OS eGFP-G3BP2 cells were transfected with siRNA to deplete LC3 homologues and test their impact on levels of cytoplasmic TDP-43 and stress granules. Cells were treated with 500uM sodium arsenite to induce formation of stress granules as well as mislocalization of TDP-43 into the cytoplasm. Stress granule formation peaks at 1hr hour and stress granules dissipate within two hours after removal of sodium arsenite. However, by knocking down essential proteins of the autophagy pathway, we expected to see a stalling of stress granule disassembly and degradation of TDP-43 in the cytoplasm. We hypothesized that one or more LC3 homologues would have a role in the degradation of stress granules and/or cytoplasmic TDP-43, and we therefore, expected to see increased levels of stress granules/cytoplasmic TDP-43 by knocking down essential homologues. Interestingly, siLC3C and siGABARAPL2 led to decreased stress granule levels at 30 minutes of recovery after 1 hour of 500uM sodium arsenite treatment (Figures 7 and 8). Additionally, GABARAP pooled knockdown also led to decreased stress granules at the same timepoint. All three Gabaraps have different results for levels of stress granules along the sodium arsenite time course, speculating different behaviours between these three homologues. Cytoplasmic TDP-43 levels were assessed among the various siRNA knockdowns of LC3 homologues. At baseline, siLC3C and siGABARAPL1 lead to increased cytoplasmic TDP-43 levels. However, there were no significant effects on cytoplasmic TDP-43 levels from knocking down LC3 homologues. Most knockdowns didn't appear to impact the clearance of cytoplasmic TDP-43 levels. A similar theme can be seen for siLC3C, suggesting cytoplasmic TDP-43 levels increased at a later recovery (Figures 9 and 10).

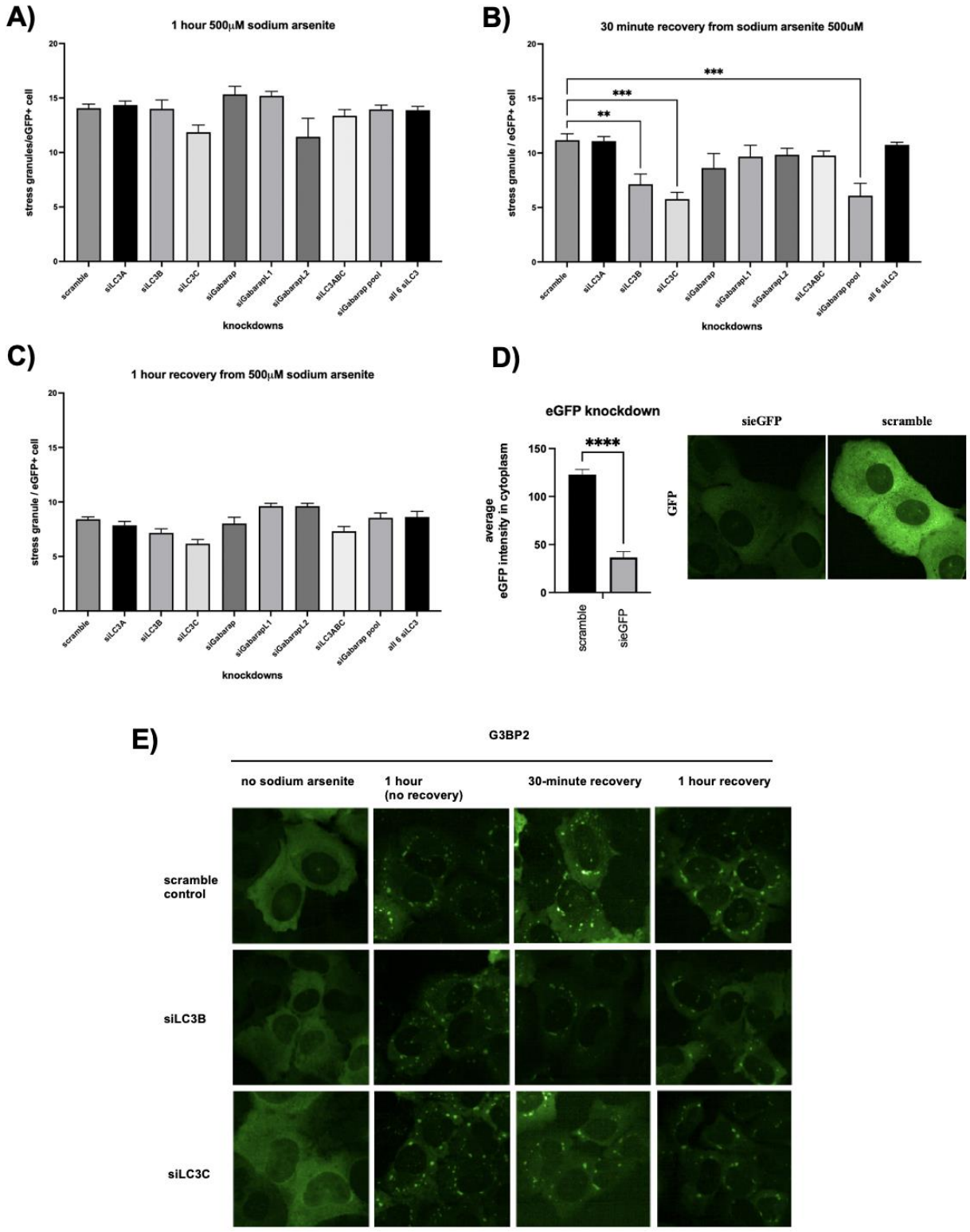

Figure 7. Decreased stress granules at 500uM sodium arsenite in U2OS eGFP-G3BP2 cells with LC3 knockdown. (A)-(C) Representative graphs of stress granules quantified among the various LC3 knockdowns in different time points of sodium arsenite. Data consisted of 5 technical replicates/knockdown. Significance testing by One way ANOVA ($p<0.05$). Data represented as means and standard error. (D) Quantification of eGFP intensity in cytoplasm to validate knockdown, with representative images. Consisted of 5-10 technical replicates per siRNA. Unpaired t-test ($p<0.05$). Data represented as means and standard error. F) Representative images of select knockdowns under various sodium arsenite timepoints, showing G3BP2 as eGFP, imaged at 40X on opera phoenix.

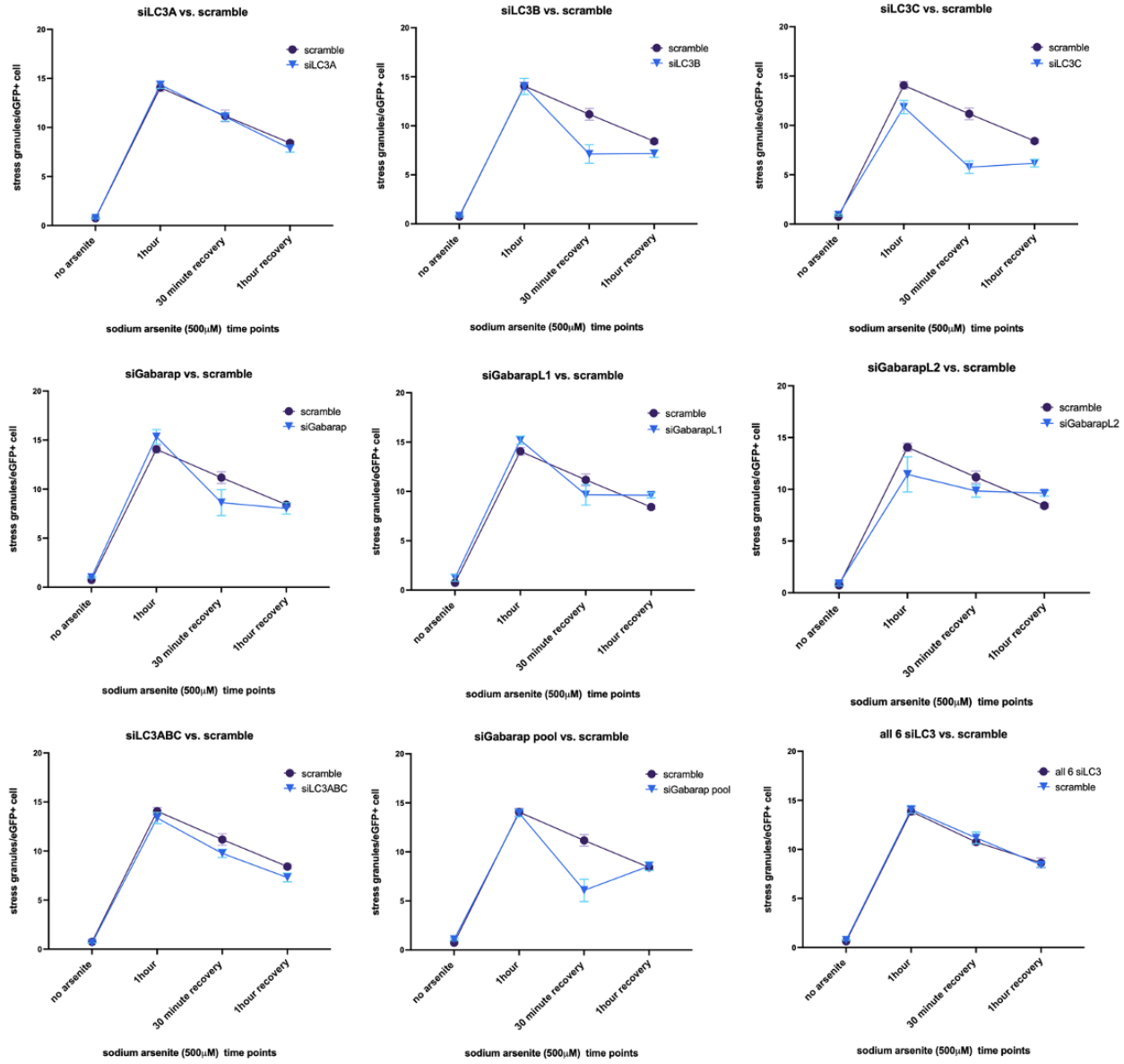

Figure 8. Stress granule levels along sodium arsenite time course Data plotted as mean and standard error, each point consisted of 5 technical replicates.

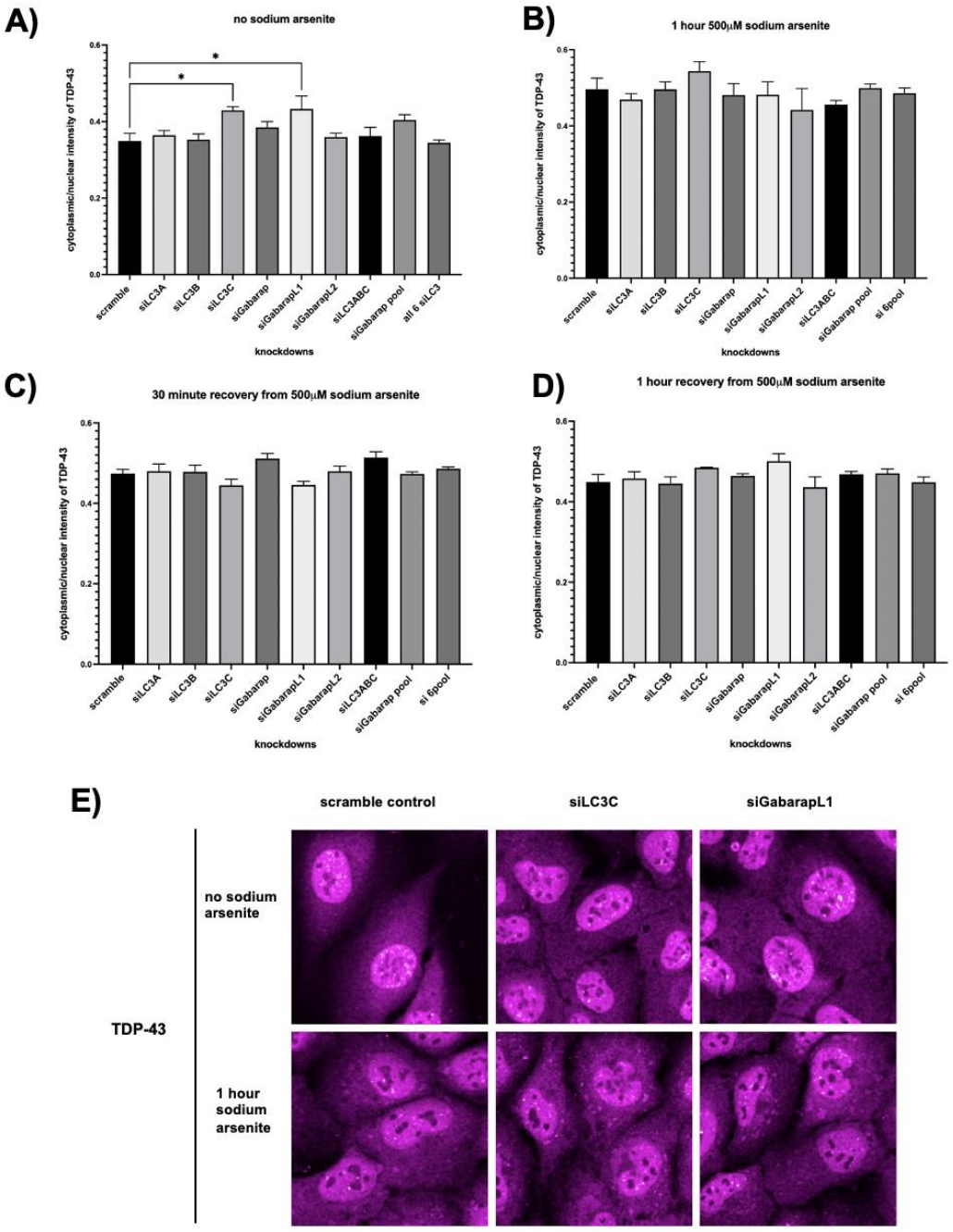

Figure 9. Increased cytoplasmic TDP-43 at baseline in LC3C and GABARAPL1 knockdown in U2OS eGFP-G3BP2 cells. (A)-(D) Representative graphs of cytoplasmic TDP-43 intensity quantified among the various LC3 knockdowns in different time points of sodium arsenite. Reported as ratio of cytoplasmic/nuclear intensity of TDP-43. Data consisted of 5 technical replicates/knockdown. Significance testing by One way anova ($p<0.05$). Data represented as means and standard error. (E) Representative images of select knockdowns under no sodium arsenite and sodium arsenite at 500uM, showing c-term TDP-43 as AF546, imaged at 40X on opera phoenix.

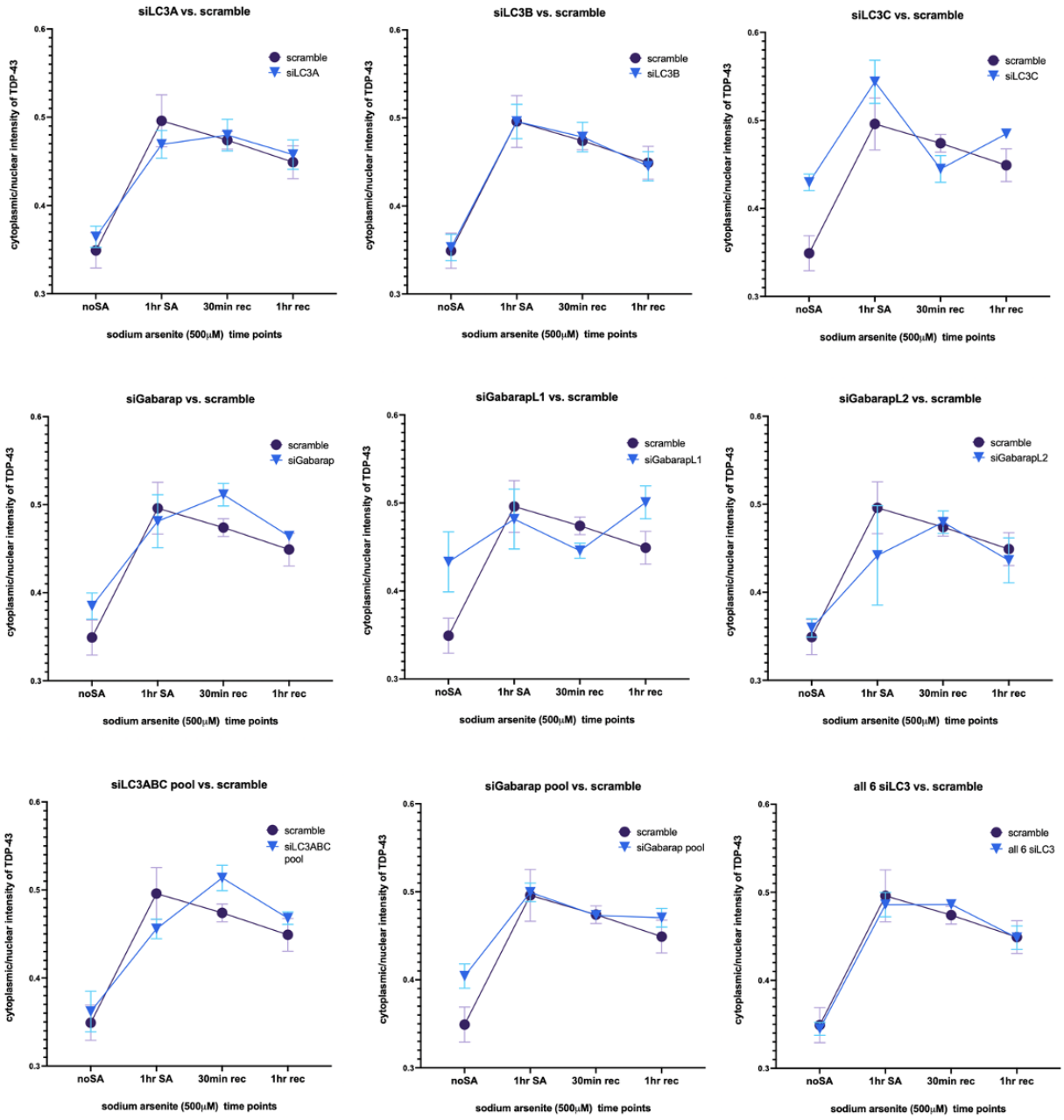

Figure 10. Cytoplasmic TDP-43 along sodium arsenite time course Data plotted as mean and standard error, each point consisted of 5 technical replicates.

3.1.3 Effects of siLC3 on stress granules and cytoplasmic TDP-43 at 100µM sodium arsenite:

We decided to repeat experiments at a lower arsenite dose to further assess the impact on clearance of stress granules and cytoplasmic TDP-43 from knockdown of LC3 homologues. 500uM sodium arsenite is at the high end of the threshold for inducing oxidative stress, we were concerned it might be overwhelming the cell and at too high of a capacity to see effects from LC3 depletion.

We repeated the previous experiment at 100uM sodium arsenite to assess levels of stress granules and cytoplasmic TDP-43 (Figure 11-13). More recovery time points were also included to see if there were any significant and long-lasting effects on clearance at later time points and a no siRNA control. Results were fairly dynamic at one hour of sodium arsenite, showing diverse effects among the various knockdowns. An sieGFP control was included to gauge the level of knockdown. Scramble showed decreased stress granule levels compared to no siRNA control, suggesting possible off-target effects of knockdown on stress granule levels and formation.

At 30 minutes of recovery from 100uM sodium arsenite, we see a decrease in numbers as expected. However, knockdown of GABARAPL1 and GABARAPL2 remain quite high, suggesting GABARAPL1 and GABARAPL2 knockdown are significantly impairing stress granule clearance and may have a significant impact in this process (Figure 11A-C). Additionally, at 1 hour of recovery and 2 hours of recovery, while most knockdowns still show the ability to recover and clear stress granules, siLC3C and siGABARAPL1 demonstrate significantly higher levels of stress granules and hinder the clearance of stress granules. Interestingly, Gabarap pooled knockdown demonstrates slightly increased levels among the three pooled knockdowns, in comparison to LC3ABC and all 6 siLC3 pool (Figure 11D). GABARAPs may have a more impactful role in stress granule clearance.

We also analyzed levels of cytoplasmic TDP-43 from the knockdowns. There were no significant effects among the various knockdowns before recovery. During this experiment, siLC3C and siGABARAPL1 did not display increased TDP-43 intensity in the cytoplasm at baseline. However, at 30 minutes of recovery, we start to see some effects. Knockdown of LC3C displayed heightened levels of cytoplasmic TDP-43 throughout 30 minutes to 1 hour of recovery. GABARAPL1 and GABARAPL2 knockdown also displayed an increase in levels of cytoplasmic TDP-43 at 30 minutes of recovery (Figure 13). The consistent increase of cytoplasmic TDP-43 in LC3C knockdown suggests that it may have a prominent role in the degradation of cytoplasmic TDP-43. GABARAPL1 and GABARAPL2 knockdown may be crucial in cytoplasmic TDP-43 clearance in earlier recovery.

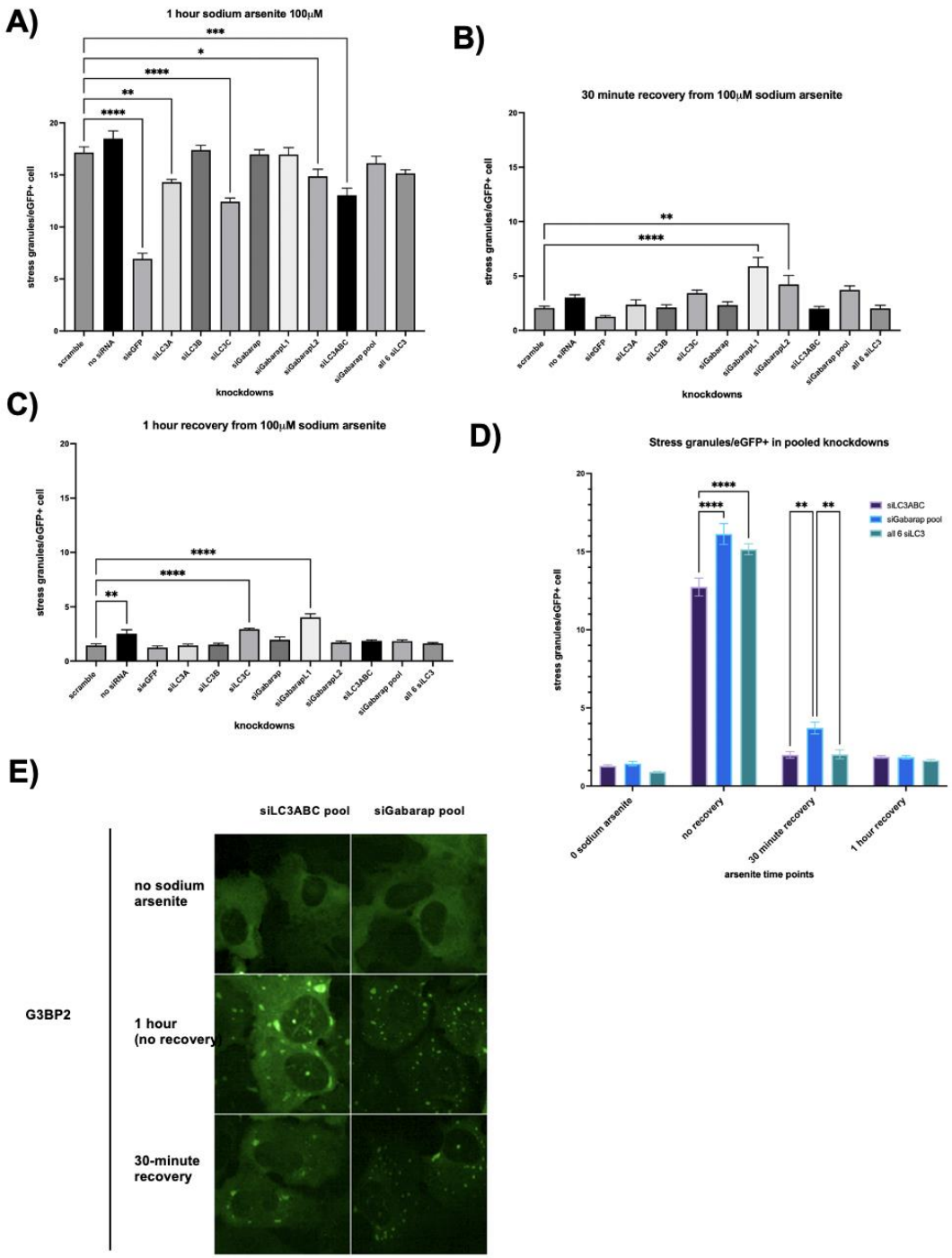

Figure 11. Stalled stress granule clearance in GABARAPL1 and GABARAP pool knockdowns in U2OS eGFP-G3BP2 cells during treatment with 100uM sodium arsenite. **(**A)-(C) Representative graphs of stress granules quantified among the various LC3 knockdowns in different timepoints of sodium arsenite. Data consisted of 5 technical replicates/knockdown. Significance testing by One way anova ($p<0.05$). Data represented as means and standard error. (D) Stress granules quantified among the different LC3 RNAi pools. Data consisted of 5 technical replicates/knockdown. Significance testing by 2-way anova ($p<0.05$). F) Representative images of pooled knockdowns under various sodium arsenite timepoints, showing G3BP2 as eGFP, imaged at 40X on opera phoenix.

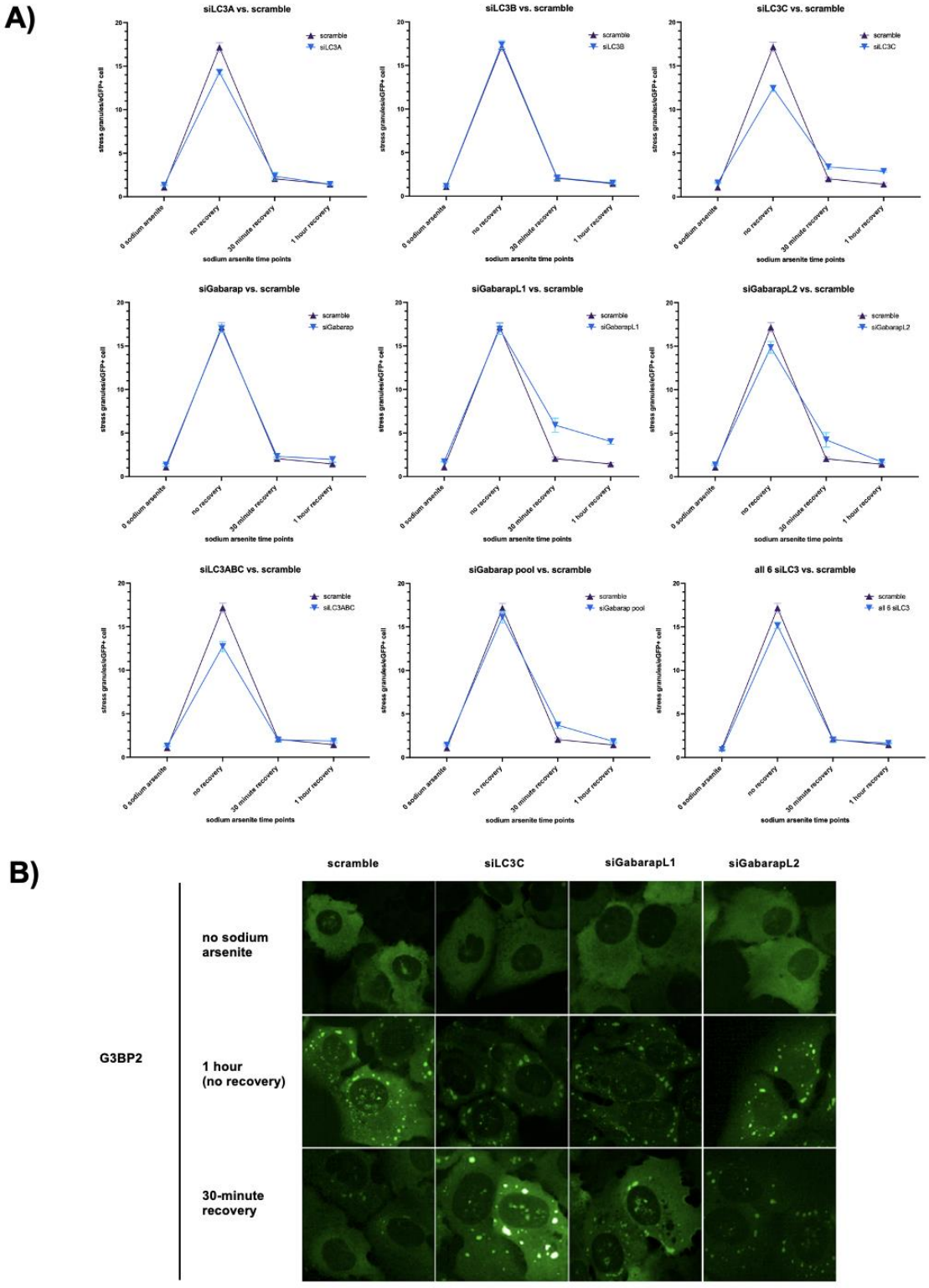

Figure 12. Stress granule levels along 100uM sodium arsenite time in U2OS eGFP-G3BP2 cells (A) Data consisted of 5 technical replicates/knockdown. Data represented as means and standard error. (B) Representative images of LC3 knockdowns under various sodium arsenite timepoints, showing G3BP2 as eGFP, imaged at 40X on opera phoenix.

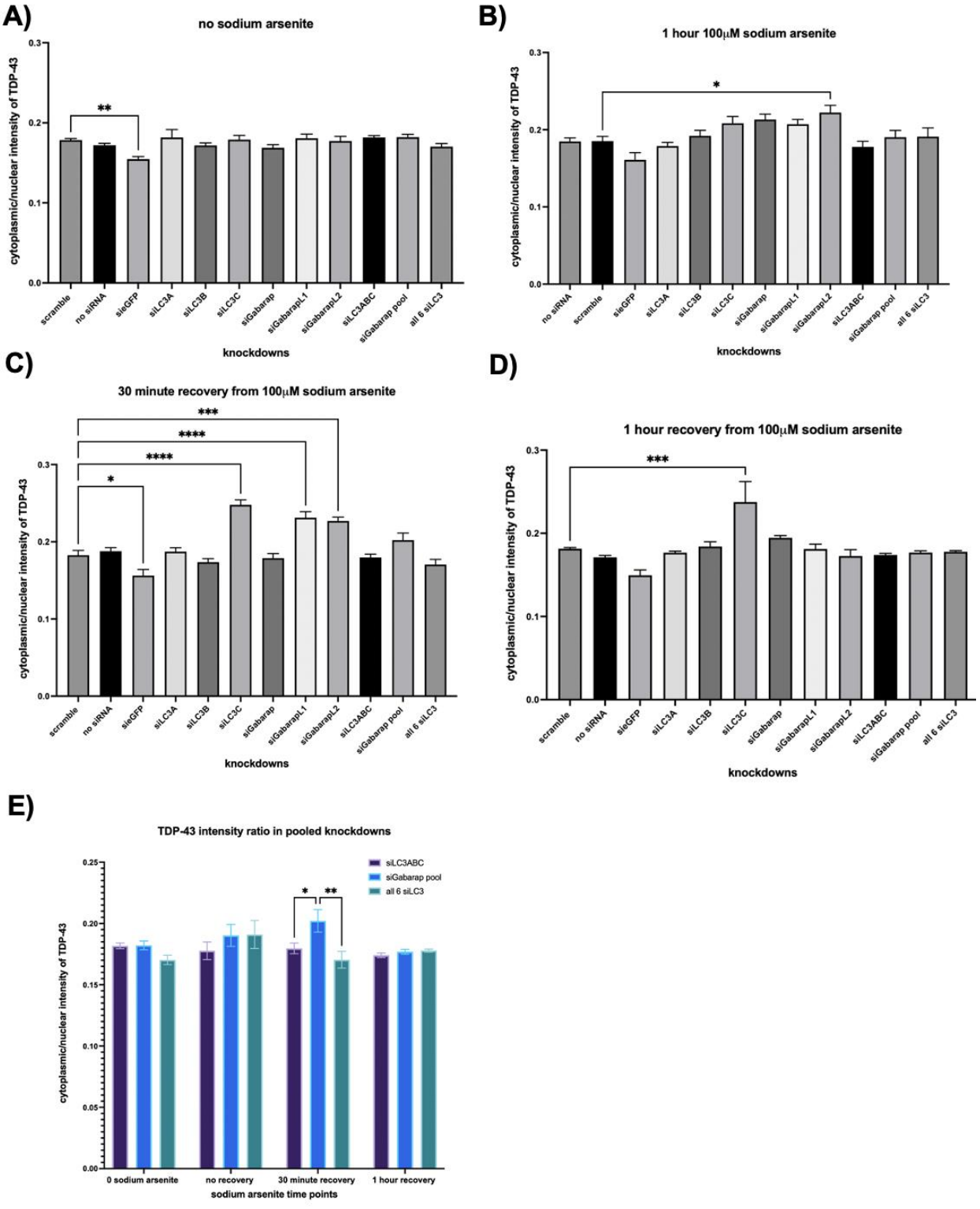

Figure 13. Increased cytoplasmic TDP-43 in LC3C knockdown in U2OS eGFP-G3BP2 cells under 100uM sodium arsenite. (A)-(D) Representative graphs of cytoplasmic TDP-43 intensity quantified among the various LC3 knockdowns in different timepoints of sodium arsenite. Reported as ratio of cytoplasmic/nuclear intensity of TDP-43. Data consisted of 5 technical replicates/knockdown. Significance testing by One way anova ($p<0.05$). Data represented as means and standard error. (E) Cytoplasmic TDP-43 levels among different LC3 RNAi pools. Data consisted of 5 technical replicates/knockdown. Significance testing by 2-way anova ($p<0.05$).

3.1.4 Validation of new siRNAs:

To validate some of these findings further, we tested a second siRNA of LC3C and GabrapL1 and the previous ones while including autophagy-related siRNAs such as ATG16L1, ATG7, and p62. We started by validating the new siRNAs for LC3C and GABARAPL1 by rt-qPCR, which yielded above 75% knockdown (Figure 14A). The other siRNAs, such as sip62, ATG16L1 and ATG7, were validated via western blot. P62 and ATG16L1 yielded strong knockdown, and ATG7 yielded moderate knockdown (Figure 14B).

3.1.5 Effects of siLC3C and siGABARAPL1 on stress granules and cytoplasmic TDP-43:

A 100uM sodium arsenite dose, was used to analyze stress granule quantification, as it displayed more effects in previous experiments. SiGABARAPL1 siRNAs displayed a significant increase in stress granules at 1 hour of sodium arsenite, which validates previous trends that siGABARAPL1 leads to increased stress granule quantity. Sip62 and siLC3C also displayed increased stress granules at 1 hour (Figures 15 and 16). However, the new siRNA for LC3C did not significantly affect stress granule levels, which contradicts previous effects from siLC3C knockdown. Interestingly, siATG7 displayed decreased stress granule levels during both time points.

A sodium arsenite dose of 500uM was used to analyze cytoplasmic TDP-43 intensities since that yielded more significant effects in previous experiments (Figure 17). Both old siRNAs for GABARAPL1 and LC3C displayed increased cytoplasmic TDP-43. However, new siRNAs for those homologues displayed no significant or opposing effects on cytoplasmic TDP-43, contradicting previous results and the true effect of siLC3C and siGabaraL1 on TDP-43.

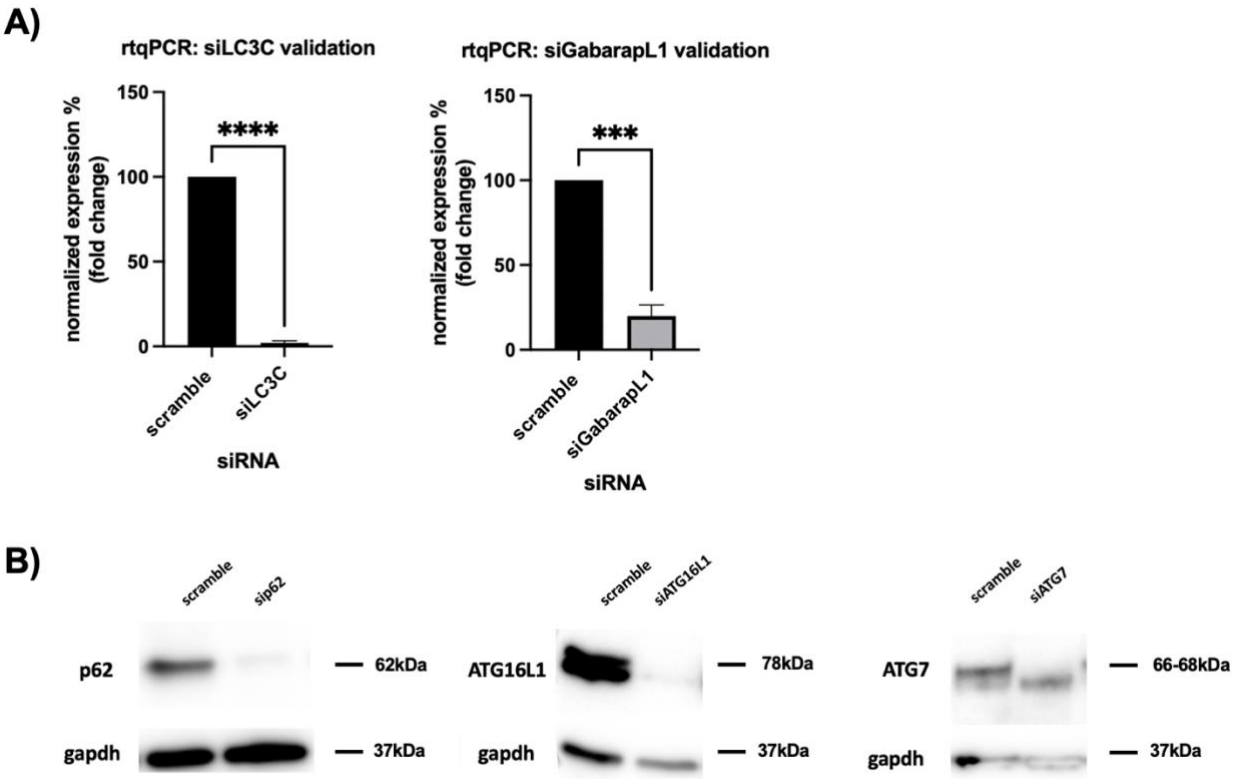

Figure 14. Validation of new siRNAs (A) rt-qPCR of new siLC3C and siGABARAPL1, representative graphs, data represented as mean and standard error (n=3). (B) Representative western blot images of autophagy related siRNAs (n=3).

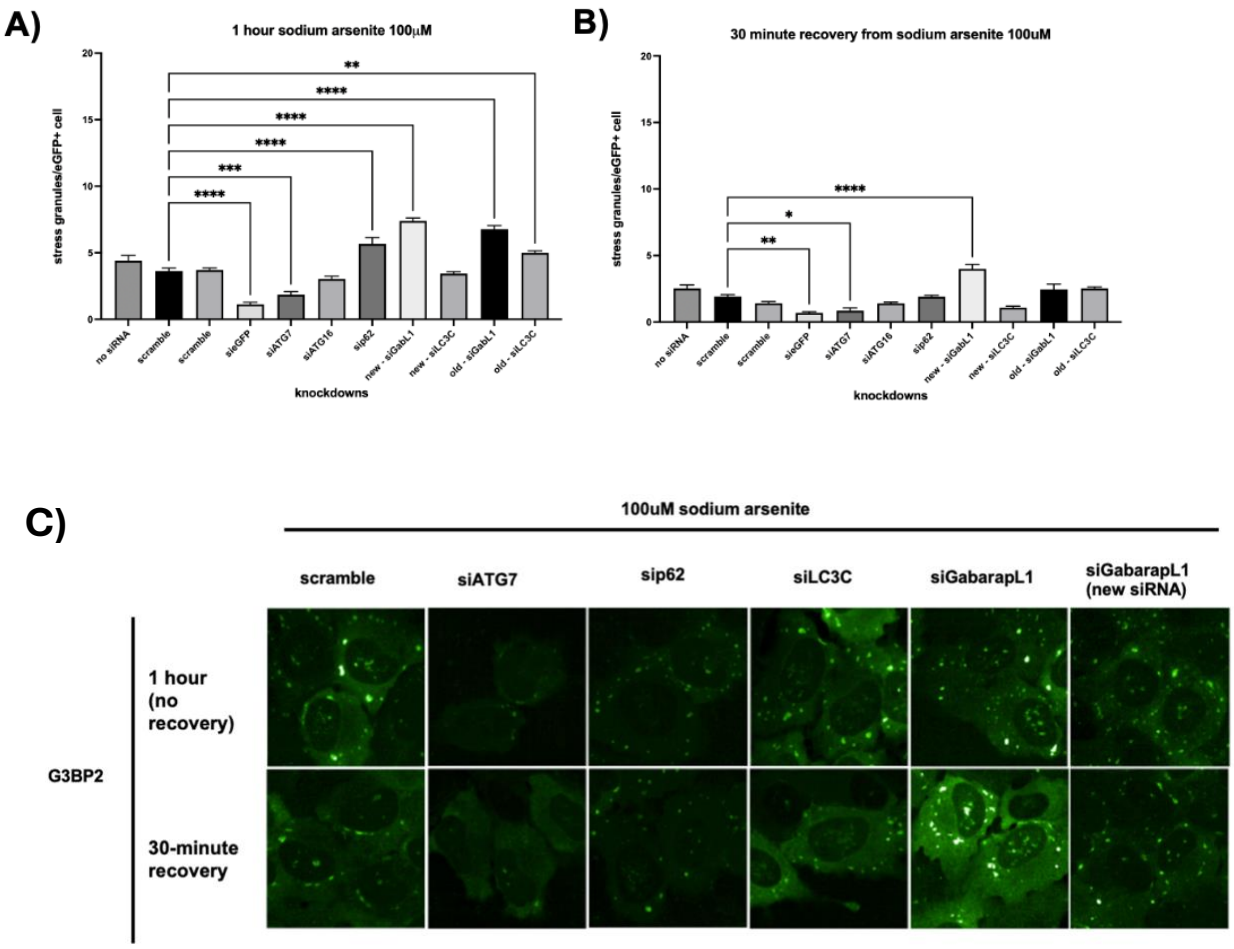

Figure 15. Validating GABARAPL1 knockdown effect in stress granule clearance in U2OS eGFP-G3BP2 cells under 100uM sodium arsenite. (A)-(B) Representative graphs of stress granules quantified among the various LC3 knockdowns in different timepoints of sodium arsenite. Data consisted of 5 technical replicates/knockdown. Significance testing by One way anova ($p<0.05$). Data represented as means and standard error. C) Representative images of select knockdowns under various sodium arsenite timepoints, showing G3BP2 as eGFP, imaged at 40X on opera phoenix.

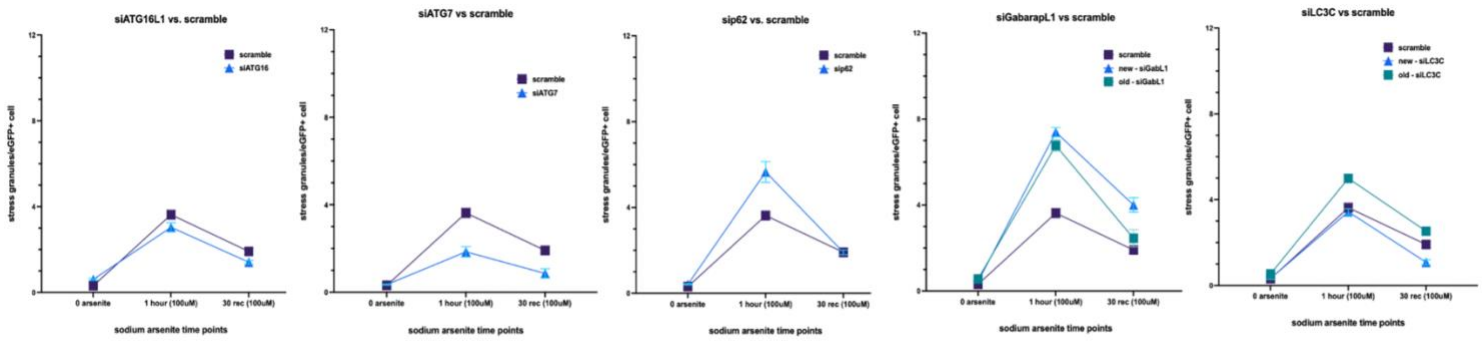

Figure 16. Stress granule levels along 100uM sodium arsenite time in U2OS eGFP-G3BP2 cells. Data consisted of 5 technical replicates/knockdown. Data represented as means and standard error.

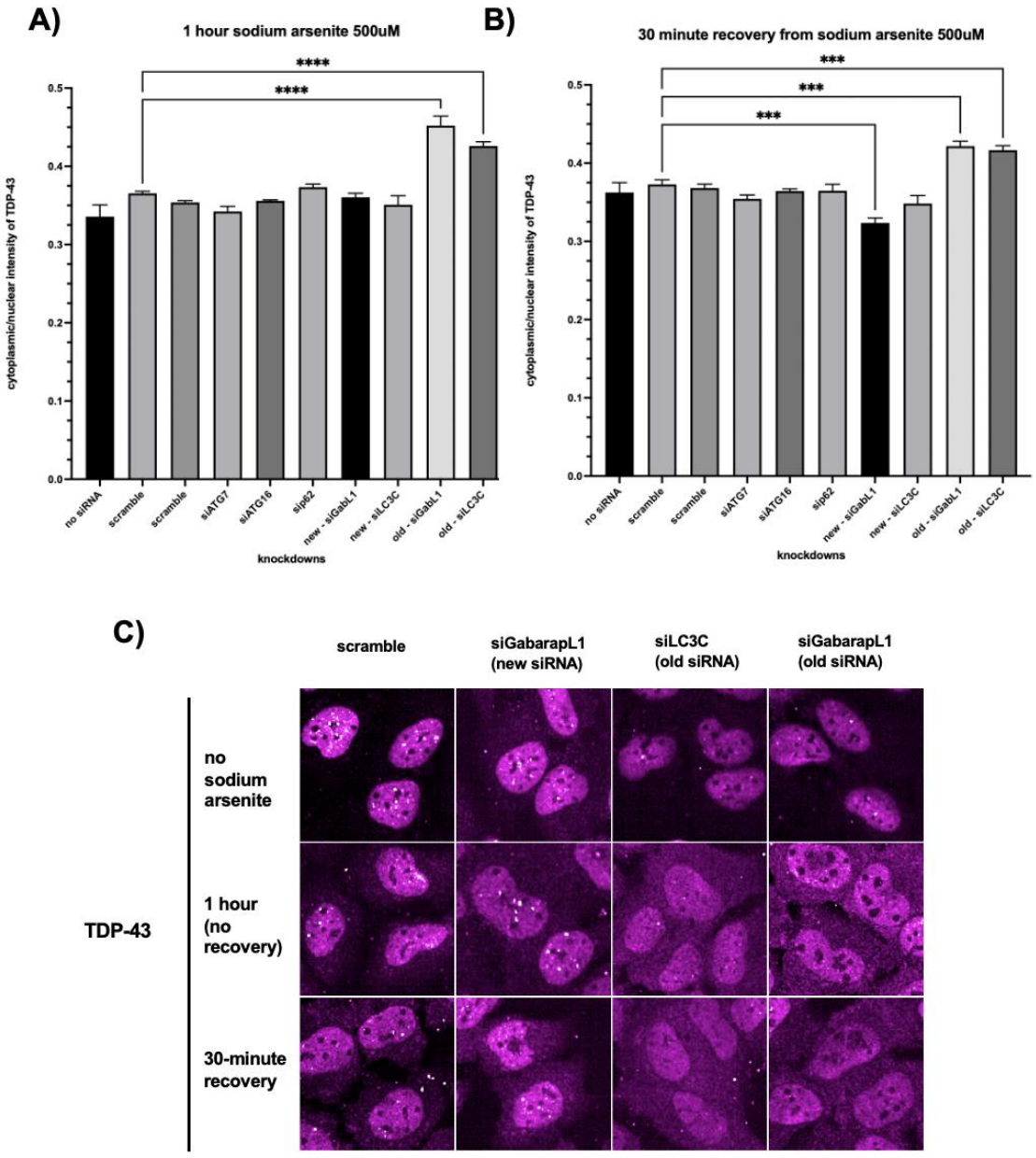

Figure 17. Effects of LC3C knockdown on TDP-43 not validated U2OS eGFP-G3BP2 cells. **(**A)-(B) Representative graphs of stress granules quantified among the various LC3 knockdowns in different timepoints of sodium arsenite. Data consisted of 5 technical replicates/knockdown. Significance testing by One way anova ($p<0.05$). Data represented as means and standard error. C) Representative images of select knockdowns under various sodium arsenite timepoints, showing G3BP2 as eGFP, imaged at 40X on opera phoenix

3.2 Mass Spectrometry:

Protein and exosomes were sent for mass spectrometry to evaluate the effects of LC3/GABARAP knockdown on the proteome of extracellular vesicles (EVs) and U2OS cells. Wild-type U2OS cells were transfected with siRNA for all 6 LC3 homologues collectively (*MAP1LC3A, MAP1LC3B, MAP1LC3C, GABARAP, GABARAPL1* and *GABARAPL2)*, creating a pooled knockdown of all 6 LC3 siRNA. SiRNA was transfected with a 30nM final concentration of the pooled siRNA, collectively. All 6 siLC3s were included in the pooled knockdown to test the effects of all homologues being knocked down collectively rather than comparing each individual LC3 homologue's effects. We first validated the pooled knockdown at increased concentration (30nM) via western blot (Figure 18). Sufficient knockdown of both LC3B and GABARAP were seen. Due to the low antibody specificity of LC3 homologue antibodies, only LC3B and GABARAP were used, which can detect all GABARAP homologues. Afterward, samples were set aside to validate via zeta view in order to confirm that small EVs were detected in extracellular vesicle samples. In our mass spectrometry results, we analyzed both cell lysates and EV samples from wild-type U2OS cells, including a scramble control and pooled knockdown of all LC3 homologues for each. EV markers from Vescilepedia were compared to the current dataset (Figures 19 and 20). All Vesiclepedia proteins were detected in the results (Figure 20). The log2 fold change of EV markers from Vesiclepedia were calculated to see if EV markers were more or less expressed when LC3 was knocked down (Figure 19). For example, RAB7A, GAPDH, PGK1, all of which are common EV markers, were significantly increased in siLC3 EVs. Other EV markers, such as YWHAQ and CFL1 were downregulated (Figure 19).

3.2.1 Upregulated Proteins in LC3/GABARAP depleted cells:

In order to analyze the effects of LC3/GABARAP knockdown in U2OS cells, log2fold change was calculated to determine the upregulation of proteins in LC3 knockdown cells relative to negative control (scramble siRNA) cells. A T-test was conducted to determine significant hits ($p \leq 0.05$) amongst the 3 biological replicates for LC3/GABARAP knockdown cells and scramble control. Amongst the proteins that were upregulated in LC3/GABARAP knockdowns, SQSTM1/p62 and ATG9 were upregulated (Figure 23). These proteins are both involved in the autophagy pathway. In addition, proteins involved in vesicle trafficking such as CHMP1A and CHMP3, as well as SNX3 and SNX5, were also found to be upregulated. CHMP1A and CHMP3 are a part of the ESCRT-III complex and are crucial players in endosomal sorting and EV biogenesis.[111] SNX3 and SNX5 are also apart of intracellular trafficking. These vesicle trafficking proteins may be upregulated due to the downregulation in autophagy, relying on extracellular release of waste.

3.2.2 Only detected in LC3/GABARAP knockdown cells:

In addition, proteins that were completely depleted in cells knocked down for LC3/GABARAP homologues were plotted separately in Figure 22. Although these proteins were not detected in knockdown cell lysate samples, they were significant ($p \leq 0.05$). Ataxin 1-Like (ATXN1L), involved in stress response, was detected, possibly reflecting the accumulation of damaged proteins from LC3 knockdown. In addition, VMA21 involved in lysosomal acidification was present, likely from impaired autophagy and, therefore defective lysosome

function. Concerning vesicle trafficking, we saw expression of TRAPPC10, which is likely upregulated to aid in enhancing vesicle transport.

3.2.3 Downregulated proteins in LC3/GABARAP depleted cells:

Some significant hits ($p \leq 0.05$) that were downregulated in LC3/GABARAP knockdown cells were linked to autophagy and vesicle trafficking processes. Such as autophagy-related proteins: AMBRA1, GABARAPL2 and MAP1LC3B, which are likely downregulated as a direct reflection of the siRNA knockdown (Figure 23). Furthermore, TBK1 was downregulated, which is involved in both autophagy and has been linked to ALS. Vesicle trafficking-related proteins such as: VPS39, VPS45 and Rab GTPase proteins: RAB35, RAB3GAP1, RAB8A were also downregulated.

3.2.4 Depleted in siLC3 cells:

Proteins that were not detected in LC3/GABARAP cell lysates, but were significant have been listed in Figure 22. Some of these included autophagy and vesicle trafficking-related proteins such as: RAB27B, which is linked to vesicle trafficking for lysosomes and exosomes. In addition, we saw a decrease in other proteins responsible for vesicle fusion, such as SNAP25 and VAMP8, which are critical for auto-lysosomal fusion.

3.2.5 EV Samples

EV samples were then analyzed to detect changes in cargo from LC3/GABARAP knockdown. Since LC3 homologues have been implicated in secretion and cargo loading for extracellular vesicles, we compared results with those from the cargo candidates listed in Leidals

et al., 2020 and Debnath et al., 2022, where these homologues were proposed to be implicated in this process. However, both studies used knockout models of ATG12 and ATG7, which are upstream from LC3 homologues. Significant EV hits were also compared to stress granule protein datasets from Anne-Claude Gingras et al., 2018 which identified 1792 stress granule interacting proteins and 144 core stress granule proteins (Figure 29).[112] ALS related proteins were also searched through the data set. Although some of the proteins did not yield significant effects ($p<0.05$), SOD1, FUS and autophagy receptor OPTN were enriched in 2 of 3 EV samples with LC3/GARABAP knockdown. Alternatively, TARDBP and G3BP2 or G3BP1 remained almost unchanged in EV samples from scramble control.

3.2.6 Upregulated proteins in LC3/GABARAP knockdown EVs:

Significant protein hits that were upregulated based on log2fold from EVs isolated from scramble control cells or only detected in LC3/GABARAP knockdown EVs were compared with: LC3B secretory candidates, ATG7 dependent EV cargo candidates and ATG12 EV dependent cargo candidates from Leidals et al.,2020 along with ATG7 dependent EV secretion candidates from BafilomycinA1 treated cells from Debnath et al., 2021. Overlapping proteins are displayed in Figure 25. These proteins were deemed dependent on autophagy machinery and assumed to rely on LC3 homologues for EV secretion. However, a significant amount was shown to be upregulated in the absence of these homologues. Some of these proteins are linked to autophagy as well as vesicle trafficking and even ALS. For example, RPTOR, a part of the mTORC1 complex that negatively regulates autophagy, was packaged into EVs; however, it was deemed dependent on ATG12 machinery.

Furthermore, many hnRNP proteins implicated in RNA binding activities were upregulated in our samples, which is contradictory to being classified as ATG7/ATG12 dependent. Specifically, HNRNPA2B1, which has been implicated in ALS and stress granule dynamics, was upregulated in our EV samples (Figure 24). In Leidal et al., 2020, HNRPNK was described as an LC3-dependent EV cargo candidate but was upregulated in our samples. Lastly, a portion of these are aligned with proteins that have been shown to interact with stress granules based on proximity-labelling studies.[112] When comparing the datasets, only two proteins overlapped with the 144 core stress granule proteins identified in Anne-Claude Gingras et al., 2018. However, 25 proteins identified in our EV hits were stress granule protein interactors (Figure 29 B). Of these 25 proteins, 24 were upregulated in EVs from cells with LC3/GABARAP knockdown. Lastly, significant hits were analyzed via GO enrichment analysis, which revealed RNA binding, protein binding and nucleic acid binding as some of the top molecular functions for proteins enriched in EVs from LC3/GABARAP knockdown (Figure 27). Similarly, GO enrichment analysis identified intracellular anatomical structure, non-membrane bounded organelle, intracellular non-membrane-bounded organelles, and cytosol as some of our EV hits' top significant cellular components (Figure 27).

3.2.7 LC3 dependent EV secretion candidates:

A similar process was repeated for our significant protein hits downregulated in our samples, compared to those datasets listing LC3-dependent EV secretion candidates (Figure 26). There was little overlap between our significant hits deemed LC3-dependent EV secretion candidates and those listed in the ATG7, ATG12 and LC3B-dependent candidates' datasets. Overlapping candidates are listed in Figure 26. Other significant hits classified as candidates in

our dataset included, MAP1LC3B and GABARAPL2, likely a direct reflection of the knockdown. Similarly, we compared our LC3-dependent EV secretion candidates with the stress granule protein datasets from Anne-Claude Gingras et al., 2018, which only revealed one protein overlap. Additionally, no significant molecular functions were identified when analyzing our significant hits on GO enrichment analysis. However, early endosome, bounding membrane organelles, early endosome membrane, endosome and vesicle membrane were the top significant cellular components for proteins downregulated in siLC3/GABARAP EVs.

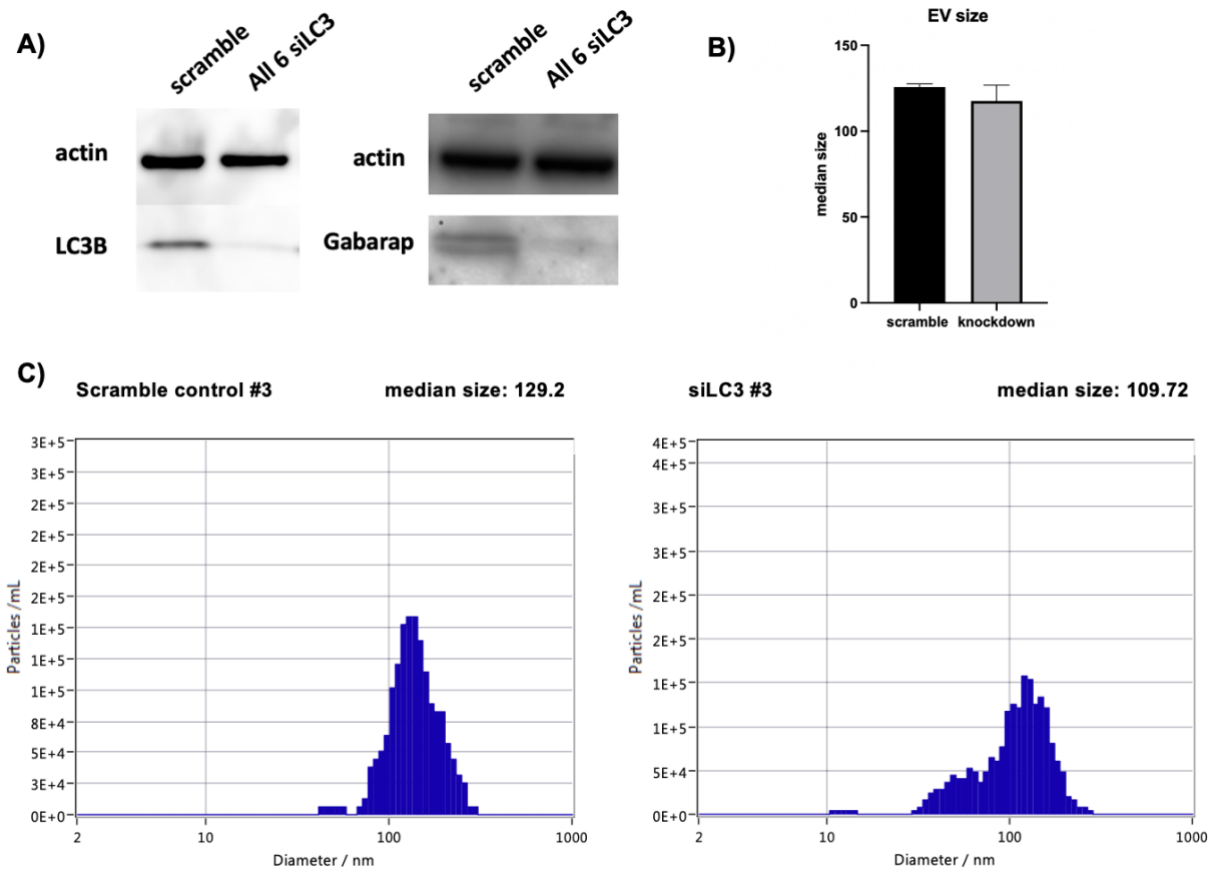

Figure 18. Knockdown validation and exosome validation for mass spectrometry experiments. (A) Representative western blots demonstrating successful knockdown of LC3B and GABARAP in pooled knockdown of all 6siLC3. (n=3). (B) Median EV size of scramble exosomes and exosomes treated with pooled LC3 RNAi. Data presented as means and standard error. (C) Representative zetaview results of EVs treated with scramble RNAi and pooled LC3 RNAi. Showing particles/mL.

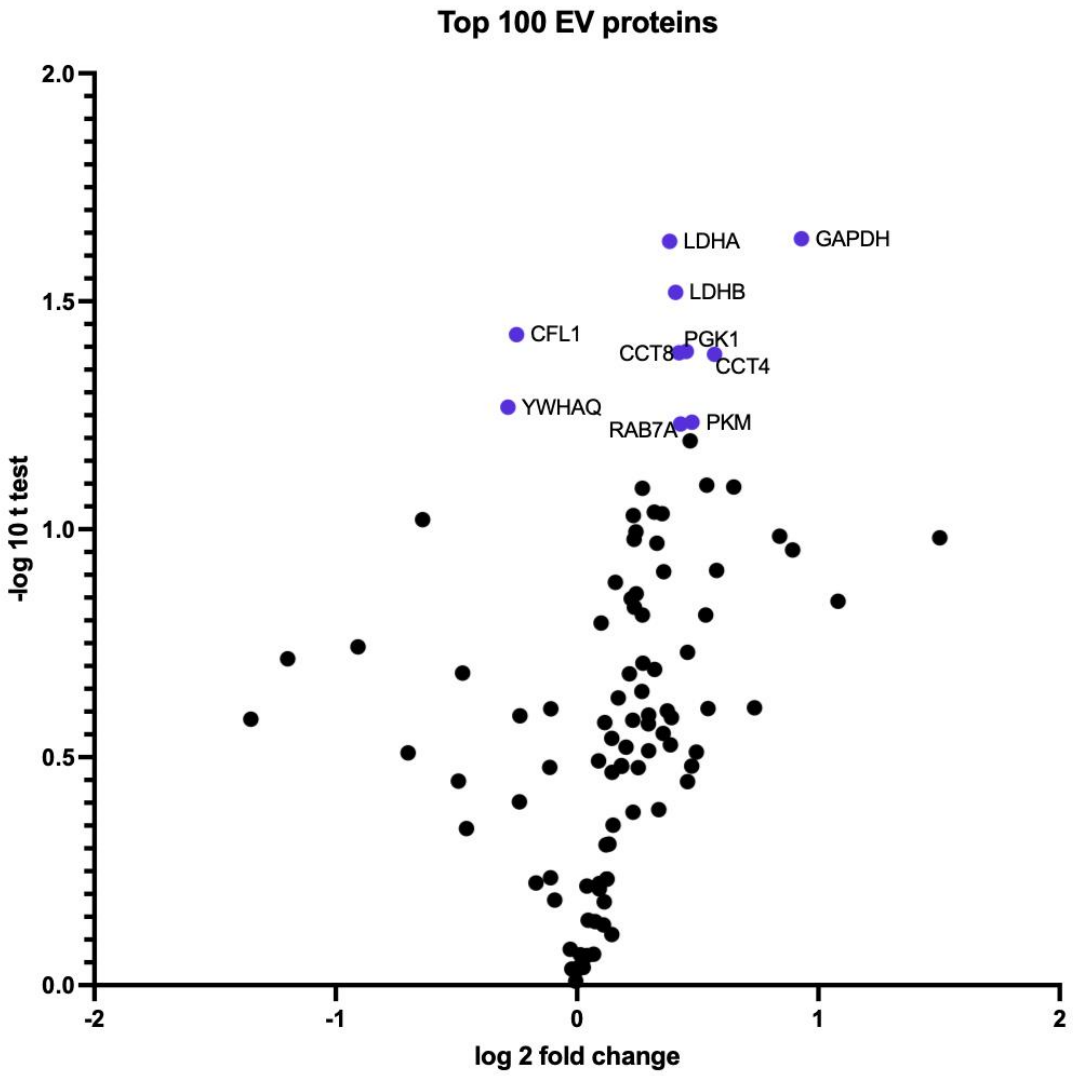

Figure 19. Volcano plot of top 100 EV markers. Purple dots represent significant EV markers ($p \leq 0.05$) that were either increased or decreased in siLC3 extracellular vesicle proteins. (n=3)

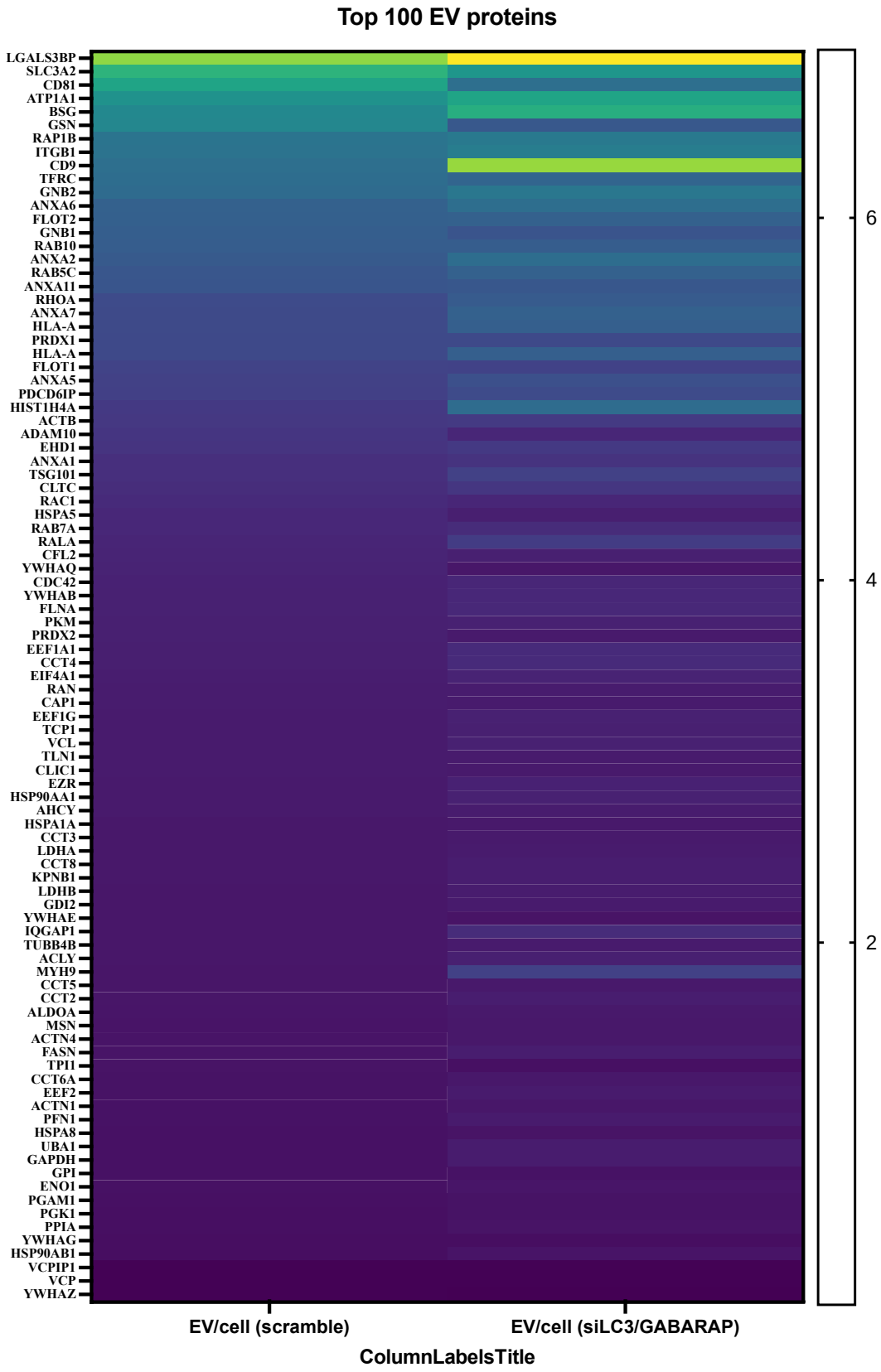

Figure 20. Heat map of top 100 EV markers. Depicted as ratio between EVs and cell samples from scramble control and LC3/GABARAP knockdown. Using top 100 EV protein list from Vesiclepedia. (n=3)

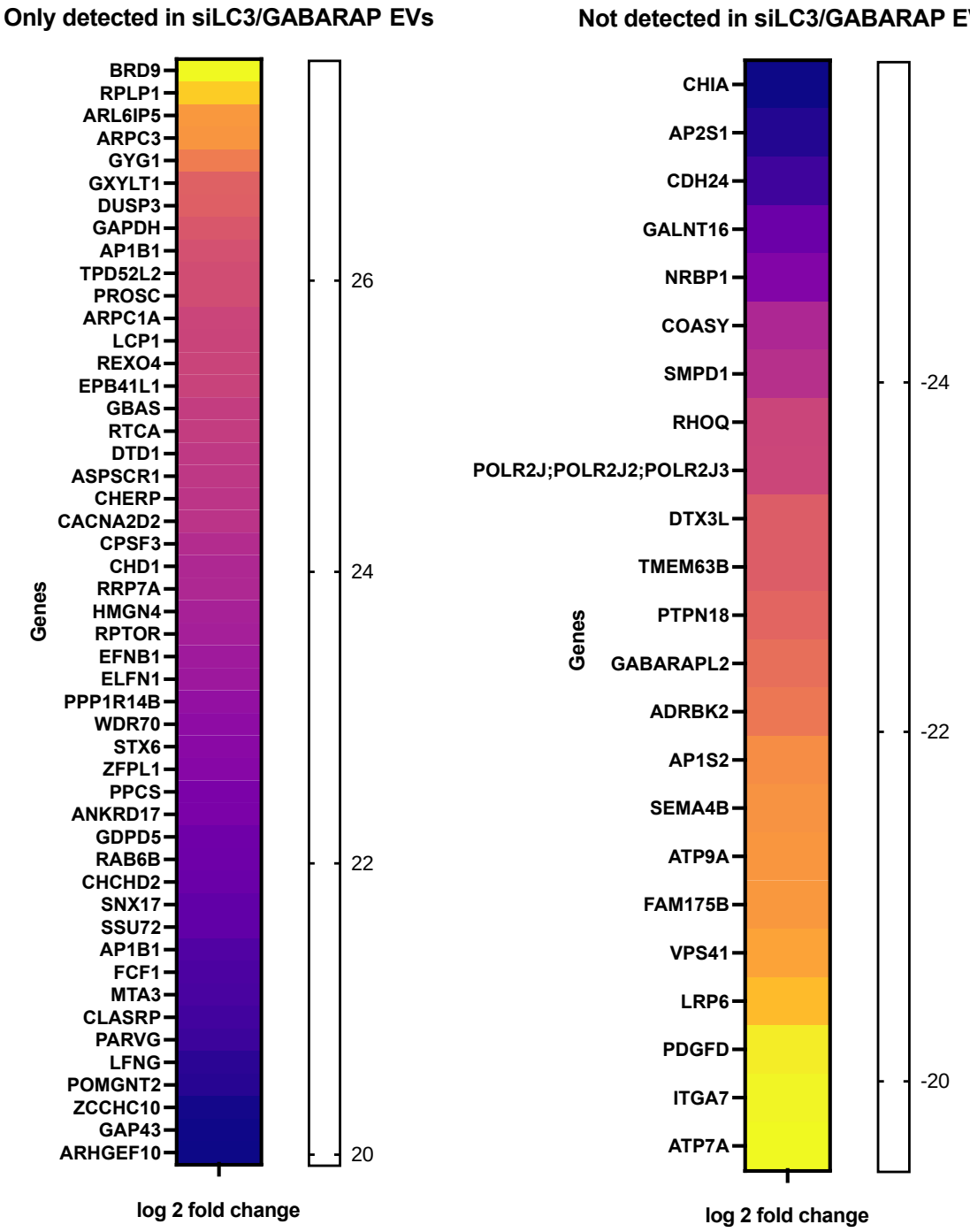

Figure 21. Heat map of genes highly expressed or not detected in siLC3/GABARAP EVs. Represented as log2fold change to wild type EVs. Represented as log2fold change relative to wild type cell lysates. All hits above were significant according to t test ($p \leq 0.05$)

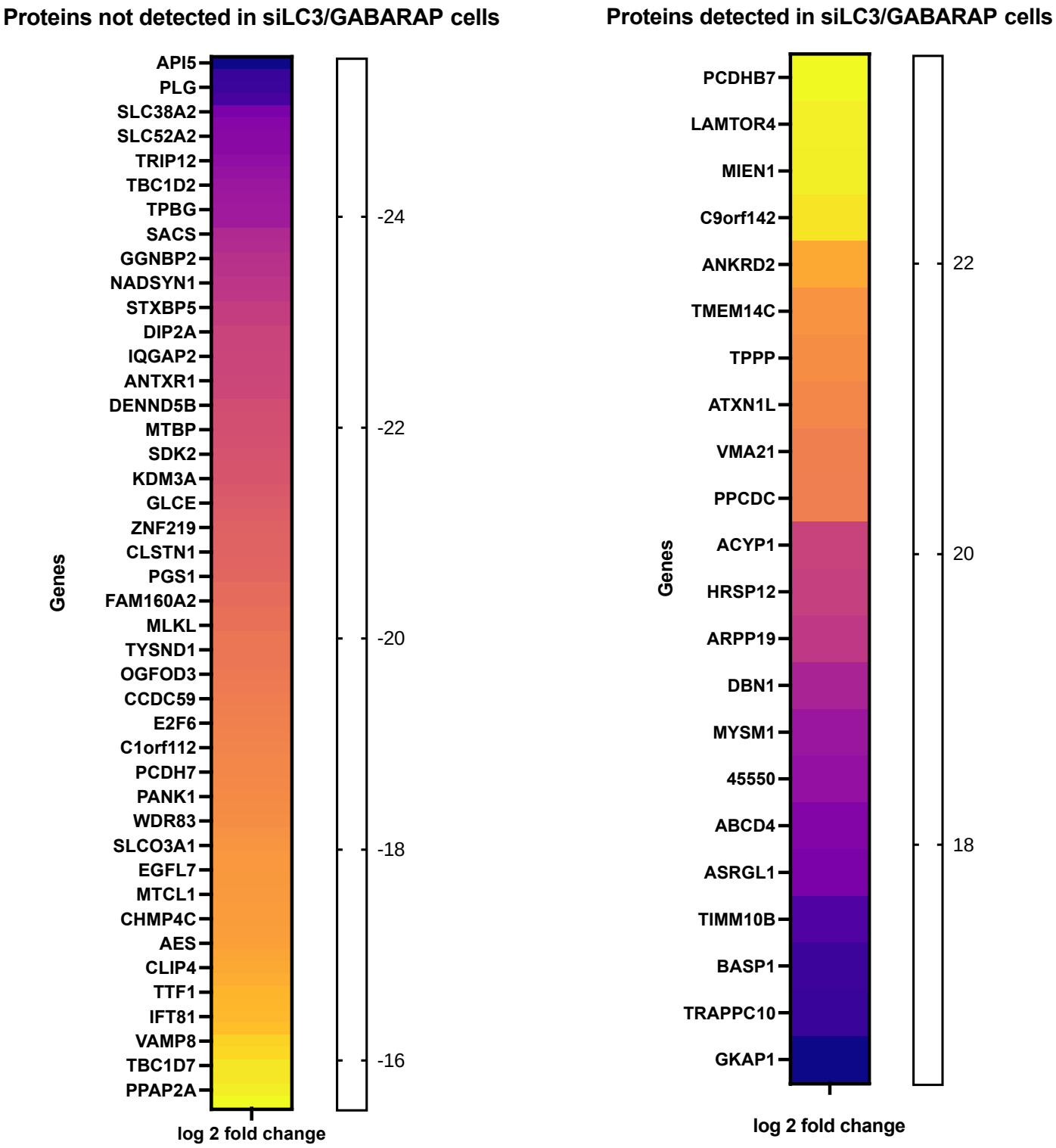

Figure 22. Heat map of genes detected or highly expressed in LC3/GABARAP knockdown cells. Represented as log2fold change relative to wild type cell lysates. All hits above were significant according to t test ($p \leq 0.05$)

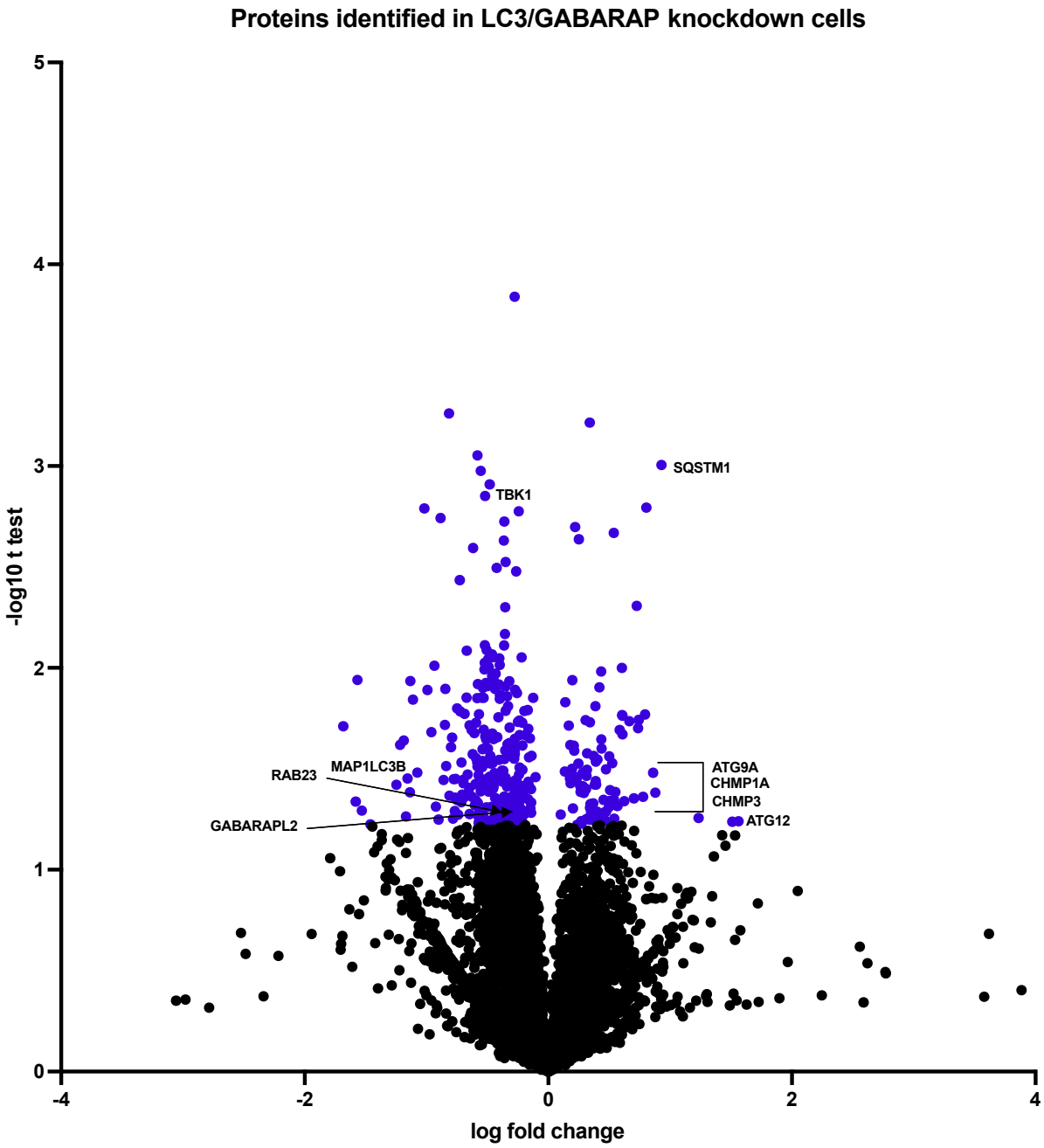

Figure 23. Log2fold change of proteins in U2OS cells with LC3/GABARAP knockdown relative to scramble control. Purple dots represent significant hits ($p \leq 0.05$). Black dots represent hits that were not significant. ATG9A, CHMP1A, CHMP3, ATG12 and P62 displayed upregulation in cells knocked down for LC3/GABARAP. MAP1LC3B, GABARAPL2, RAB23 and TBK1 display downregulation in cells knocked down for LC3/GABARAP.

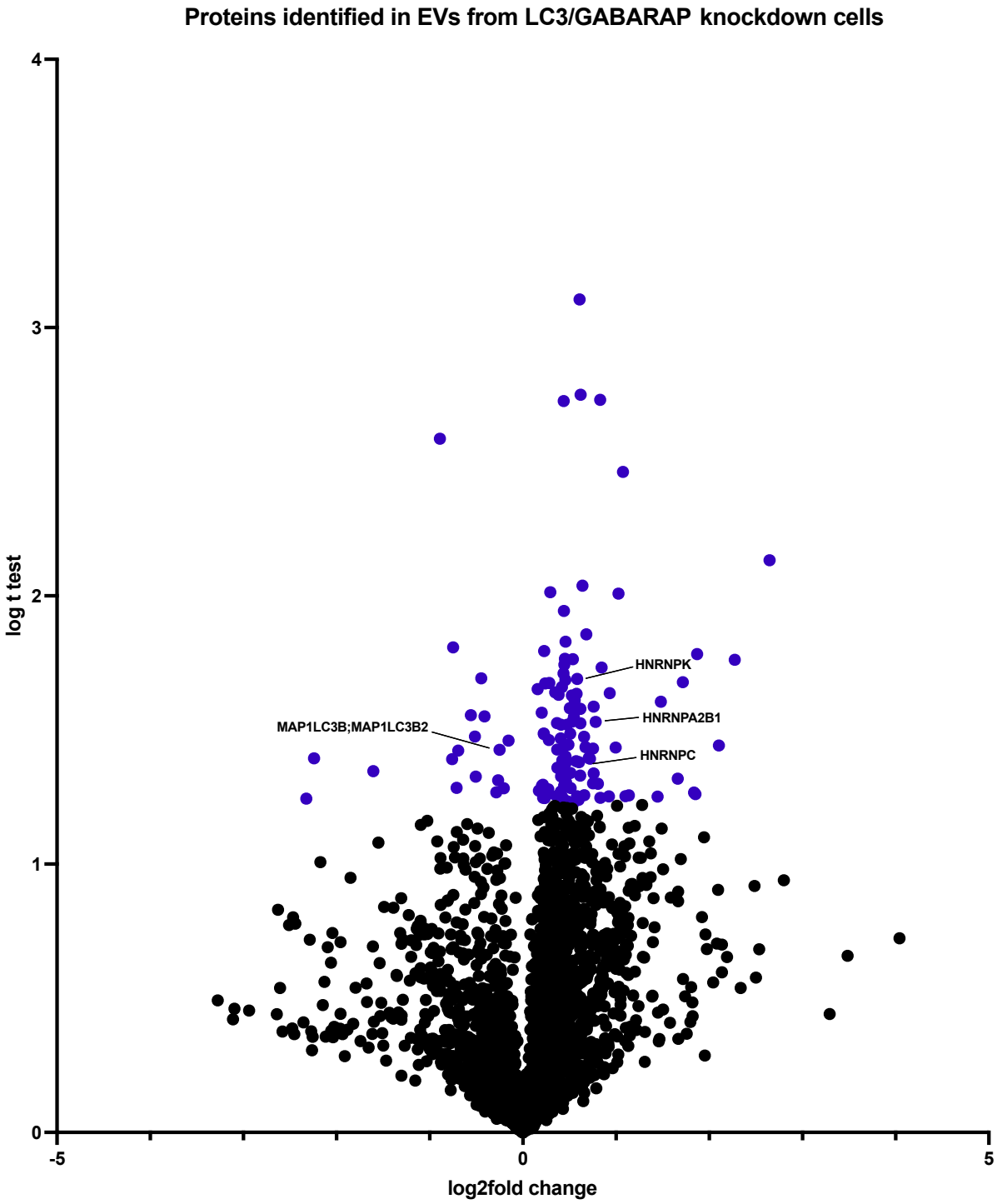

Figure 24. Log2fold change of proteins in EVs from U2OS cells with LC3/GABARAP knockdown relative to EVs from scramble control. Purple dots represent significant hits ($p \leq 0.05$). Black dots represent hits that were not significant. HNRNPK, HNRNPA2B1, HNRNPC displayed upregulation in cells knocked down for LC3/GABARAP. MAP1LC3B, display downregulation in cells knocked down for LC3/GABARAP.

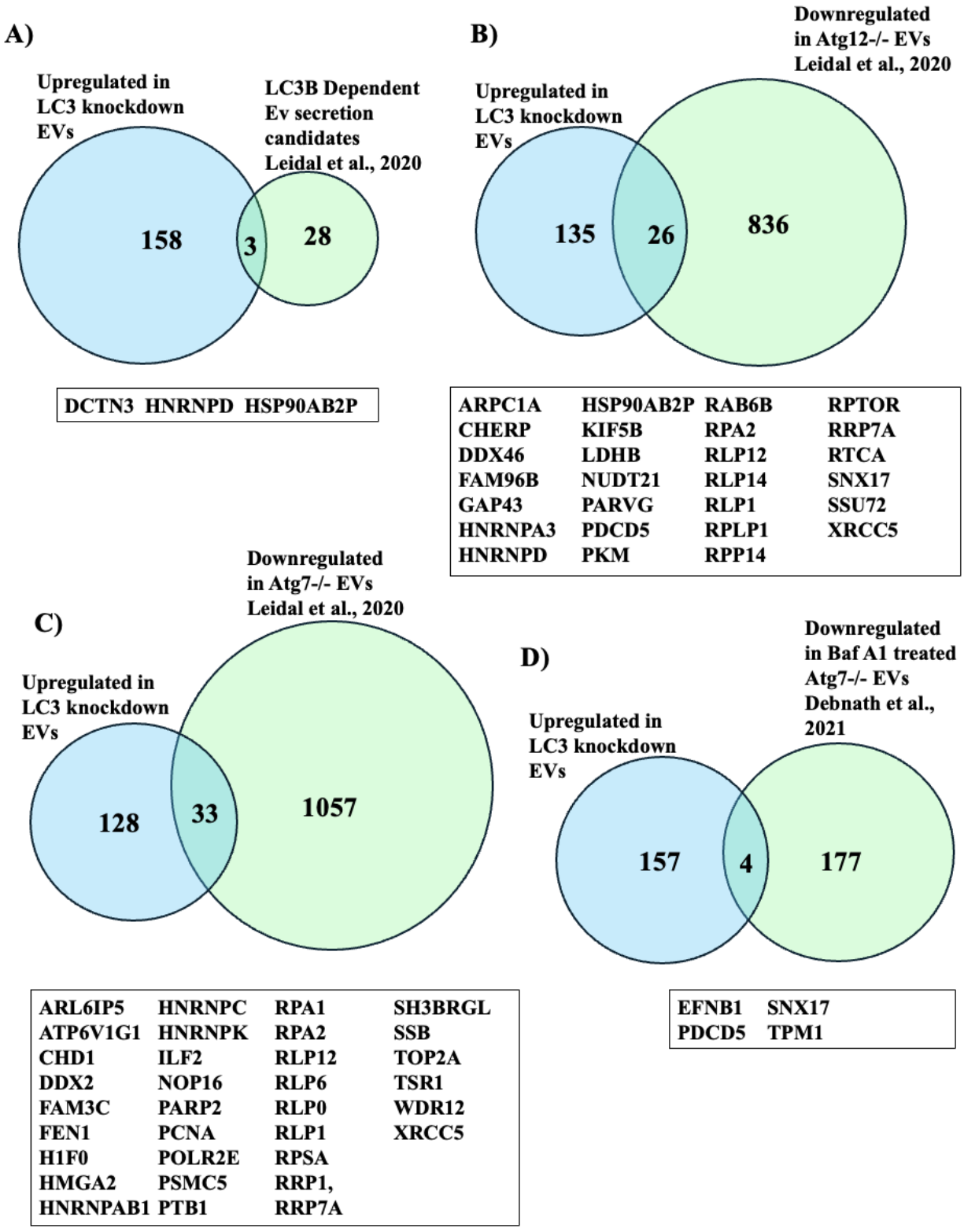

Figure 25. Venn Diagram of overlapping proteins between datasets. Overlap between upregulated proteins in EVs from LC3/GABARAP knockdown cells and A) LC3B Dependent EV secretion candidates from Leidal et al., 2020 B) Downregulated in ATG7-/- EVs from Leidal et al., 2020 C) Downregulated in ATG7-/- EVs from Leidals et al., 2020 D) Downregulated in BafA1 treated ATG7-/- Debnath et al., 2021.

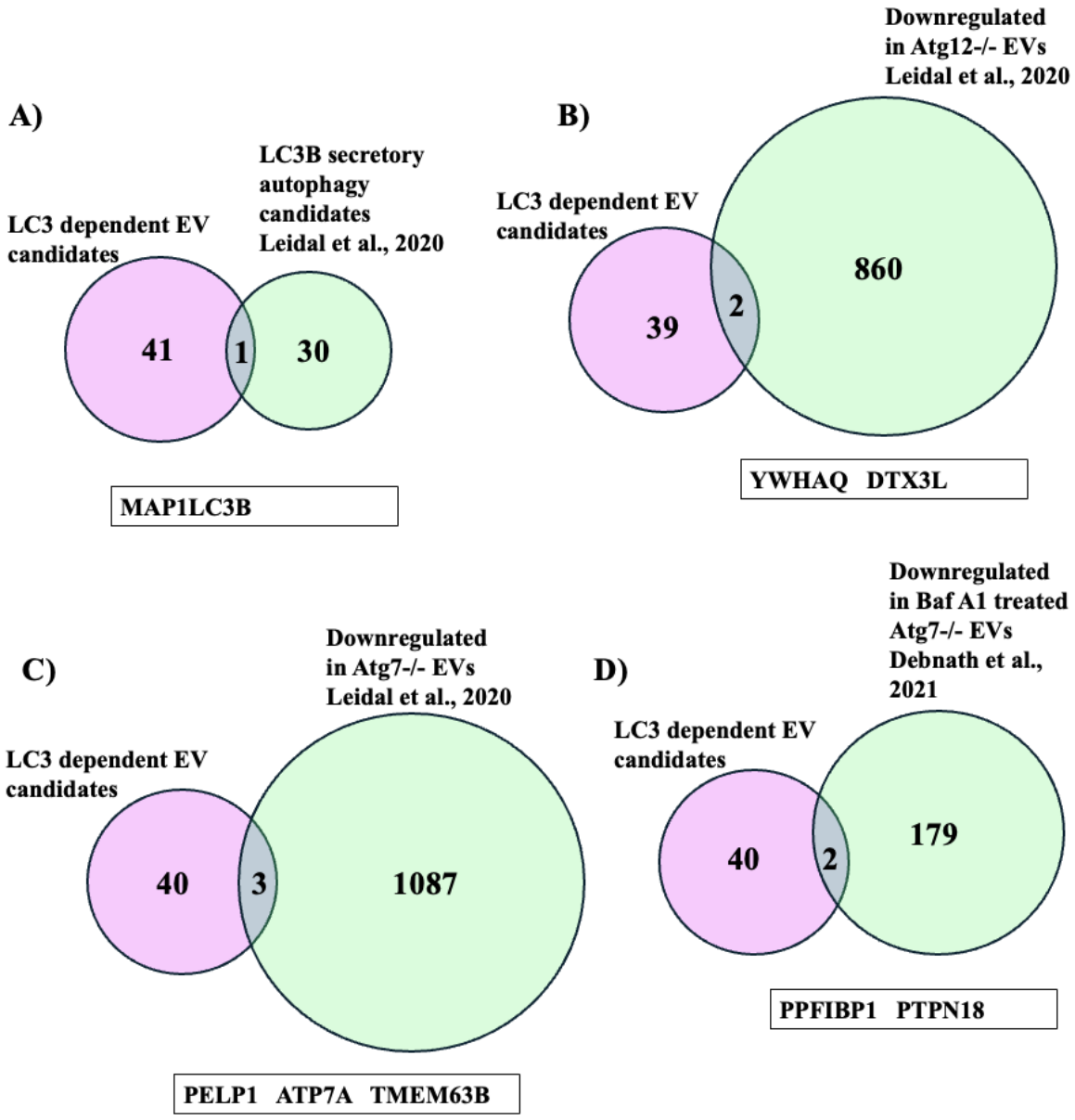

Figure 26. Venn Diagram of overlapping proteins between datasets. Overlap between downregulared proteins in EVs from LC3/GABARAP knockdown cells/LC3 dependent EV candidates and A) LC3B Dependent EV secretion candidates from Leidal et al., 2020 B) Downregulated in ATG7-/- EVs from Leidal et al., 2020 C) Downregulated in ATG7-/- EVs from Leidals et al., 2020 D) Downregulated in BafA1 treated ATG7-/- Debnath et al., 2021.

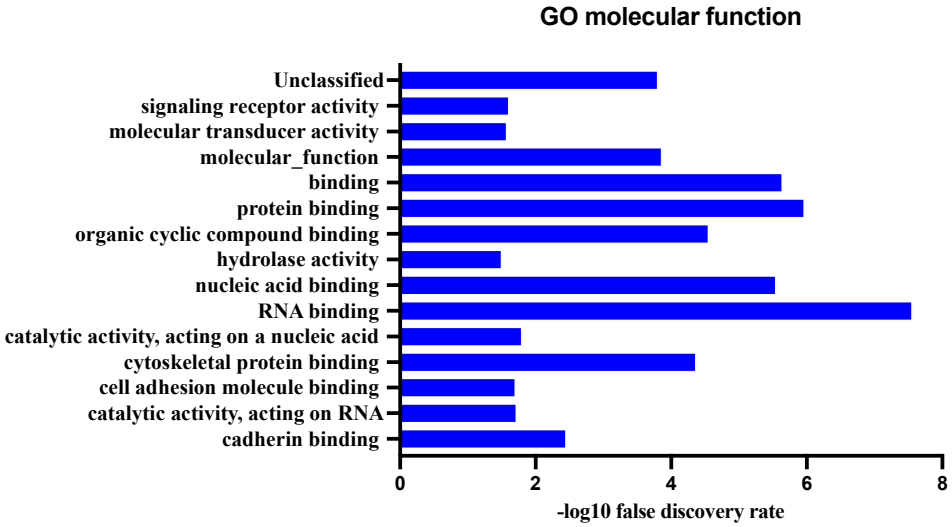
GO molecular function
Unclassified
signaling receptor activity
molecular transducer activity
molecular_function
binding
protein binding
organic cyclic compound binding
hydrolase activity
nucleic acid binding
RNA binding
catalytic activity, acting on a nucleic acid
cytoskeletal protein binding
cell adhesion molecule binding
catalytic activity, acting on RNA
cadherin binding
0
2
4
6
8
-log10 false discovery rate

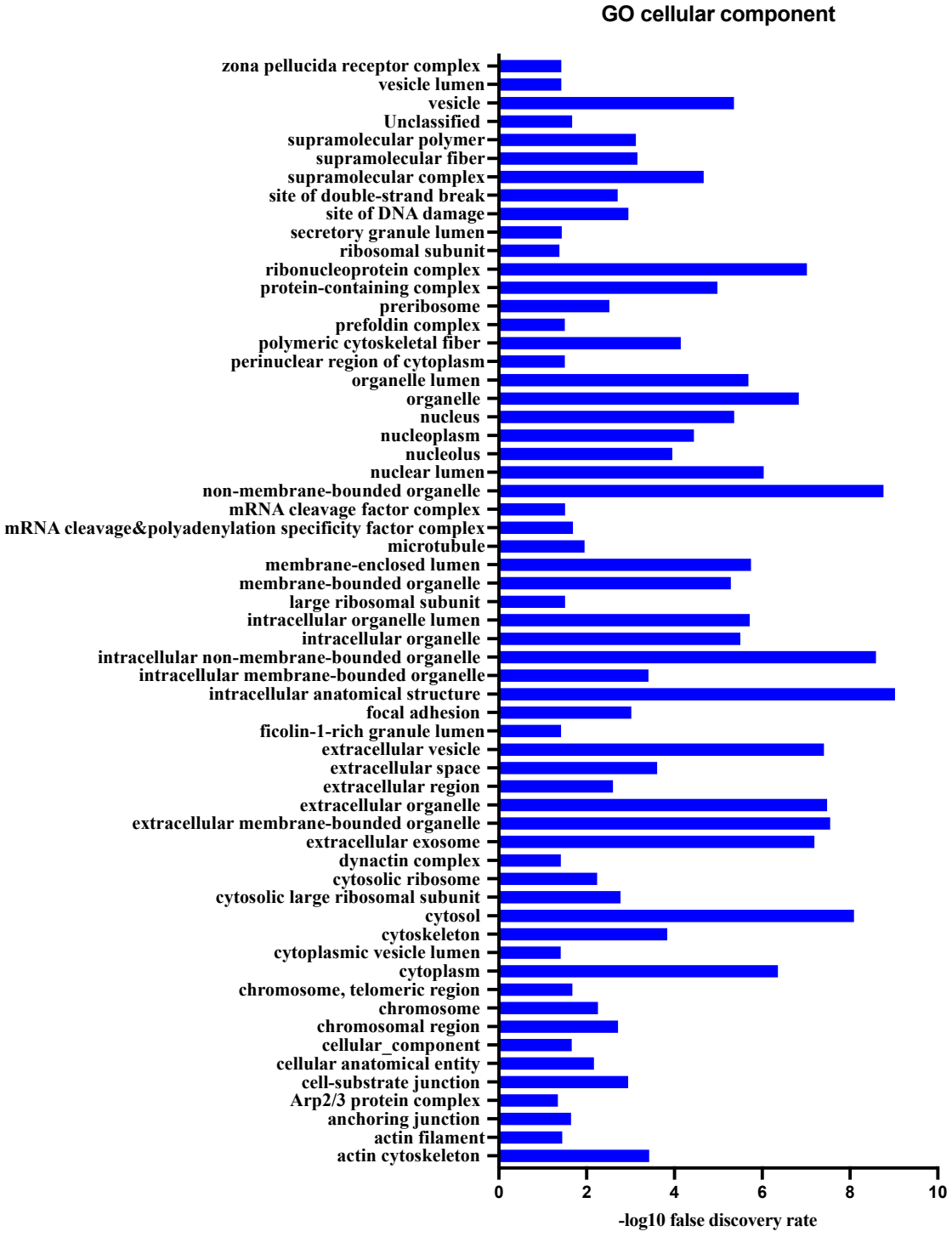
GO cellular component
zona pellucida receptor complex
vesicle lumen
vesicle
Unclassified
supramolecular polymer
supramolecular fiber
supramolecular complex
site of double-strand break
site of DNA damage
secretory granule lumen
ribosomal subunit
ribonucleoprotein complex
protein-containing complex
preribosome
prefoldin complex
polymeric cytoskeletal fiber
perinuclear region of cytoplasm
organelle lumen
organelle
nucleus
nucleoplasm
nucleolus
nuclear lumen
non-membrane-bounded organelle
mRNA cleavage factor complex
mRNA cleavage&polyadenylation specificity factor complex
microtubule
membrane-enclosed lumen
membrane-bounded organelle
large ribosomal subunit
intracellular organelle lumen
intracellular organelle
intracellular non-membrane-bounded organelle
intracellular membrane-bounded organelle
intracellular anatomical structure
focal adhesion
ficolin-1-rich granule lumen
extracellular vesicle
extracellular space
extracellular region
extracellular organelle
extracellular membrane-bounded organelle
extracellular exosome
dynactin complex
cytosolic ribosome
cytosolic large ribosomal subunit
cytosol
cytoskeleton
cytoplasmic vesicle lumen
cytoplasm
chromosome, telomeric region
chromosome
chromosomal region
cellular_component
cellular anatomical entity
cell-substrate junction
Arp2/3 protein complex
anchoring junction
actin filament
actin cytoskeleton
0
2
4
6
8
10
-log10 false discovery rate

Figure 27. Gene Ontology (GO) enrichment analysis of proteins upregulated in EV samples from LC3/GABARAP knockdown. Top Graft demonstrates GO term molecular function, and bottom graft demonstrates GO cellular component. Plotted as -log10 false discovery rate (FDR) ($p \leq 0.05$). Statistical significance determines by Fisher's Exact test.

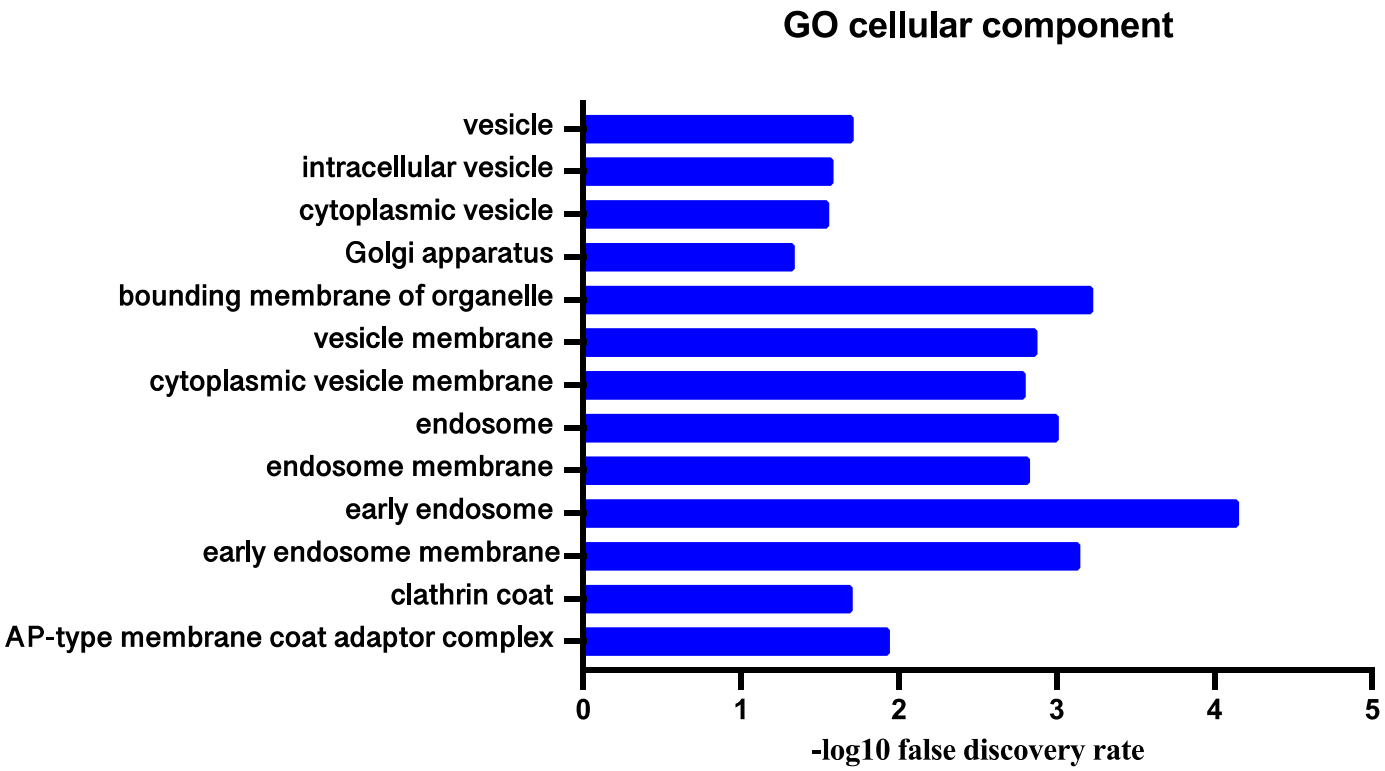

Figure 28. Gene Ontology (GO) enrichment analysis of proteins downregulated in EV samples from LC3/GABARAP knockdown. GO term molecular function, plotted as -log10 false discovery rate (FDR) ($p \leq 0.05$). Statistical significance determines by Fisher's Exact test.

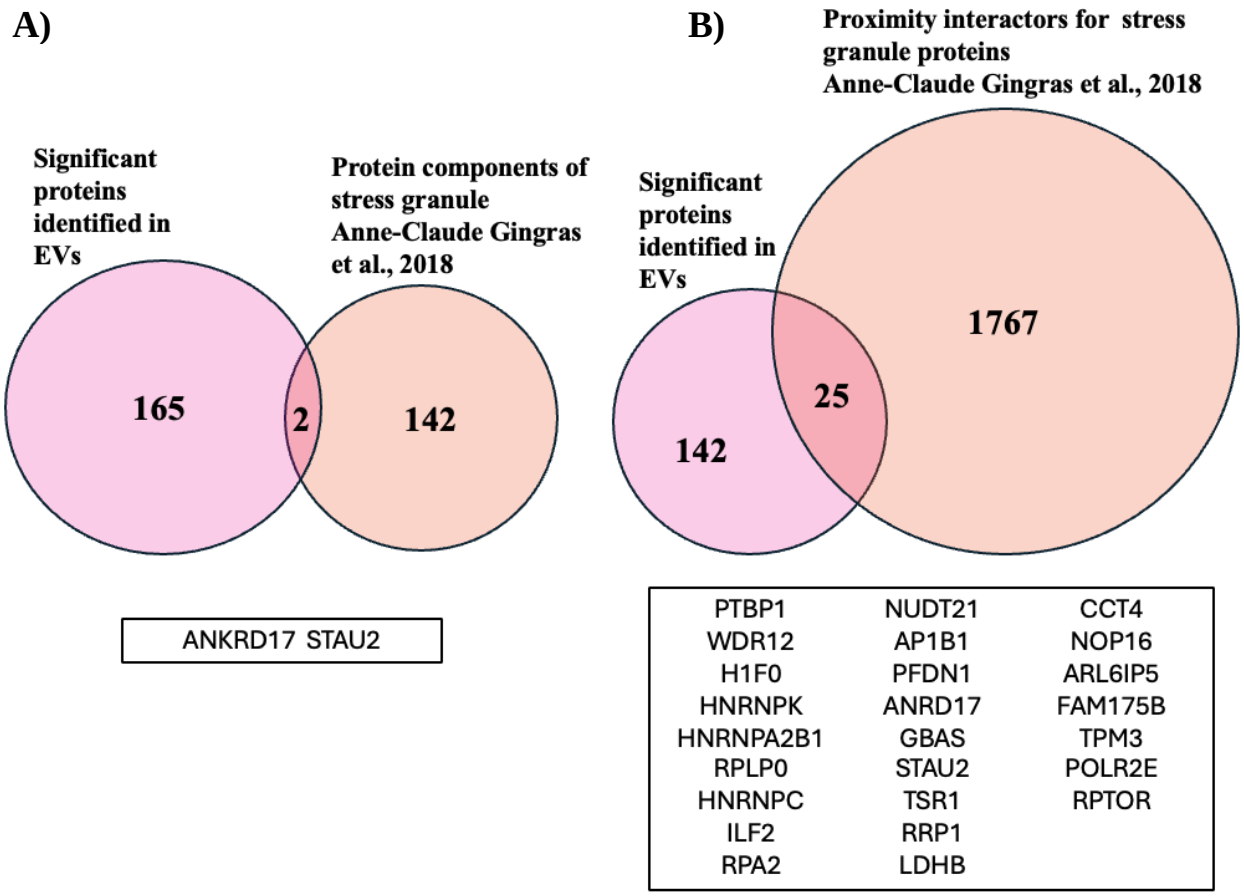

Figure 29. Many proteins in EVs are stress granule proteins. Overlap between significant proteins identified in EVs and A) Top 144 core stress granule proteins identified from Anne-Claude Gringas et al., 2018. B) Top 1792 stress granule protein interactors identified from Anne-Clause Gringas et al., 2018.

Chapter 4: Discussion

The autophagy pathway, termed "self-eating" was discovered in 1963 by Christian de Duve, nearly 8 years later after his discovery of the lysosome.[113] It wasn't until 2000 when the LC3 homologues were discovered. This field is continuously growing as we uncover more mechanisms underlying autophagy. Overtime, autophagy has shown crucial significance in the role of disease as a pathway to target for therapeutic purposes. In many neurodegenerative diseases, we see impairments and defects of the autophagy pathway and amelioration when induced, as well as worsening when further impaired.[83] The functions of autophagy are crucial for proper protein and organelle quality control, proteostasis, and keeping the cell in a healthy state, avoiding extreme cell stress or death.[10] We see examples of this in ALS, where there is a disruption in the autophagy pathway, accumulated autophagy machinery puncta, damaged organelles, increased cell stress and increased protein aggregates. Most ALS cases are sporadic, meaning there are no known family history or identifiable genetic mutations.[1] Although basal autophagy is vital for regular protein quality control, it becomes even more vital in the context of cell stress or disease. Overall, in ALS, we see lower autophagy capacity and flux, which further aids in the pathogenesis of the disease.[83] Currently, there are no cures or effective treatments for the disease, showcasing a need to research better avenues and targets for therapy at the cellular level.

This project aimed to research a set of essential proteins in the autophagy pathway, known as the LC3 homologues. These proteins are essential in the autophagy pathway, as they are responsible for the elongation, formation and closure of the phagophore and the docking sites for targeted cargo. Consisting of 6 proteins total, with unique interactomes and crucial roles in this pathway, each of the homologues displays some individuality, hinting that each may be

crucial for different types of degradation.[32,48,49,114] Not all autophagy receptors have been shown to interact with all LC3 homologues, and some LC3 homologues, for example, LC3C, are crucial in different types of selective autophagy, such as mitophagy.[51] In contrast, other homologues show less interaction with mitophagy-related machinery.[51] In many neurodegenerative diseases, including ALS, impaired autophagy prevents aggregate degradation and leads to persistent stress granules. Autophagy receptors colocalize with substrates such as TDP-43 in ALS, suggesting that their ability to dock on the LC3 and be incorporated into the autophagosome is impaired. By studying each of the 6 homologues, we hope to find one or more homologue that may be more crucial in the clearance of ALS substrates, such as TDP-43 and stress granules.[3,92,115]

The first objective aimed to compare the effects of knocking down each LC3 separately and in pools to determine which knockdown may be more impactful to cytoplasmic TDP-43 and stress granule clearance. This was done using high-throughput imaging microscopy to quantify stress granules per cell in each knockdown and cytoplasmic TDP-43 intensity levels. Although our 500uM sodium arsenite treatment displayed dynamic results and decreased stress granule numbers, the concentration may have influenced this. A very high dose of sodium arsenite may overwhelm the cell's stress responses and survival mechanisms, making it challenging to see effects on stress granule clearance or even stress granule formation. In this same experiment, when we quantified cytoplasmic TDP-43, there was an increase in intensity at baseline in LC3C and GABARAPL1 knockdown. Although this was an interesting effect, it was not consistent in replicates of the experiments. This trend was also inconsistent when using a new siRNA of each homologue. Therefore, this could have been an off-target effect from siRNA transfections.

Furthermore, due to the lack of effects from knockdowns on stress granule clearance at 500uM and concerns that the dosage may have been too high, we repeated the same experiment

at a lower dose of sodium arsenite, still sufficient to see some degree of mislocalization of TDP-43 and formation of stress granules. Both knockdown of GABARAPL1 and GABARAPL2 displayed increased stress granule formation at early recovery from 100uM of sodium arsenite. However, GABARAPL1 knockdown displayed consistent effects through half-hour recovery and one hour. Additionally, LC3C displayed increased stress granules at a later time point. Overall, this highlighted the potential role GABARAPL1 may have on stress granule clearance. Although GABARAPL1 did not consistently affect cytoplasmic TDP-43 clearance, the knockdown of LC3C did throughout the recovery of 100uM sodium arsenite. This highlights the possible specificity of LC3 homologues in the clearance of ALS-related substrates.

4.1 Effects of LC3C may be off target and require further investigation:

However, when we tested a new siRNA for LC3C, the previous effects from siLC3C were not consistent in stalling cytoplasmic TDP-43 clearance. Although the previously used siRNA for LC3C displayed increased cytoplasmic TDP-43 again, we cannot determine whether this is a true effect from this homologue. The inconsistency between the siRNAs for LC3C could be due to off-target effects; using a third siRNA for LC3C or switching to a knockdown model instead would offer clarification. If the trend of LC3C knockdown causing increased cytoplasmic TDP-43 does not reoccur, then we can conclude that the initial effects may have been specific to that siRNA. However, if the trend repeats, other experimental methods, such as validating effects via western blot after subcellular fractionation of cytoplasmic TDP-43, could further elucidate the role.

4.2 GABARAPs display a more significant effect in the clearance of stress granules than LC3s

When comparing the three different pooled knockdowns, siLC3ABC, siGABARAP pool and all 6 siLC3, the siGABARAP pool alone displayed increased stress granules per cell compared to the LC3ABC pool and knockdown of all 6 LC3s collectively. This suggests that the GABARAPs could be more crucial in clearance of stress granules and have a higher specificity for granulophagy than the LC3 homologues. GABARAPs are more essential for the later stages of autophagosome biogenesis than LC3 homologues.[42] Therefore, knockdown of GABARAPs may significantly impact autophagic degradation and the fusion process of the autophagosome and lysosome. This effect could also highlight a higher affinity for stress granule clearance from this sub-family. A similar trend was seen previously in a knockout model, where GABARAP knockouts displayed a higher impact on Parkin mitophagy than the LC3 subfamily knockout, showing that the GABARAP subfamily was more essential for this type of mitophagy. [116] Although this is not directly correlated to stress granule clearance, it further elucidates the specificity in autophagic degradation between LC3 homologues and sub-families. This is thought to be influenced by the different N-terminals amongst the homologues, which are thought to mediate other protein interactions and, therefore, affinity for certain types of autophagy.[36,116,117] Previous proteomic studies have also displayed different interactomes amongst each homologue.[52] Lastly, further validation of these findings is needed to verify the effects of GABARAP sub-family depletion in clearance of stress granules. Repeating this with different siRNA, generating a knockout model, and testing it with different stress granule proteins such as TIA1 could further elucidate this dynamic.

4.3 Knockdown of GABARAPL1 stalls stress granule clearance:

However, both the previously used siRNA and new siRNA for GABARAPL1 displayed increased stress granules from sodium arsenite treatment, further highlighting the potential role of GABARAPL1 in clearance of stress granules. As previously described, different LC3 homologues prefer certain types of autophagy, likely determined by their varying N-terminal structures responsible for protein-protein interactions.[117] The hydrophobic pockets in the N-terminal are responsible for interacting with proteins containing an LIR motif and are shown to display binding preferences with certain LIR containing proteins.[52,117] GABARAPL1 has been shown to interact with p62, which is implicated in stress granule clearance. However, many other LC3 homologues also interact with this receptor. VCP has been identified as an autophagosomal substrate for GABARAPL1 from proximity-labelling experiments. [51] VCP has also been implicated in stress granule disassembly and clearance.[115,118] Investigating the interaction of GABARAPL1 and stress granules by using other stress granule markers in a knockout model and pursuing proteomic-based approaches such as proximity labelling or pulldowns could further elucidate the role this homologue has on stress granule clearance. Lastly, it would be valuable to investigate the relationship and interaction between VCP and GABARAPL1 and whether this is a mechanism by which stress granules are cleared through autophagy. Lastly, GABARAPL1, VCP, and G3BP2 all share interactions with ULK1, and VCP and G3BP1 show direct interactions.[51] How these interact and collectively influence stress granule clearance is unclear, however, we can speculate a possible mechanism in which GABARAPL1 may be essential in this pathway.

4.5 Effects of LC3/GABARAP knockdown on autophagic machinery and ALS substrates:

Our last objective was to investigate the impact of LC3/GABARAP knockdown via siRNA on autophagic machinery and ALS substrates such as TDP-43 and stress granule proteins. Although the LC3/GABARAP knockdown did not display a significant decrease/increase in TDP-43 or G3BP1/G3BP2 levels, however, we detected a substantial increase in autophagy related proteins p62, ATG12 and ATG9A. Increased levels of SQSTM1/p62 are associated with disrupted autophagic degradation and, therefore, accumulated autophagy receptors.[116] This suggests that knockdown of LC3 homologues alone is enough to cause some impairment downstream in the pathway. ATG9A is involved in phagophore nucleation, while ATG12 is a part of the ATG12-ATG5-ATG16L1 complex, which assists in LC3 lipidation to the phagophore.[119] We can speculate that ATG9A and ATG12 may be upregulated due to impaired autophagy and the possible need to upregulate upstream in the pathway to overcompensate for autophagic impairment. Lastly, we see a rise in proteins associated with autophagy, such as ESCRT components CHMP1A and CHMP3.[111,120] The ESCRT complex is involved in the later stages of autophagy, such as autophagosome maturation as well as the release of ILVs from MVBs in late endosomes.[120] The upregulation of ESCRT-III components may be a compensatory response to continue autophagosome maturation in the absence of LC3 homologues or upregulate EV secretion. Knockdown of RAB27b can lead to LC3 and p62 accumulation, likely from inhibited autophagic flux, which suggests its involvement in later stages of autophagy.[121] Therefore, the depletion of RAB27b during knockdown of LC3/GABARAP homologues may reflect a mutual influence of these proteins.[121] More specifically, RAB23 has been implicated in the fusion of Golgi-derived autophagic vesicles (GcAVs) with lysosomes, displaying an important role in later stages of autophagy.[122] Lastly, we

see a depletion of VAMP8, which is also involved in autophagosome-lysosome fusion.[123] The downregulation of these proteins involved in later stages of autophagy from LC3/GABARAP knockdown highlights the possible impairment in autophagosome biogenesis and connection to these homologues. Lastly, TBK1, which is involved in the early stages of autophagy, such as recruitment of ATGs to the PI3KC3 complex, was downregulated. Loss of function mutations in TBK1 are linked to ALS; therefore, this offers another mechanism by which TBK1 and autophagy might be implicated in the disease.[111,123] If TBK1 is downregulated after LC3/GABARAP knockdown, this could further impair the autophagy pathway.

4.6 LC3 independent EV secretion candidates:

LC3 homologues have been implicated as crucial players in autophagy, although they have also been associated with secretory pathways such as the loading of cargo and secretion of EVs. Literature has proposed several pathways, such as SALI and LDELS, which implicate the importance of LC3 homologues in loading extracellular vesicles. Specifically, SALI implies that when the lysosome is inhibited or there is a disruption to the lysosomal degradation of autophagic cargo, the cargo is redirected for secretion via EVs. The LDELS paper implied that LC3 was responsible for loading RBPs into EVs based on ATG7 and ATG12 knockout models, similar to the SALI paper. Although they also analyzed the LC3B secretome, we know that each homologue has a unique interactome, meaning the LC3B secretome is not an accurate glimpse of the influence in EV secretion from LC3 homologues.[51,52] Lastly, although ATG7 and ATG12 knockout models provided a significant impact on cargo loading of EVs and implicated an essential role for ATG homologues outside of classical autophagy, it is hard to say if LC3 homologues themselves are responsible for these results.

In our results, many significant hits from Debnath et al., 2021 and Leidal et al., 2020 were upregulated in our data. For example, the hnRNP proteins, particularly HNRNPK, were suggested to interact with LC3 and be enriched in LC3 lipidated EVs. However, during the knockdown of these homologues, HNRNPK was upregulated in EV samples. The presence of numerous ATG7, ATG12 and LC3B EV cargo candidates in our samples, despite the knockdown of LC3/GABARAP, suggests that the packing of those proteins could be directly associated with ATG7 or ATG12 themselves or influences by another protein upstream from LC3. Further investigation using other LC3 homologues for proximity labelling could better decipher their secretomes. Another protein worth noting was the increased secretion of HNRNPA2B1 and other hnRNPs.[2] HnRNP proteins have been associated with ALS, specifically HNRNPA2B1, suggesting that increased secretion into EVs may reflect the cell trying to mitigate accumulated hnRNPs in the cytoplasm due to LC3 knockdown. Lastly, many of the proteins upregulated in these EV samples demonstrated overlap with stress granule interacting proteins identified in proteomics studies.[112] Furthermore, when we performed GO enrichment analysis, some of the top molecular functions consisted of RNA and protein binding. Lastly, GO analysis revealed intracellular non-membrane-bounded organelles as one of the top cellular components which align with stress granules. We can suggest that the rise in RBPs and stress granule related proteins is a sign of accumulated RBPs in the cytoplasm due to LC3/GABARAP knockdown. Knockdown of LC3/GABARAP impairs autophagy and, therefore is likely to increase cell stress, rerouting stress granule related proteins into EVs as a way to reroute and secrete accumulated cytoplasmic proteins outside of the cell.

4.5 LC3-dependent EV cargo candidates don't align with ATG-dependent cargo candidates:

Many of our significant hits downregulated in EVs from LC3/GABARAP knockdown cells did not align with those from Debnath et al., 2021 and LDELS et al., 2020. Of 1092 proteins identified as ATG7 dependent, only four were significantly downregulated in LC3/GABARAP knockdown EVs, such as TOP2A, PELP1, ATP8A and TMEM63B. Comparing the significant hits in EVs listed in our dataset with those deemed ATG12 dependent from the same paper, only two were downregulated in our siLC3 EVs. Similarly, RAB27a and SNAP29 were identified as a required protein for EV secretion of autophagy cargo when the lysosome is inhibited, and when depleted, displayed accumulation intracellularly of p62.[5] We did not see any effects on RAB27a or SNAP29 in our dataset, although there was cellular accumulation of p62. Although there appears to be little overlap with the secretome identified in SALI and LDELS studies, there is no doubt that silencing LC3 homologues has a negative impact on vesicle trafficking-related proteins and downstream effects on autophagic machinery. However, the mechanism of exporting autophagic cargo through the secretion of EVs may be a pathway exercised when LC3 is knocked down, demonstrating that the path may rely on other autophagic machinery rather than LC3 homologues themselves. Knockout models may help further elucidate this role and investigate the interaction of upstream ATG proteins in EV pathways. However, one limitation of this study was the absence of chemical stressors that induce a more ALS-related model. Using a bafilomycin treatment to impair lysosomal degradation may have demonstrated more overlap with the Debnath et al. dataset. Using sodium arsenite to induce stress granule formation and TDP-43 mislocalization could have provided a better insight into the effects of LC3/GABARAP knockdown on a larger scale.

Chapter 5: Conclusion

This thesis further demonstrates the differences and selectivity among the various LC3 homologues and their targets. Among the various LC3 homologues, not all have an equal impact on the degradation of ALS-related substrates, TDP-43 and G3BP2; the latter being a core stress granule marker. Although there was no consistently significant impact on the clearance of cytoplasmic TDP-43, GABARAPL1 significantly impacted the degradation of stress granules. Further experiments analyzing the degradation of stress granules by GABARAPL1 using other stress granule markers such as TIA1 and FUS may provide better insight. Investigating the role of VCP and GABARAPL1 in the clearance of stress granules may offer a new mechanism in which autophagy is responsible for the clearance of stress granules and how depletion of GABARAPL1 may be implicated in ALS pathogenesis. Expanding the role of GABARAPL1 and its interactome may provide great insight into its role in stress granule dynamics. This could be accomplished through sodium arsenite treatment (to mimic ALS cell phenotypes) in conjunction with proximity labelling and pulldowns.

Further investigation into the role of LC3C in the degradation of TDP-43 may clarify the relationship using knockout models or another siRNA. Similarly, although our proteomics did not reveal many ALS-related proteins to be accumulated, there was a significant increase in autophagy-related components. Specifically, the upregulation of p62, which signals impaired autophagy and increased ATG proteins, will likely compensate for LC3 knockdown.

Additionally, downstream proteins of LC3 were downregulated, suggesting a possible interruption in autolysosome fusion events and providing further evidence that these homologues are crucial for downstream events in autophagy. It is unclear whether LC3 proteins are responsible for the secretion of autophagy receptors and other cargo candidates, as suggested by

Leidal et al., 2020 and Debnath et al., 2021. However, the knockdown of LC3 homologues displayed increased secretion for many of these candidates, contradicting the role of these homologues that have been previously suggested. Specifically, multiple RBPs and stress granule interacting proteins were upregulated in EVs from LC3/GABARAP knockdown cells, suggesting an accumulation of these proteins in the cytoplasm due to autophagy impairment and shunting these proteins for secretion via EVs in an LC3-independent manner. Further experiments investigating the proteomic effects of various LC3 knock outs and knock downs would elucidate their effects on TDP-43 and stress granule clearance, and cargo loading into EVs. Sodium arsenite treatment would better depict what might happen at the proteomic level when LC3 homologues are depleted during oxidative stress.

LC3 homologues alone inflicted impaired autophagic degradation, displaying that these proteins may be beneficial to target therapeutically in the context of ALS and other neurodegenerative diseases with impaired autophagy. Lastly, the relationship between GABARAPL1 and stress granule clearance may offer insight into how these dynamics are perturbed in ALS and intertwined with the autophagy pathway. If autophagy is disrupted in ALS, autophagy-related cargo could be released through EVs as a compensatory mechanism; therefore, disruption to this pathway would promote further accumulation of aggregated proteins in the cytoplasm. Further research to narrow down what this pathway relies on could help determine a therapeutic target.

References:

1. Suk TR, Rousseaux MWC. The role of TDP-43 mislocalization in amyotrophic lateral sclerosis. *Mol Neurodegener*. 2020;15(1). doi:10.1186/s13024-020-00397-1
2. Wolozin B, Ivanov P. Stress granules and neurodegeneration. *Nat Rev Neurosci*. 2019;20(11):649-666. doi:10.1038/s41583-019-0222-5
3. Monahan Z, Shewmaker F, Pandey UB. Stress granules at the intersection of autophagy and ALS. *Brain Res*. 2016;1649:189-200. doi:10.1016/j.brainres.2016.05.022
4. Leidal AM, Huang HH, Marsh T, et al. The LC3-conjugation machinery specifies the loading of RNA-binding proteins into extracellular vesicles. *Nat Cell Biol*. 2020;22(2):187-199. doi:10.1038/s41556-019-0450-y
5. Solvik TA, Nguyen TA, Lin YHT, et al. Secretory autophagy maintains proteostasis upon lysosome inhibition. *Journal of Cell Biology*. 2022;221(6). doi:10.1083/jcb.202110151
6. Parzych KR, Klionsky DJ. An overview of autophagy: Morphology, mechanism, and regulation. *Antioxid Redox Signal*. 2014;20(3):460-473. doi:10.1089/ars.2013.5371
7. Raffeiner M, Zhu S, González-Fuente M, Üstün S. Interplay between autophagy and proteasome during protein turnover. *Trends Plant Sci*. 2023;28(6):698-714. doi:10.1016/j.tplants.2023.01.013
8. Bashore C, Prakash S, Johnson MC, et al. Targeted degradation via direct 26S proteasome recruitment. *Nat Chem Biol*. 2023;19(1):55-63. doi:10.1038/s41589-022-01218-w
9. Dikic I, Elazar Z. Mechanism and medical implications of mammalian autophagy. *Nat Rev Mol Cell Biol*. 2018;19(6):349-364. doi:10.1038/s41580-018-0003-4
10. Yang Z, Klionsky DJ. Mammalian autophagy: Core molecular machinery and signaling regulation. *Curr Opin Cell Biol*. 2010;22(2):124-131. doi:10.1016/j.ceb.2009.11.014
11. He C, Klionsky DJ. Regulation mechanisms and signaling pathways of autophagy. *Annu Rev Genet*. 2009;43:67-93. doi:10.1146/annurev-genet-102808-114910
12. Jewell JL, Russell RC, Guan KL. Amino acid signalling upstream of mTOR. *Nat Rev Mol Cell Biol*. 2013;14(3):133-139. doi:10.1038/nrm3522
13. Russell RC, Yuan HX, Guan KL. Autophagy regulation by nutrient signaling. *Cell Res*. 2014;24(1):42-57. doi:10.1038/cr.2013.166
14. King KE, Losier TT, Russell RC. Regulation of Autophagy Enzymes by Nutrient Signaling. *Trends Biochem Sci*. 2021;46(8):687-700. doi:10.1016/j.tibs.2021.01.006
15. Zhang W, Li X, Wang S, Chen Y, Liu H. Regulation of TFEB activity and its potential as a therapeutic target against kidney diseases. *Cell Death Discov*. 2020;6(1). doi:10.1038/s41420-020-0265-4
16. Sardiello M, Palmieri M, di Ronza A, et al. A Gene Network Regulating Lysosomal Biogenesis and Function. *Science (1979)*. 2009;325(5939):473-477. doi:10.1126/science.1174447
17. Settembre C, Zoncu R, Medina DL, et al. A lysosome-to-nucleus signalling mechanism senses and regulates the lysosome via mTOR and TFEB. *EMBO Journal*. 2012;31(5):1095-1108. doi:10.1038/emboj.2012.32
18. Nguyen A, Faesen AC. The role of the HORMA domain proteins ATG13 and ATG101 in initiating autophagosome biogenesis. *FEBS Lett*. 2024;598(1):114-126. doi:10.1002/1873-3468.14717
19. Nishimura T, Tooze SA. Emerging roles of ATG proteins and membrane lipids in autophagosome formation. *Cell Discov*. 2020;6(1). doi:10.1038/s41421-020-0161-3

20. Sakoh-Nakatogawa M, Matoba K, Asai E, et al. Atg12-Atg5 conjugate enhances E2 activity of Atg3 by rearranging its catalytic site. *Nat Struct Mol Biol*. 2013;20(4):433-439. doi:10.1038/nsmb.2527
21. Lamb CA, Yoshimori T, Tooze SA. The autophagosome: Origins unknown, biogenesis complex. *Nat Rev Mol Cell Biol*. 2013;14(12):759-774. doi:10.1038/nrm3696
22. Mailler E, Guardia CM, Bai X, et al. The autophagy protein ATG9A enables lipid mobilization from lipid droplets. *Nat Commun*. 2021;12(1). doi:10.1038/s41467-021-26999-x
23. Cherra SJ, Kulich SM, Uechi G, et al. Regulation of the autophagy protein LC3 by phosphorylation. *Journal of Cell Biology*. 2010;190(4):533-539. doi:10.1083/jcb.201002108
24. Jiang W, Chen X, Ji C, et al. Key regulators of autophagosome closure. *Cells*. 2021;10(11). doi:10.3390/cells10112814
25. Takahashi Y, He H, Tang Z, et al. An autophagy assay reveals the ESCRT-III component CHMP2A as a regulator of phagophore closure. *Nat Commun*. 2018;9(1). doi:10.1038/s41467-018-05254-w
26. McEwan DG, Popovic D, Gubas A, et al. PLEKHM1 regulates autophagosome-lysosome fusion through HOPS complex and LC3/GABARAP proteins. *Mol Cell*. 2015;57(1):39-54. doi:10.1016/j.molcel.2014.11.006
27. Mauvezin C, Nagy P, Juhász G, Neufeld TP. Autophagosome-lysosome fusion is independent of V-ATPase-mediated acidification. *Nat Commun*. 2015;6. doi:10.1038/ncomms8007
28. Nakatogawa H, Ichimura Y, Ohsumi Y. Atg8, a Ubiquitin-like Protein Required for Autophagosome Formation, Mediates Membrane Tethering and Hemifusion. *Cell*. 2007;130(1):165-178. doi:10.1016/j.cell.2007.05.021
29. Weidberg H, Shvets E, Shpilka T, Shimron F, Shinder V, Elazar Z. LC3 and GATE-16/GABARAP subfamilies are both essential yet act differently in autophagosome biogenesis. *EMBO Journal*. 2010;29(11):1792-1802. doi:10.1038/emboj.2010.74
30. Kabeya Y, Mizushima N, Yamamoto A, Oshitani-Okamoto S, Ohsumi Y, Yoshimori T. LC3, GABARAP and GATE16 localize to autophagosomal membrane depending on form-II formation. *J Cell Sci*. 2004;117(13):2805-2812. doi:10.1242/jcs.01131
31. Kabeya Yukiko, Noboro Mizushima, Takashi Ueno, et al. LC3, a mammalian homologue of yeast Apg8p, is localized in autophagosome membranes after processing. *EMBO J*. Published online September 11, 2000. Accessed October 10, 2024. https://doi.org/10.1093%2Femboj%2F19.21.5720
32. Johansen T, Lamark T. Selective Autophagy: ATG8 Family Proteins, LIR Motifs and Cargo Receptors. *J Mol Biol*. 2020;432(1):80-103. doi:10.1016/j.jmb.2019.07.016
33. Varga VB, Keresztes F, Sigmond T, Vellai T, Kovács T. The evolutionary and functional divergence of the Atg8 autophagy protein superfamily. *Biol Futur*. 2022;73(4):375-384. doi:10.1007/s42977-022-00123-6
34. Jatana N, Ascher DB, Pires DEV, Gokhale RS, Thukral L. Human LC3 and GABARAP subfamily members achieve functional specificity via specific structural modulations. *Autophagy*. 2020;16(2):239-255. doi:10.1080/15548627.2019.1606636
35. Paz Y, Elazar Z, Fass D. Structure of GATE-16, membrane transport modulator and mammalian ortholog of autophagocytosis factor Aut7p. *Journal of Biological Chemistry*. 2000;275(33):25445-25450. doi:10.1074/jbc.C000307200

36. Wesch N, Kirkin V, Rogov V V. Atg8-Family Proteins-Structural Features and Molecular Interactions in Autophagy and Beyond. *Cells*. 2020;9(9). doi:10.3390/cells9092008
37. Chakrama FZ, Seguin-Py S, Le Grand JN, et al. GABARAPL1 (GEC1) associates with autophagic vesicles. *Autophagy*. 2010;6(4):495-505. doi:10.4161/auto.6.4.11819
38. Costa JR, Prak K, Aldous S, Gewinner CA, Ketteler R. *Autophagy Gene Expression Profiling Identifies a Defective Microtubule-Associated Protein Light Chain 3A Mutant in Cancer*. Vol 7. www.impactjournals.com/oncotarget
39. Herhaus L, Bhaskara RM, Lystad AH, et al. TBK1-mediated phosphorylation of LC3C and GABARAP-L2 controls autophagosome shedding by ATG4 protease. *EMBO Rep*. 2020;21(1). doi:10.15252/embr.201948317
40. Huang R, Xu Y, Wan W, et al. Deacetylation of nuclear LC3 drives autophagy initiation under starvation. *Mol Cell*. 2015;57(3):456-466. doi:10.1016/j.molcel.2014.12.013
41. Jia R, Bonifacino JS. Negative regulation of autophagy by UBA6-BIRC6-mediated ubiquitination of LC3. doi:10.7554/eLife.50034.001
42. Weidberg H, Shpilka T, Shvets E, Abada A, Shimron F, Elazar Z. LC3 and GATE-16 N Termini Mediate Membrane Fusion Processes Required for Autophagosome Biogenesis. *Dev Cell*. 2011;20(4):444-454. doi:10.1016/j.devcel.2011.02.006
43. Vaites LP, Paulo JA, Huttlin EL, Harper JW. Systematic Analysis of Human Cells Lacking ATG8 Proteins Uncovers Roles for GABARAPs and the CCZ1/MON1 Regulator C18orf8/RMC1 in Macroautophagic and Selective Autophagic Flux. Published online 2017. doi:10.1128/MCB
44. Nguyen TN, Padman BS, Usher J, Oorschot V, Ramm G, Lazarou M. Atg8 family LC3/GAB ARAP proteins are crucial for autophagosome-lysosome fusion but not autophagosome formation during PINK1/Parkin mitophagy and starvation. *Journal of Cell Biology*. 2016;215(6):857-874. doi:10.1083/jcb.201607039
45. Pankiv S, Clausen TH, Lamark T, et al. p62/SQSTM1 binds directly to Atg8/LC3 to facilitate degradation of ubiquitinated protein aggregates by autophagy*[S]. *Journal of Biological Chemistry*. 2007;282(33):24131-24145. doi:10.1074/jbc.M702824200
46. Kirkin V, Lamark T, Sou YS, et al. A Role for NBR1 in Autophagosomal Degradation of Ubiquitinated Substrates. *Mol Cell*. 2009;33(4):505-516. doi:10.1016/j.molcel.2009.01.020
47. von Muhlinen N, Akutsu M, Ravenhill BJ, et al. LC3C, Bound Selectively by a Noncanonical LIR Motif in NDP52, Is Required for Antibacterial Autophagy. *Mol Cell*. 2012;48(3):329-342. doi:10.1016/j.molcel.2012.08.024
48. Wirth M, Zhang W, Razi M, et al. Molecular determinants regulating selective binding of autophagy adapters and receptors to ATG8 proteins. *Nat Commun*. 2019;10(1). doi:10.1038/s41467-019-10059-6
49. Zellner S, Behrends C. Autophagosome content profiling reveals receptor-specific cargo candidates. *Autophagy*. 2021;17(5):1281-1283. doi:10.1080/15548627.2021.1909410
50. Behrends C, Sowa ME, Gygi SP, Harper JW. Network organization of the human autophagy system. *Nature*. 2010;466(7302):68-76. doi:10.1038/nature09204
51. Le Guerroué F, Eck F, Jung J, et al. Autophagosomal Content Profiling Reveals an LC3C-Dependent Piecemeal Mitophagy Pathway. *Mol Cell*. 2017;68(4):786-796.e6. doi:10.1016/j.molcel.2017.10.029
52. Behrends C, Sowa ME, Gygi SP, Harper JW. Network organization of the human autophagy system. *Nature*. 2010;466(7302):68-76. doi:10.1038/nature09204

53. Leidal AM, Debnath J. LC3-dependent extracellular vesicle loading and secretion (LDELS). *Autophagy*. 2020;16(6):1162-1163. doi:10.1080/15548627.2020.1756557
54. Zhang H, Fracchiolla D, Sawa-Makarska J, et al. Mechanism of cargo-directed Atg8 conjugation during selective autophagy. Published online 2016. doi:10.7554/eLife.18544.001
55. Stolz A, Ernst A, Dikic I. Cargo recognition and trafficking in selective autophagy. *Nat Cell Biol*. 2014;16(6):495-501. doi:10.1038/ncb2979
56. Deng Z, Purtell K, Lachance V, Wold MS, Chen S, Yue Z. Autophagy Receptors and Neurodegenerative Diseases. *Trends Cell Biol*. 2017;27(7):491-504. doi:10.1016/j.tcb.2017.01.001
57. Birgisdottir ÅB, Lamark T, Johansen T. The LIR motif - crucial for selective autophagy. *J Cell Sci*. 2013;126(15):3237-3247. doi:10.1242/jcs.126128
58. Khaminets A, Behl C, Dikic I. Ubiquitin-Dependent And Independent Signals In Selective Autophagy. *Trends Cell Biol*. 2016;26(1):6-16. doi:10.1016/j.tcb.2015.08.010
59. Kirkin V, Lamark T, Sou YS, et al. A Role for NBR1 in Autophagosomal Degradation of Ubiquitinated Substrates. *Mol Cell*. 2009;33(4):505-516. doi:10.1016/j.molcel.2009.01.020
60. Daroszewska A, Ralston SH. Mechanisms of disease: Genetics of Paget's disease of bone and related disorders. *Nat Clin Pract Rheumatol*. 2006;2(5):270-277. doi:10.1038/ncprheum0172
61. Farrawell NE, McAlary L, Lum JS, et al. Ubiquitin Homeostasis Is Disrupted in TDP-43 and FUS Cell Models of ALS. *iScience*. 2020;23(11). doi:10.1016/j.isci.2020.101700
62. Scotter EL, Vance C, Nishimura AL, et al. Differential roles of the ubiquitin proteasome system and autophagy in the clearance of soluble and aggregated TDP-43 species. *J Cell Sci*. 2014;127(6):1263-1278. doi:10.1242/jcs.140087
63. Wong YC, Holzbaur ELF. Optineurin is an autophagy receptor for damaged mitochondria in parkin-mediated mitophagy that is disrupted by an ALS-linked mutation. *Proc Natl Acad Sci U S A*. 2014;111(42):E4439-E4448. doi:10.1073/pnas.1405752111
64. Novak I, Kirkin V, McEwan DG, et al. Nix is a selective autophagy receptor for mitochondrial clearance. *EMBO Rep*. 2010;11(1):45-51. doi:10.1038/embor.2009.256
65. Chitiprolu M, Jagow C, Tremblay V, et al. A complex of C9ORF72 and p62 uses arginine methylation to eliminate stress granules by autophagy. *Nat Commun*. 2018;9(1). doi:10.1038/s41467-018-05273-7
66. Menzies FM, Fleming A, Rubinsztein DC. Compromised autophagy and neurodegenerative diseases. *Nat Rev Neurosci*. 2015;16(6):345-357. doi:10.1038/nrn3961
67. Heckmann BL, Teubner BJW, Boada-Romero E, et al. *Noncanonical Function of an Autophagy Protein Prevents Spontaneous Alzheimer's Disease*. Vol 6.; 2020. https://www.science.org
68. Li Z, Wang C, Wang Z, et al. Allele-selective lowering of mutant HTT protein by HTT–LC3 linker compounds. *Nature*. 2019;575(7781):203-209. doi:10.1038/s41586-019-1722-1
69. Barmada SJ, Serio A, Arjun A, et al. Autophagy induction enhances TDP43 turnover and survival in neuronal ALS models. *Nat Chem Biol*. 2014;10(8):677-685. doi:10.1038/nchembio.1563

70. Bjørkøy G, Lamark T, Brech A, et al. p62/SQSTM1 forms protein aggregates degraded by autophagy and has a protective effect on huntingtin-induced cell death. *Journal of Cell Biology*. 2005;171(4):603-614. doi:10.1083/jcb.200507002
71. Wong YC, Holzbaur ELF. Optineurin is an autophagy receptor for damaged mitochondria in parkin-mediated mitophagy that is disrupted by an ALS-linked mutation. *Proc Natl Acad Sci U S A*. 2014;111(42):E4439-E4448. doi:10.1073/pnas.1405752111
72. Teyssou E, Takeda T, Lebon V, et al. Mutations in SQSTM1 encoding p62 in amyotrophic lateral sclerosis: Genetics and neuropathology. *Acta Neuropathol*. 2013;125(4):511-522. doi:10.1007/s00401-013-1090-0
73. Rubino E, Rainero I, Chiò A, et al. *SQSTM1 Mutations in Frontotemporal Lobar Degeneration and Amyotrophic Lateral Sclerosis*.; 2012. www.softgenetics.com
74. Rudnick ND, Griffey CJ, Guarnieri P, et al. Distinct roles for motor neuron autophagy early and late in the SOD1G93A mouse model of ALS. *Proc Natl Acad Sci U S A*. 2017;114(39):E8294-E8303. doi:10.1073/pnas.1704294114
75. Hardiman O, Van Den Berg LH, Kiernan MC. Clinical diagnosis and management of amyotrophic lateral sclerosis. *Nat Rev Neurol*. 2011;7(11):639-649. doi:10.1038/nrneurol.2011.153
76. Ragagnin AMG, Shadfar S, Vidal M, Jamali MS, Atkin JD. Motor neuron susceptibility in ALS/FTD. *Front Neurosci*. 2019;13(JUN). doi:10.3389/fnins.2019.00532
77. Deng H, Gao K, Jankovic J. The role of FUS gene variants in neurodegenerative diseases. *Nat Rev Neurol*. 2014;10(6):337-348. doi:10.1038/nrneurol.2014.78
78. Ito D, Hatano M, Suzuki N. *RNA Binding Proteins and the Pathological Cascade in ALS/FTD Neurodegeneration*.; 2017. https://www.science.org
79. Pinkerton M, Lourenco G, Pacheco MT, Halliday GM, Kiernan MC, Tan RH. Survival in sporadic ALS is associated with lower p62 burden in the spinal cord. *J Neuropathol Exp Neurol*. 2023;82(9):769-773. doi:10.1093/jnen/nlad051
80. Johnson JO, Mandrioli J, Benatar M, et al. Exome Sequencing Reveals VCP Mutations as a Cause of Familial ALS. *Neuron*. 2010;68(5):857-864. doi:10.1016/j.neuron.2010.11.036
81. Deng HX, Chen W, Hong ST, et al. Mutations in UBQLN2 cause dominant X-linked juvenile and adult-onset ALS and ALS/dementia. *Nature*. 2011;477(7363):211-215. doi:10.1038/nature10353
82. Saxena S, Cabuy E, Caroni P. A role for motoneuron subtype-selective ER stress in disease manifestations of FALS mice. *Nat Neurosci*. 2009;12(5):627-636. doi:10.1038/nn.2297
83. Chua JP, De Calbiac H, Kabashi E, Barmada SJ. Autophagy and ALS: mechanistic insights and therapeutic implications. *Autophagy*. Published online 2021. doi:10.1080/15548627.2021.1926656
84. Sasaki S. *Autophagy in Spinal Cord Motor Neurons in Sporadic Amyotrophic Lateral Sclerosis*.; 2011. https://academic.oup.com/jnen/article/70/5/349/2917295
85. Cascella R, Bigi A, Giorgino Riffert D, et al. *A Quantitative Biology Approach Correlates Neuronal Toxicity with the Largest Inclusions of TDP-43*. Vol 8.; 2022. https://www.science.org
86. Dewey CM, Cenik B, Sephton CF, Johnson BA, Herz J, Yu G. TDP-43 aggregation in neurodegeneration: Are stress granules the key? *Brain Res*. 2012;1462:16-25. doi:10.1016/j.brainres.2012.02.032

87. Sephton CF, Good SK, Atkin S, et al. TDP-43 is a developmentally regulated protein essential for early embryonic development. *Journal of Biological Chemistry*. 2010;285(9):6826-6834. doi:10.1074/jbc.M109.061846
88. Buratti E. TDP-43 post-translational modifications in health and disease. *Expert Opin Ther Targets*. 2018;22(3):279-293. doi:10.1080/14728222.2018.1439923
89. Tripathi P, Guo H, Dreser A, et al. Pathomechanisms of ALS8: altered autophagy and defective RNA binding protein (RBP) homeostasis due to the VAPB P56S mutation. *Cell Death Dis*. 2021;12(5). doi:10.1038/s41419-021-03710-y
90. Schmitt D, Bozkurt S, Henning-Domres P, et al. Lipid and protein content profiling of isolated native autophagic vesicles. *EMBO Rep*. Published online December 6, 2022. doi:10.15252/embr.202153065
91. Kumar S, Phaneuf D, Cordeau P, Boutej H, Kriz J, Julien JP. Induction of autophagy mitigates TDP-43 pathology and translational repression of neurofilament mRNAs in mouse models of ALS/FTD. *Mol Neurodegener*. 2021;16(1). doi:10.1186/s13024-020-00420-5
92. Kuusisto E, Kauppinen T, Alafuzoff I. Use of p62/SQSTM1 antibodies for neuropathological diagnosis. *Neuropathol Appl Neurobiol*. 2008;34(2):169-180. doi:10.1111/j.1365-2990.2007.00884.x
93. Protter DSW, Parker R. Principles and Properties of Stress Granules. *Trends Cell Biol*. 2016;26(9):668-679. doi:10.1016/j.tcb.2016.05.004
94. Colombrita C, Zennaro E, Fallini C, et al. TDP-43 is recruited to stress granules in conditions of oxidative insult. *J Neurochem*. 2009;111(4):1051-1061. doi:10.1111/j.1471-4159.2009.06383.x
95. Molliex A, Temirov J, Lee J, et al. *Phase Separation by Low Complexity Domains Promotes Stress Granule Assembly and Drives Pathological Fibrillization*. Vol 163.; 2015.
96. Monahan Z, Shewmaker F, Pandey UB. Stress granules at the intersection of autophagy and ALS. *Brain Res*. 2016;1649:189-200. doi:10.1016/j.brainres.2016.05.022
97. Buchan JR, Kolaitis RM, Paul Taylor J, Parker R. *Eukaryotic Stress Granules Are Cleared by Granulophagy and Cdc48/VCP Function*.; 2013.
98. Jo M, Lee S, Jeon YM, Kim S, Kwon Y, Kim HJ. The role of TDP-43 propagation in neurodegenerative diseases: integrating insights from clinical and experimental studies. *Exp Mol Med*. 2020;52(10):1652-1662. doi:10.1038/s12276-020-00513-7
99. Colombrita C, Zennaro E, Fallini C, et al. TDP-43 is recruited to stress granules in conditions of oxidative insult. *J Neurochem*. 2009;111(4):1051-1061. doi:10.1111/j.1471-4159.2009.06383.x
100. Khalfallah Y, Kuta R, Grasmuck C, Prat A, Durham HD, Vande Velde C. TDP-43 regulation of stress granule dynamics in neurodegenerative disease-relevant cell types /631/80/304 /631/378/87 /13/1 /13/31 /13/51 /13/109 /13/106 /13/89 /14/19 /14/32 /82/80 article. *Sci Rep*. 2018;8(1). doi:10.1038/s41598-018-25767-0
101. Nguyen DKH, Thombre R, Wang J. Autophagy as a common pathway in amyotrophic lateral sclerosis. *Neurosci Lett*. 2019;697:34-48. doi:10.1016/j.neulet.2018.04.006
102. Wang IF, Guo BS, Liu YC, et al. Autophagy activators rescue and alleviate pathogenesis of a mouse model with proteinopathies of the TAR DNA-binding protein 43. *Proc Natl Acad Sci U S A*. 2012;109(37):15024-15029. doi:10.1073/pnas.1206362109

103. Ryu HH, Jun MH, Min KJ, et al. Autophagy regulates amyotrophic lateral sclerosis-linked fused in sarcoma-positive stress granules in neurons. *Neurobiol Aging*. 2014;35(12):2822-2831. doi:10.1016/j.neurobiolaging.2014.07.026
104. Kocak M, Ezazi Erdi S, Jorba G, et al. Targeting autophagy in disease: established and new strategies. *Autophagy*. 2022;18(3):473-495. doi:10.1080/15548627.2021.1936359
105. Nalawansha DA, Crews CM. PROTACs: An Emerging Therapeutic Modality in Precision Medicine. *Cell Chem Biol*. 2020;27(8):998-1014. doi:10.1016/j.chembiol.2020.07.020
106. Takahashi D, Moriyama J, Nakamura T, et al. AUTACs: Cargo-Specific Degraders Using Selective Autophagy. *Mol Cell*. 2019;76(5):797-810.e10. doi:10.1016/j.molcel.2019.09.009
107. Li Z, Wang C, Wang Z, et al. Allele-selective lowering of mutant HTT protein by HTT–LC3 linker compounds. *Nature*. 2019;575(7781):203-209. doi:10.1038/s41586-019-1722-1
108. Debnath J, Leidal AM. Secretory autophagy during lysosome inhibition (SALI). *Autophagy*. 2022;18(10):2498-2499. doi:10.1080/15548627.2022.2095788
109. Doyle LM, Wang MZ. Overview of extracellular vesicles, their origin, composition, purpose, and methods for exosome isolation and analysis. *Cells*. 2019;8(7). doi:10.3390/cells8070727
110. Gagliardi D, Bresolin N, Comi G Pietro, Corti S. Extracellular vesicles and amyotrophic lateral sclerosis: from misfolded protein vehicles to promising clinical biomarkers. *Cellular and Molecular Life Sciences*. 2021;78(2):561-572. doi:10.1007/s00018-020-03619-3
111. Bertin A, de Franceschi N, de la Mora E, et al. Human ESCRT-III polymers assemble on positively curved membranes and induce helical membrane tube formation. *Nat Commun*. 2020;11(1). doi:10.1038/s41467-020-16368-5
112. Youn JY, Dunham WH, Hong SJ, et al. High-Density Proximity Mapping Reveals the Subcellular Organization of mRNA-Associated Granules and Bodies. *Mol Cell*. 2018;69(3):517-532.e11. doi:10.1016/j.molcel.2017.12.020
113. Mizushima N. A brief history of autophagy from cell biology to physiology and disease. *Nat Cell Biol*. 2018;20(5):521-527. doi:10.1038/s41556-018-0092-5
114. Wild P, McEwan DG, Dikic I. The LC3 interactome at a glance. *J Cell Sci*. 2014;127(1):3-9. doi:10.1242/jcs.140426
115. Buchan JR, Kolaitis RM, Taylor JP, Parker R. XEukaryotic stress granules are cleared by autophagy and Cdc48/VCP function. *Cell*. 2013;153(7):1461. doi:10.1016/j.cell.2013.05.037
116. Nguyen TN, Padman BS, Usher J, Oorschot V, Ramm G, Lazarou M. Atg8 family LC3/GAB ARAP proteins are crucial for autophagosome-lysosome fusion but not autophagosome formation during PINK1/Parkin mitophagy and starvation. *Journal of Cell Biology*. 2016;215(6):857-874. doi:10.1083/jcb.201607039
117. Rogov V, Dötsch V, Johansen T, Kirkin V. Interactions between Autophagy Receptors and Ubiquitin-like Proteins Form the Molecular Basis for Selective Autophagy. *Mol Cell*. 2014;53(2):167-178. doi:10.1016/j.molcel.2013.12.014
118. Wang B, Maxwell BA, Joo JH, et al. ULK1 and ULK2 Regulate Stress Granule Disassembly Through Phosphorylation and Activation of VCP/p97. *Mol Cell*. 2019;74(4):742-757.e8. doi:10.1016/j.molcel.2019.03.027

119. Feng Y, He D, Yao Z, Klionsky DJ. The machinery of macroautophagy. *Cell Res*. 2014;24(1):24-41. doi:10.1038/cr.2013.168
120. Hurley JH, Hanson PI. Membrane budding and scission by the ESCRT machinery: It's all in the neck. *Nat Rev Mol Cell Biol*. 2010;11(8):556-566. doi:10.1038/nrm2937
121. Underwood R, Wang B, Carico C, Whitaker RH, Placzek WJ, Yacoubian TA. The GTPase Rab27b regulates the release, autophagic clearance, and toxicity of alpha-synuclein. *Journal of Biological Chemistry*. 2020;295(23):8005-8016. doi:10.1074/JBC.RA120.013337
122. Ao X, Zou L, Wu Y. Regulation of autophagy by the Rab GTPase network. *Cell Death Differ*. 2014;21(3):348-358. doi:10.1038/cdd.2013.187
123. Yamamoto H, Zhang S, Mizushima N. Autophagy genes in biology and disease. *Nat Rev Genet*. 2023;24(6):382-400. doi:10.1038/s41576-022-00562-w